

Supporting Information

Halogen Bonding and Mechanochemistry Combined: Synthesis, Characterization, and Application of *N*-Iodosaccharin-based Pyridine Complexes

Christian Schumacher,^{a,b,‡} Khai-Nghi Truong,^{a,‡} Jas S. Ward,^{a,‡} Anssi Rajala,^a Elias Lassila,^a
Carsten Bolm,^b Kari Rissanen^{a,*}

[‡] These authors contributed equally.

^a University of Jyväskylä, Department of Chemistry, P.O. Box 35, Surfontie 9 B, 40014 Jyväskylä, Finland.

^b Institute of Organic Chemistry, RWTH Aachen University, Landoltweg 1, 52074 Aachen, Germany

Correspondence to: Kari Rissanen (kari.t.rissanen@jyu.fi)

Table of Contents

1 Analytical Methods.....	4
1.1 Single-Crystal X-ray Diffraction (SCXRD) Analysis.....	4
1.2 Powder X-ray Diffraction (PXRD) Analysis.....	4
1.3 Melting Point Determination.....	4
1.4 Nuclear Magnetic Resonance Spectroscopy.....	4
1.5 Infrared Spectroscopy.....	5
1.6 Mass Spectrometry.....	5
1.7 Elemental Analysis.....	5
2 Equipment and Materials.....	6
2.1 Microwave-assisted Reactions.....	6
2.2 Mechanochemical Reactions.....	6
2.3 Chemicals.....	7
2.4 Flash Column Chromatography.....	7
2.5 Thin-Layer Chromatography.....	7
2.6 Crystal growing.....	7
3 Crystallographic Data.....	8
3.1 Crystal Data.....	8
3.2 Displacement Ellipsoid Plots and Crystal Packing.....	12
4 IR Ex-Situ Analysis.....	28
5 PXRD Ex-Situ Analysis.....	46
6 General Synthetic Procedures and Scale-Up Experiments.....	52
6.1 General Procedure 1 (GP1) – Microwave-assisted Synthesis of 4-Substituted Pyridines.....	52
6.2 General Procedure 2 (GP2) – Solution Synthesis of XB Complexes using DMAP, MPY, PiPY.....	52
6.3 Scale-Up Experiments.....	53
6.4 General Procedure 3 (GP3) – Ex-situ Analysis of the XB Complex Formation by IR and PXRD Analysis.....	54
6.5 General Procedure 4 (GP4) – Mechanochemical Synthesis of the XB Complexes (Mortar and Pestle).....	54
6.6 General Procedure 5 (GP5) – Mechanochemical Synthesis of XB Complex [NISac-DMAP] (Planetary Mill).....	54
6.7 General Procedure 6 (GP6) – Ex-situ Analysis of the Iodonium Complex Formation by IR and PXRD Analysis.....	55
6.8 General Procedure 7 (GP7) – Mechanochemical Synthesis of [I(DMAP) ₂]NSac.....	56
6.9 General Procedure 8 (GP8) – Iodination of Antipyrine (Solution).....	56
6.10 General Procedure 9 (GP9) – Iodination of Antipyrine (Planetary Mill).....	56
7 Analytical Data.....	57

7.1 Starting Materials	57
7.2 Products	59
7.2.1 XB Complexes	59
7.2.2 Iodine(I) Complexes.....	61
7.2.3 Iodinated Products	65
7.2.4 Recovery of Starting Materials	66
8 References.....	68
9 Spectra	70

1 Analytical Methods

1.1 Single-Crystal X-ray Diffraction (SCXRD) Analysis

The single crystal X-ray data for **2d**, **4ab**, **4ac**, **4bd**, **4d**, **8**, [(MPYH)NSac_1], [(MPYH)NSac_2], [(MPYH)NSac_3], [(PiPYH)I₃], [(PPYH)I], [(PPYH)NSac_1], and [(PPYH)NSac_2] were collected at 120 K using an Agilent SuperNova dual wavelength diffractometer with an Atlas detector using mirror-monochromated Cu-K α ($\lambda = 1.54184 \text{ \AA}$) or Mo-K α ($\lambda = 0.71073 \text{ \AA}$) radiation. The single crystal X-ray data for **3a**, **3b**, **3c**, **3d**, **4a**·H₂O, **4a_1**, **4a_2**, **4c_1**, **4c_2**, **4c_3**, **4cd**, [I(DMAP)₂]I_{3_1}, and [I(DMAP)₂]I_{3_2} were collected at 170 K using Bruker-Nonius Kappa CCD diffractometer with an APEX-II detector with graphite-monochromatised Mo-K α ($\lambda = 0.71073 \text{ \AA}$) radiation, with the COLLECT program for data collection and DENZO/SCALEPACK for the data reduction.^{1,2} The X-ray single crystal data and CCDC numbers 2255940-2255965 of all new structures are included below.

1.2 Powder X-ray Diffraction (PXRD) Analysis

Powder X-ray diffraction patterns were recorded on a PANALYTICAL X'PERT PRO MPD diffractometer. The X-ray source was Cu-K α_2 radiation with a wavelength of $\lambda = 1.544256 \text{ \AA}$. The PXRD patterns were recorded in 2 θ range from 3-60° and a step size of D2 $\theta = 0.0167^\circ$.

1.3 Melting Point Determination

Melting points (mp) were determined as melting point ranges (starting from analyte starts to melt until it is completely molten) on a BÜCHI M-560 melting point apparatus using open-end capillaries. A heating rate of 5 °C·min⁻¹ was applied, color changes and decomposing samples are marked as such (decomp.). The given values are uncorrected.

1.4 Nuclear Magnetic Resonance Spectroscopy

Nuclear magnetic resonance (NMR) spectra were recorded on a Bruker Avance Neo 400, Bruker Avance Neo 600, Varian VNMRS 300, Varian VNMRS 400 or Varian VNMRS 600 at ambient temperature (25 °C), if not mentioned otherwise. Carbon NMR spectra were recorded as proton broadband decoupled spectra, indicated as ¹³C{¹H}. Chemical shifts (δ) are given in ppm (parts per million) and are reported from downfield to upfield. The spin-spin coupling constants (J) are reported in Hertz. Corresponding multiplicities are reported as s (singlet), d (doublet), t (triplet), q (quartet), quint (quintet), m (multiplet), br (broad signal) and combinations thereof. ¹H and ¹³C{¹H} spectra were referenced to the solvent (residual) signal of the (non)-deuterated NMR solvent (Table S1).³

Table S1. ^1H and $^{13}\text{C}\{^1\text{H}\}$ NMR data of the used NMR solvents.

NMR Solvent	^1H NMR of solvent residual signal δ [ppm]	$^{13}\text{C}\{^1\text{H}\}$ NMR solvent signals: δ [ppm]
CDCl_3	7.26 (CHCl_3)	77.16
CD_2Cl_2	5.32 (CHDCl_2)	53.84
$(\text{CD}_3)_2\text{CO}$	2.05 [$(\text{CH}_3)_2\text{CO}$]	206.26, 29.84
CD_3CN	1.94 (CH_3CN)	118.26, 1.32
$(\text{CD}_3)_2\text{SO}$	2.50 [$(\text{CH}_3)_2\text{SO}$]	39.52

1.5 Infrared Spectroscopy

Infrared (IR) spectra for reaction analysis during the optimization process was recorded in transmission mode on a Bruker Tensor 27 FTIR spectrometer by placing the material on an ATR sample compartment. The measurements were performed with 128 scans and a resolution of 4 cm^{-1} .

IR spectra for analysis of pure compounds were recorded neat and in transmission mode on a PerkinElmer Spectrum 100 FT-IR spectrometer. Single reflection measurement was achieved using an attached UATR device with a KRS-5 crystal.

1.6 Mass Spectrometry

Low resolution mass spectra were recorded on a Finnigan SSQ 7000 mass spectrometer either in electron ionization (EI) mode operating at 70 eV or in chemical ionization (CI) mode applying 100 eV and methane as conditions. Signals are reported according to their m/z values. The relative intensities are compared to the base peak ($I = 100\%$) and given in parentheses. Positive electrospray ionization (ESI) spectra were recorded on a ThermoFisher Scientific LTQ Orbitrap XL mass spectrometer.

1.7 Elemental Analysis

Elemental analysis (CHN) was performed either on a Elementar varioEL or Elementar varioEL cube CHN analyzer. The values for both the calculated and the found results are reported in percentages.

2 Equipment and Materials

2.1 Microwave-assisted Reactions

Microwave-assisted reactions were performed using a CEM Discover microwave (Figure S1) equipped with the IntelliVent pressure measurement option. Reaction tubes were always of 10 mL volume and equipped with a magnetic stirring bar.

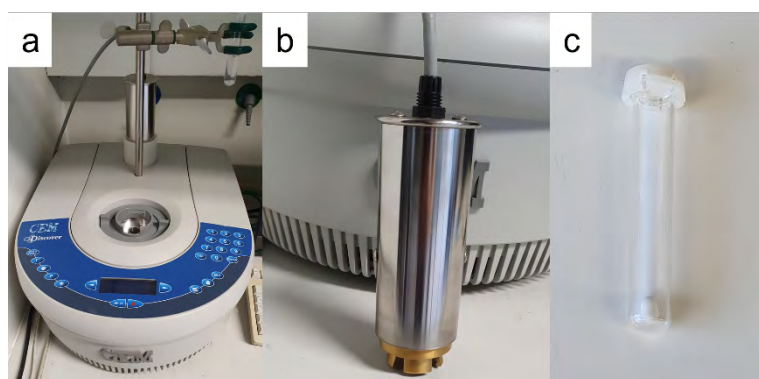


Figure S1. Used microwave equipment. a) Microwave; b) attached pressure device; c) reaction tube equipped with used stirring bar.

2.2 Mechanochemical Reactions

Mechanochemical reactions were performed using either a mortar and a pestle or a planetary mill (Figure S2). For ball milling reactions a FRITSCH Planetary Micro Mill PULVERISETTE 7 classic line was used. Milling containers (12 mL) and balls (5 or 10 mm in \varnothing) were always of the same material (agate).

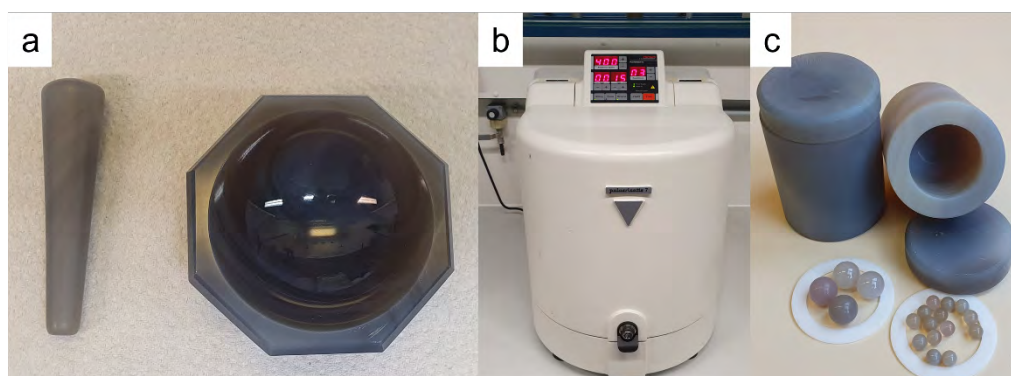


Figure 2. Mechanochemical equipment used. a) agate mortar and pestle; b) FRITSCH planetary mill PULVERISETTE 7 classic line; c) 12 mL agate milling containers and milling balls (10 and 5 mm in \varnothing).

2.3 Chemicals

Solvents for crystallizations or reactions have been of HPLC grade. The pyridine derivatives [4-dimethylaminopyridine (DMAP, Sigma Aldrich), 4-(pyrrolidino)pyridine (PPY, Fluka), 4-morpholinopyridine (MPY, Fluorochem), 4-piperidinopyridine (PiPY, Fluorochem)], *N*-iodosaccharin (TCI), iodine (TCI and Merck), saccharin (TCI and Acros), phenyliodine(III) diacetate (PIDA, BLD Pharm), and antipyrine (Alfa Aesar) have been used as received. 2,4-Dimethylaniline (J&K Scientific) was distilled prior to use. Unless otherwise mentioned, all other chemicals were obtained from commercial suppliers and were used as received.

2.4 Flash Column Chromatography

Solvents for column chromatography were of technical grade and were distilled prior to use. Eluent mixtures are always understood as volume-to-volume ratios (*v/v*). Flash column chromatography was always performed on silica gel 60 M (0.04–0.063 mm) purchased from Machery-Nagel. The to be purified product was impregnated on silica. Therefore, it was dissolved in an appropriate solvent, a suitable amount of silica was added, and the solvent was removed under reduced pressure using a rotary evaporator. The obtained free flowing powder was placed on top of the column for purification. Appropriate fractions were identified by thin-layer chromatography (TLC) analysis and combined.

2.5 Thin-Layer Chromatography

TLC analysis was performed on TLC silica gel 60 F254 aluminum sheets purchased from Merck. Products were visualized using UV light ($\lambda = 254$ nm). Retention factors (R_f) are defined as the travelled distance of analyte divided by the distance of the eluent.

2.6 Crystal growing

A few milligrams of the to be (co-)crystallized substances were filled into a 4 ml glass vial. In case of co-crystallization the stoichiometry was set according to the needs of the crystal approach. Then, the solids were dissolved in 1-2 ml of the chosen solvent (HPLC grade), if required gentle heating was applied. The solution was filtered into another 4 ml glass vial using a glass pipette filter. The sample was stored, covered with perforated parafilm for slow evaporation in the dark either at room temperature, 4 °C, or -20 °C, and were checked from time to time for crystalline materials that were analyzed by SCXRD (and/or IR).

3 Crystallographic Data

3.1 Crystal Data

Crystal data for **2d**: C₁₀H₁₄N₂, M = 162.23, colourless plate, 0.05 × 0.21 × 0.26 mm, tetragonal, space group *I*-42*d*, a = 12.6737(7) Å, c = 11.6271(5) Å, V = 11.6271(5) Å³, Z = 8, D_{calc} = 1.154 gcm⁻³, F(000) = 704, μ = 0.07 mm⁻¹, T = 120.0(1) K, θ_{max} = 26.3°, 931 total reflections, 793 with I_o > 2σ(I_o), R_{int} = 0.049, 931 data, 76 parameters, no restraints, GooF = 1.08, 0.11 < dΔρ < -0.13 eÅ⁻³, R[F² > 2σ(F²)] = 0.043, wR(F²) = 0.102, CCDC 2255940.

Crystal data for **3a**: C₁₄H₁₄IN₃O₃S, M = 431.24, colourless needle, 0.13 × 0.16 × 0.28 mm, monoclinic, space group *P*2₁/*n*, a = 9.0129(2) Å, b = 12.312(4) Å, c = 14.5193(5) Å, β = 101.611(1)°, V = 1578.2(5) Å³, Z = 4, D_{calc} = 1.815 gcm⁻³, F(000) = 848, μ = 2.18 mm⁻¹, T = 170(1) K, θ_{max} = 30.9°, 4891 total reflections, 3756 with I_o > 2σ(I_o), R_{int} = 0.033, 4891 data, 201 parameters, no restraints, GooF = 1.02, 0.45 < dΔρ < -0.52 eÅ⁻³, R[F² > 2σ(F²)] = 0.036, wR(F²) = 0.071, CCDC 2255941.

Crystal data for **3b**: C₁₆H₁₆IN₃O₃S, M = 457.28, colourless plate, 0.07 × 0.31 × 0.36 mm, triclinic, space group *P*-1 (No. 2), a = 7.9856(2) Å, b = 8.3116(4) Å, c = 13.2390(6) Å, α = 78.275(1)°, β = 89.168(2)°, γ = 75.710(1)°, V = 833.17(6) Å³, Z = 2, D_{calc} = 1.823 gcm⁻³, F(000) = 452, μ = 2.07 mm⁻¹, T = 170(1) K, θ_{max} = 26.3°, 3353 total reflections, 2766 with I_o > 2σ(I_o), R_{int} = 0.044, 3353 data, 217 parameters, no restraints, GooF = 1.05, 0.74 < dΔρ < -0.73 eÅ⁻³, R[F² > 2σ(F²)] = 0.051, wR(F²) = 0.109, CCDC 2255942.

Crystal data for **3c**: C₁₆H₁₆IN₃O₄S, M = 473.28, colourless block, 0.20 × 0.24 × 0.29 mm, triclinic, space group *P*-1 (No. 2), a = 8.1810(3) Å, b = 8.3001(4) Å, c = 15.0946(9) Å, α = 94.226(2)°, β = 101.222(2)°, γ = 118.108(3)°, V = 870.45(8) Å³, Z = 2, D_{calc} = 1.806 gcm⁻³, F(000) = 468, μ = 1.99 mm⁻¹, T = 170(1) K, θ_{max} = 26.3°, 3476 total reflections, 2633 with I_o > 2σ(I_o), R_{int} = 0.050, 3476 data, 226 parameters, 9 restraints, GooF = 1.10, 1.14 < dΔρ < -1.13 eÅ⁻³, R[F² > 2σ(F²)] = 0.059, wR(F²) = 0.134, CCDC 2255943.

Crystal data for **3d**: C₁₇H₁₈IN₃O₃S, M = 471.30, colourless plate, 0.03 × 0.14 × 0.17 mm, triclinic, space group *P*-1 (No. 2), a = 8.2544(4) Å, b = 8.3834(5) Å, c = 13.5305(9) Å, α = 78.889(2)°, β = 91.709(3)°, γ = 77.131(2)°, V = 893.09(9) Å³, Z = 2, D_{calc} = 1.753 gcm⁻³, F(000) = 468, μ = 1.93 mm⁻¹, T = 170(1) K, θ_{max} = 26.3°, 3581 total reflections, 2558 with I_o > 2σ(I_o), R_{int} = 0.053, 3581 data, 226 parameters, no restraints, GooF = 1.02, 0.91 < dΔρ < -0.75 eÅ⁻³, R[F² > 2σ(F²)] = 0.067, wR(F²) = 0.141, CCDC 2255944.

Crystal data for **4a·H₂O**: [C₁₄H₂₀IN₄][C₇H₄NO₃S]·2(H₂O), M = 589.44, colourless plate, 0.05 × 0.20 × 0.27 mm, triclinic, space group *P*-1 (No. 2), a = 10.4392(7) Å, b = 11.0639(7) Å, c = 11.6234(8) Å, α = 106.974(3)°, β = 97.528(2)°, γ = 105.542(3)°, V = 1204.74(14) Å³, Z = 2, D_{calc} = 1.625 gcm⁻³, F(000) = 596, μ = 1.46 mm⁻¹, T = 170(1) K, θ_{max} = 25.0°, 4182 total reflections, 2284 with I_o > 2σ(I_o), R_{int} = 0.117,

4182 data, 314 parameters, 37 restraints, GooF = 1.05, $1.13 < d\Delta\rho < -0.78 \text{ e}\text{\AA}^{-3}$, $R[F^2 > 2\sigma(F^2)] = 0.079$, $wR(F^2) = 0.163$, CCDC 2255947.

Crystal data for **4a_1**: $[\text{C}_{14}\text{H}_{20}\text{IN}_4][\text{C}_7\text{H}_4\text{NO}_3\text{S}]$, M = 553.41, colourless needle, $0.09 \times 0.13 \times 0.21 \text{ mm}$, monoclinic, space group $P2_1/c$, $a = 16.2893(14) \text{ \AA}$, $b = 7.8087(7) \text{ \AA}$, $c = 19.0946(19) \text{ \AA}$, $\beta = 109.270(3)^\circ$, $V = 2292.7(4) \text{ \AA}^3$, $Z = 4$, $D_{\text{calc}} = 1.603 \text{ gcm}^{-3}$, $F(000) = 1112$, $\mu = 1.52 \text{ mm}^{-1}$, $T = 170(1) \text{ K}$, $\theta_{\text{max}} = 25.3^\circ$, 4115 total reflections, 1353 with $I_o > 2\sigma(I_o)$, $R_{\text{int}} = 0.162$, 4115 data, 304 parameters, 99 restraints, GooF = 1.00, $1.22 < d\Delta\rho < -0.84 \text{ e}\text{\AA}^{-3}$, $R[F^2 > 2\sigma(F^2)] = 0.092$, $wR(F^2) = 0.181$, CCDC 2255945.

Crystal data for **4a_2**: $[\text{C}_{14}\text{H}_{20}\text{IN}_4][\text{C}_7\text{H}_4\text{NO}_3\text{S}]$, M = 553.41, colourless plate, $0.05 \times 0.13 \times 0.16 \text{ mm}$, orthorhombic, space group $Pbca$, $a = 9.1690(3) \text{ \AA}$, $b = 15.4714(4) \text{ \AA}$, $c = 31.904(1) \text{ \AA}$, $V = 4525.8(2) \text{ \AA}^3$, $Z = 8$, $D_{\text{calc}} = 1.624 \text{ gcm}^{-3}$, $F(000) = 2224$, $\mu = 1.54 \text{ mm}^{-1}$, $T = 170(1) \text{ K}$, $\theta_{\text{max}} = 26.3^\circ$, 4565 total reflections, 3063 with $I_o > 2\sigma(I_o)$, $R_{\text{int}} = 0.073$, 4565 data, 284 parameters, no restraints, GooF = 1.03, $0.35 < d\Delta\rho < -0.37 \text{ e}\text{\AA}^{-3}$, $R[F^2 > 2\sigma(F^2)] = 0.042$, $wR(F^2) = 0.073$, CCDC 2255946.

Crystal data for **4ab**: $[\text{C}_{16}\text{H}_{22}\text{IN}_4][\text{C}_7\text{H}_4\text{NO}_3\text{S}] \cdot \text{CH}_2\text{Cl}_2$, M = 664.37, colourless plate, $0.07 \times 0.24 \times 0.25 \text{ mm}$, triclinic, space group $P-1$ (No. 2), $a = 8.1076(6) \text{ \AA}$, $b = 10.3354(9) \text{ \AA}$, $c = 17.7279(14) \text{ \AA}$, $\alpha = 75.849(2)^\circ$, $\beta = 84.311(2)^\circ$, $\gamma = 68.506(1)^\circ$, $V = 1340.19(19) \text{ \AA}^3$, $Z = 2$, $D_{\text{calc}} = 1.646 \text{ gcm}^{-3}$, $F(000) = 668$, $\mu = 1.51 \text{ mm}^{-1}$, $T = 120.0(1) \text{ K}$, $\theta_{\text{max}} = 25.3^\circ$, 4837 total reflections, 3269 with $I_o > 2\sigma(I_o)$, $R_{\text{int}} = 0.048$, 4837 data, 327 parameters, 18 restraints, GooF = 1.07, $1.44 < d\Delta\rho < -0.78 \text{ e}\text{\AA}^{-3}$, $R[F^2 > 2\sigma(F^2)] = 0.078$, $wR(F^2) = 0.192$, CCDC 2255948.

Crystal data for **4ac**: $[\text{C}_{16}\text{H}_{22}\text{IN}_4\text{O}][\text{C}_7\text{H}_4\text{NO}_3\text{S}]$, M = 595.45, colourless plate, $0.03 \times 0.19 \times 0.28 \text{ mm}$, orthorhombic, space group $Cmca$, $a = 18.6425(10) \text{ \AA}$, $b = 8.1736(3) \text{ \AA}$, $c = 35.9127(16) \text{ \AA}$, $V = 5472.2(4) \text{ \AA}^3$, $Z = 8$, $D_{\text{calc}} = 1.445 \text{ gcm}^{-3}$, $F(000) = 2400$, $\mu = 10.21 \text{ mm}^{-1}$, $T = 120.0(1) \text{ K}$, $\theta_{\text{max}} = 70.0^\circ$, 2684 total reflections, 1736 with $I_o > 2\sigma(I_o)$, $R_{\text{int}} = 0.099$, 2684 data, 185 parameters, 2 restraints, GooF = 1.02, $1.91 < d\Delta\rho < -0.84 \text{ e}\text{\AA}^{-3}$, $R[F^2 > 2\sigma(F^2)] = 0.048$, $wR(F^2) = 0.130$, CCDC 2255949.

Crystal data for **4bd**: $[\text{C}_{19}\text{H}_{26}\text{IN}_4][\text{C}_7\text{H}_4\text{NO}_3\text{S}] \cdot 2(\text{CH}_2\text{Cl}_2)$, M = 789.36, colourless plate, $0.10 \times 0.20 \times 0.23 \text{ mm}$, monoclinic, space group $C2/m$, $a = 20.5334(8) \text{ \AA}$, $b = 19.1220(7) \text{ \AA}$, $c = 8.3713(3) \text{ \AA}$, $\beta = 95.740(2)^\circ$, $V = 3270.4(2) \text{ \AA}^3$, $Z = 4$, $D_{\text{calc}} = 1.603 \text{ gcm}^{-3}$, $F(000) = 1592$, $\mu = 11.61 \text{ mm}^{-1}$, $T = 120.0(1) \text{ K}$, $\theta_{\text{max}} = 70.0^\circ$, 3203 total reflections, 2631 with $I_o > 2\sigma(I_o)$, $R_{\text{int}} = 0.034$, 3203 data, 255 parameters, 47 restraints, GooF = 1.08, $0.87 < d\Delta\rho < -1.09 \text{ e}\text{\AA}^{-3}$, $R[F^2 > 2\sigma(F^2)] = 0.051$, $wR(F^2) = 0.154$, CCDC 2255950.

Crystal data for **4c_1**: $2([\text{C}_{18}\text{H}_{24}\text{IN}_4\text{O}_2][\text{C}_7\text{H}_4\text{NO}_3\text{S}]) \cdot \text{C}_3\text{H}_6\text{O}$, M = 1333.04, colourless plate, $0.04 \times 0.14 \times 0.28 \text{ mm}$, triclinic, space group $P-1$ (No. 2), $a = 8.3294(5) \text{ \AA}$, $b = 10.2425(8) \text{ \AA}$, $c = 19.2668(15) \text{ \AA}$, $\alpha = 76.797(2)^\circ$, $\beta = 88.922(3)^\circ$, $\gamma = 66.018(4)^\circ$, $V = 1457.06(19) \text{ \AA}^3$, $Z = 1$, $D_{\text{calc}} = 1.519 \text{ gcm}^{-3}$, $F(000) = 676$, $\mu = 1.22 \text{ mm}^{-1}$, $T = 170(1) \text{ K}$, $\theta_{\text{max}} = 25.3^\circ$, 5250 total reflections, 2505 with $I_o > 2\sigma(I_o)$, $R_{\text{int}} = 0.067$, 5250 data, 349 parameters, 57 restraints, GooF = 1.04, $4.58 < d\Delta\rho < -1.03 \text{ e}\text{\AA}^{-3}$, $R[F^2 > 2\sigma(F^2)] = 0.093$, $wR(F^2) = 0.241$, CCDC 2255951.

Crystal data for **4c_2**: [C₁₈H₂₄IN₄O₂][C₇H₄NO₃S], M = 637.48, colourless plate, 0.06 × 0.25 × 0.32 mm, monoclinic, space group *C2/m*, a = 37.415(4) Å, b = 9.3673(9) Å, c = 4.1753(4) Å, β = 91.294(2)°, V = 1463.0(3) Å³, Z = 2, D_{calc} = 1.447 gcm⁻³, F(000) = 644, μ = 1.21 mm⁻¹, T = 170(1) K, θ_{max} = 25.3°, 1366 total reflections, 670 with I_o > 2σ(I_o), R_{int} = 0.096, 1366 data, 122 parameters, 63 restraints, GooF = 1.07, 0.70 < dΔρ < -1.16 eÅ⁻³, R[F² > 2σ(F²)] = 0.085, wR(F²) = 0.230, CCDC 2255952.

Crystal data for **4c_3**: [C₁₈H₂₄IN₄O₂][C₇H₄NO₃S]·CHCl₃, M = 756.85, colourless plate, 0.04 × 0.16 × 0.17 mm, triclinic, space group *P*-1 (No. 2), a = 8.3347(4) Å, b = 10.3539(5) Å, c = 19.4385(10) Å, α = 76.182(2)°, β = 87.595(3)°, γ = 66.362(2)°, V = 1489.53(13) Å³, Z = 2, D_{calc} = 1.687 gcm⁻³, F(000) = 760, μ = 1.46 mm⁻¹, T = 170(1) K, θ_{max} = 25.3°, 5391 total reflections, 3507 with I_o > 2σ(I_o), R_{int} = merged (refined as 2 component twin), 5391 data, 382 parameters, no restraints, GooF = 1.09, 1.25 < dΔρ < -1.53 eÅ⁻³, R[F² > 2σ(F²)] = 0.078, wR(F²) = 0.194, CCDC 2255953.

Crystal data for **4cd**: [C₁₉H₂₆IN₄O][C₇H₄NO₃S]·CH₂Cl₂, M = 635.51, colourless plate, 0.04 × 0.12 × 0.14 mm, triclinic, space group *P*-1 (No. 2), a = 8.3752(7) Å, b = 10.3497(8) Å, c = 19.4856(14) Å, α = 101.771(3)°, β = 92.584(2)°, γ = 113.863(3)°, V = 1496.7(2) Å³, Z = 2, D_{calc} = 1.410 gcm⁻³, F(000) = 644, μ = 1.18 mm⁻¹, T = 170(1) K, θ_{max} = 25.3°, 5383 total reflections, 1935 with I_o > 2σ(I_o), R_{int} = merged (refined as 2 component twin), 5383 data, 323 parameters, 186 restraints, GooF = 1.02, 1.46 < dΔρ < -0.78 eÅ⁻³, R[F² > 2σ(F²)] = 0.105, wR(F²) = 0.219, CCDC 2255954.

Crystal data for **4d**: [C₂₀H₂₈IN₄][C₇H₄NO₃S]·2(CH₂Cl₂), M = 803.39, colourless plate, 0.13 × 0.28 × 0.32 mm, monoclinic, space group *P2₁/c*, a = 8.7802(3) Å, b = 19.1082(7) Å, c = 20.1659(8) Å, β = 94.418(2)°, V = 3373.3(2) Å³, Z = 4, D_{calc} = 1.582 gcm⁻³, F(000) = 1624, μ = 1.37 mm⁻¹, T = 120.0(1) K, θ_{max} = 26.3°, 6800 total reflections, 5312 with I_o > 2σ(I_o), R_{int} = 0.042, 6800 data, 398 parameters, 27 restraints, GooF = 1.05, 1.57 < dΔρ < -1.80 eÅ⁻³, R[F² > 2σ(F²)] = 0.046, wR(F²) = 0.115, CCDC 2255955.

Crystal data for **8**: C₈H₁₀IN, M = 247.07, colourless plate, 0.04 × 0.11 × 0.27 mm, orthorhombic, space group *Iba2*, a = 22.1896(17) Å, b = 15.5327(11) Å, c = 4.9667(5) Å, V = 1711.8(2) Å³, Z = 8, D_{calc} = 1.917 gcm⁻³, F(000) = 944, μ = 3.67 mm⁻¹, T = 120.0(1) K, θ_{max} = 25.2°, 1539 total reflections, 1084 with I_o > 2σ(I_o), R_{int} = 0.129, 1539 data, 93 parameters, 40 restraints, GooF = 1.03, 2.30 < dΔρ < -0.89 eÅ⁻³, R[F² > 2σ(F²)] = 0.051, wR(F²) = 0.124, CCDC 2255956. Compound **8** was obtained for a test iodination reaction of 2,4-xylylidine with Barluenga's reagent. A 10 mL screw cap vial equipped with a magnetic stirring bar was charged with 2,4-xylylidine (24.2 mg, 0.2 mmol, 1.00 equiv.), which was dissolved in DCM (0.5 mL). Then, Barluenga's reagent (0.20 mmol, 1.00 equiv.) was added, and the reaction mixture was stirred for 15 min at rt. It was separated between DCM and water (each 20 mL) and aq. sat. Na₂S₂O₃ solution (10 mL) were added. After phase separation, the organic phase was dried over Na₂SO₄, and the product was purified by column chromatography. For further details, see Section 7.2.3 Iodinated Products.

Crystal data for [(MPYH)NSac_1]: [C₉H₁₃N₂O][C₇H₄NO₃S], M = 347.38, colourless block, 0.35 × 0.38 × 0.38 mm, monoclinic, space group *P*₂₁/*n*, a = 13.5609(16) Å, b = 8.0439(9) Å, c = 14.5581(18) Å, β = 98.598(2)°, V = 1570.2(3) Å³, Z = 4, D_{calc} = 1.469 gcm⁻³, F(000) = 728, μ = 0.23 mm⁻¹, T = 120.0(1) K, θ_{max} = 26.3°, 3114 total reflections, 2174 with I_o > 2σ(I_o), R_{int} = 0.045, 6800 data, 263 parameters, 72 restraints, GooF = 1.03, 0.40 < dΔρ < -0.65 eÅ⁻³, R[F² > 2σ(F²)] = 0.076, wR(F²) = 0.167, CCDC 2255957.

Crystal data for [(MPYH)NSac_2]: [C₉H₁₃N₂O][C₇H₄NO₃S], M = 347.38, colourless block, 0.40 × 0.40 × 0.45 mm, monoclinic, space group *P*₂₁, a = 9.8114(3) Å, b = 7.9038(2) Å, c = 10.9507(3) Å, β = 105.784(2)°, V = 817.18(4) Å³, Z = 2, D_{calc} = 1.412 gcm⁻³, F(000) = 364, μ = 0.22 mm⁻¹, T = 120.0(1) K, θ_{max} = 26.3°, 3284 total reflections, 3100 with I_o > 2σ(I_o), R_{int} = 0.026, 3284 data, 217 parameters, 1 restraint, GooF = 1.05, 0.21 < dΔρ < -0.28 eÅ⁻³, R[F² > 2σ(F²)] = 0.035, wR(F²) = 0.078, CCDC 2255958.

Crystal data for [(MPYH)NSac_3]: [C₉H₁₃N₂O][C₇H₄NO₃S], M = 347.38, colourless plate, 0.07 × 0.21 × 0.27 mm, triclinic, space group *P*-1 (No. 2), a = 8.0402(6) Å, b = 13.5547(9) Å, c = 14.5596(11) Å, α = 98.518(3)°, β = 91.675(2)°, γ = 91.455(2)°, V = 1567.9(2) Å³, Z = 4, D_{calc} = 1.472 gcm⁻³, F(000) = 728, μ = 0.23 mm⁻¹, T = 120.0(1) K, θ_{max} = 26.3°, 6297 total reflections, 2853 with I_o > 2σ(I_o), R_{int} = 0.086, 6297 data, 433 parameters, no restraints, GooF = 1.02, 1.00 < dΔρ < -0.44 eÅ⁻³, R[F² > 2σ(F²)] = 0.109, wR(F²) = 0.271, CCDC 2255959.

Crystal data for [(PiPYH)I₃]: [C₂₀H₂₉N₄]I₃, M = 706.17, orange block, 0.20 × 0.20 × 0.23 mm, triclinic, space group *P*-1 (No. 2), a = 13.1946(7) Å, b = 15.4088(10) Å, c = 19.6477(14) Å, α = 71.888(2)°, β = 80.519(3)°, γ = 70.237(2)°, V = 3565.1(4) Å³, Z = 6, D_{calc} = 1.973 gcm⁻³, F(000) = 2016, μ = 3.96 mm⁻¹, T = 120.0(1) K, θ_{max} = 26.3°, 14353 total reflections, 7527 with I_o > 2σ(I_o), R_{int} = 0.079, 14353 data, 730 parameters, 144 restraints, GooF = 1.00, 1.65 < dΔρ < -1.71 eÅ⁻³, R[F² > 2σ(F²)] = 0.059, wR(F²) = 0.125, CCDC 2255960.

Crystal data for [(PPYH)I]: [C₉H₁₃N₂]I, M = 276.11, colourless needle, 0.13 × 0.13 × 0.43 mm, monoclinic, space group *P*₂₁/*c*, a = 7.3437(3) Å, b = 15.2166(6) Å, c = 18.5687(7) Å, β = 95.139(2)°, V = 2066.64(14) Å³, Z = 8, D_{calc} = 1.775 gcm⁻³, F(000) = 1072, μ = 3.05 mm⁻¹, T = 120.0(1) K, θ_{max} = 26.2°, 4148 total reflections, 3017 with I_o > 2σ(I_o), R_{int} = 0.047, 4148 data, 217 parameters, no restraints, GooF = 1.05, 1.40 < dΔρ < -1.05 eÅ⁻³, R[F² > 2σ(F²)] = 0.049, wR(F²) = 0.092, CCDC 2255961.

Crystal data for [(PPYH)NSac_1]: [C₉H₁₃N₂][C₇H₄NO₃S], M = 331.38, colourless plate, 0.08 × 0.22 × 0.23 mm, monoclinic, space group *P*₂₁/*c*, a = 7.4609(6) Å, b = 13.0907(14) Å, c = 15.3663(17) Å, β = 92.576(3)°, V = 1499.3(3) Å³, Z = 4, D_{calc} = 1.468 gcm⁻³, F(000) = 696, μ = 0.24 mm⁻¹, T = 120.0(1) K, θ_{max} = 26.3°, 3013 total reflections, 1613 with I_o > 2σ(I_o), R_{int} = 0.106, 3013 data, 208 parameters, 18

restraints, GooF = 1.01, $0.74 < d\Delta\rho < -0.54 \text{ e}\text{\AA}^{-3}$, $R[F^2 > 2\sigma(F^2)] = 0.087$, $wR(F^2) = 0.206$, CCDC 2255962.

Crystal data for [(PPYH)NSac_2]: $[\text{C}_9\text{H}_{13}\text{N}_2][\text{C}_7\text{H}_4\text{NO}_3\text{S}]$, $M = 331.38$, colourless plate, $0.04 \times 0.17 \times 0.17 \text{ mm}$, monoclinic, space group $P2_1/n$, $a = 8.0985(3) \text{ \AA}$, $b = 8.1635(3) \text{ \AA}$, $c = 23.2286(8) \text{ \AA}$, $\beta = 93.541(3)^\circ$, $V = 1532.76(10) \text{ \AA}^3$, $Z = 4$, $D_{\text{calc}} = 1.436 \text{ gcm}^{-3}$, $F(000) = 696$, $\mu = 2.05 \text{ mm}^{-1}$, $T = 120.0(1) \text{ K}$, $\theta_{\text{max}} = 70.0^\circ$, 2886 total reflections, 2103 with $I_o > 2\sigma(I_o)$, $R_{\text{int}} =$ merged (refined as 2 component twin), 2886 data, 209 parameters, no restraints, GooF = 1.09, $0.79 < d\Delta\rho < -0.70 \text{ e}\text{\AA}^{-3}$, $R[F^2 > 2\sigma(F^2)] = 0.087$, $wR(F^2) = 0.215$, CCDC 2255963.

Crystal data for [(DMAP)₂I₃_1]: $[\text{C}_{14}\text{H}_{20}\text{IN}_4]\text{I}_3 \cdot \text{CH}_2\text{Cl}_2$, $M = 836.86$, orange block, $0.17 \times 0.25 \times 0.26 \text{ mm}$, monoclinic, space group $P2_1/m$, $a = 9.7430(4) \text{ \AA}$, $b = 9.7275(5) \text{ \AA}$, $c = 12.9505(7) \text{ \AA}$, $\beta = 94.585(2)^\circ$, $V = 1223.46(10) \text{ \AA}^3$, $Z = 2$, $D_{\text{calc}} = 2.272 \text{ gcm}^{-3}$, $F(000) = 772$, $\mu = 5.32 \text{ mm}^{-1}$, $T = 170(1) \text{ K}$, $\theta_{\text{max}} = 26.3^\circ$, 2599 total reflections, 1973 with $I_o > 2\sigma(I_o)$, $R_{\text{int}} = 0.041$, 2599 data, 132 parameters, 21 restraints, GooF = 1.06, $1.47 < d\Delta\rho < -1.19 \text{ e}\text{\AA}^{-3}$, $R[F^2 > 2\sigma(F^2)] = 0.047$, $wR(F^2) = 0.101$, CCDC 2255965.

Crystal data for [(DMAP)₂I₃_2]: $[\text{C}_{14}\text{H}_{20}\text{IN}_4]\text{I}_3$, $M = 751.94$, orange plate, $0.10 \times 0.28 \times 0.32 \text{ mm}$, triclinic, space group $P-1$ (No. 2), $a = 7.9392(6) \text{ \AA}$, $b = 7.9371(7) \text{ \AA}$, $c = 9.4443(9) \text{ \AA}$, $\alpha = 110.712(3)^\circ$, $\beta = 91.993(2)^\circ$, $\gamma = 103.844(3)^\circ$, $V = 535.80(8) \text{ \AA}^3$, $Z = 1$, $D_{\text{calc}} = 2.330 \text{ gcm}^{-3}$, $F(000) = 344$, $\mu = 5.82 \text{ mm}^{-1}$, $T = 170(1) \text{ K}$, $\theta_{\text{max}} = 26.2^\circ$, 2155 total reflections, 1866 with $I_o > 2\sigma(I_o)$, $R_{\text{int}} = 0.034$, 2155 data, 105 parameters, no restraints, GooF = 1.03, $1.51 < d\Delta\rho < -1.54 \text{ e}\text{\AA}^{-3}$, $R[F^2 > 2\sigma(F^2)] = 0.038$, $wR(F^2) = 0.087$, CCDC 2255964.

3.2 Displacement Ellipsoid Plots and Crystal Packing

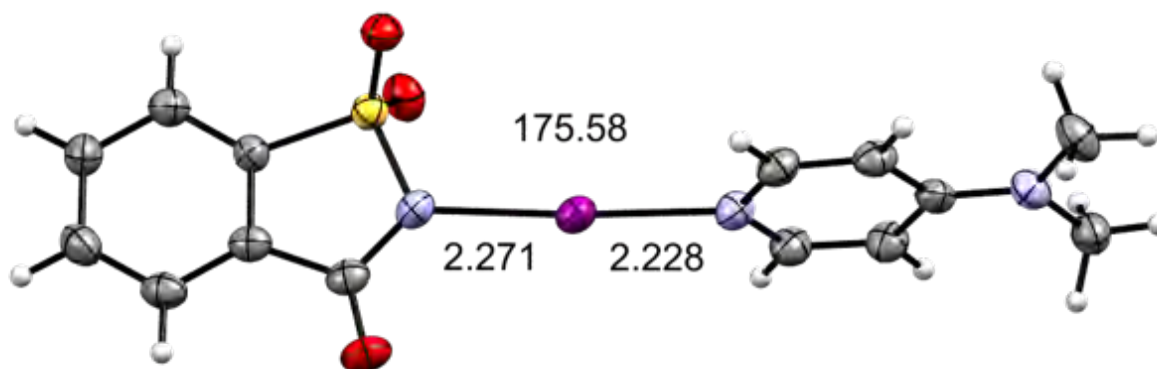


Figure S3. Displacement ellipsoid plot of XB complex **3a**. Displacement ellipsoids are drawn at the 50% probability level. Distances are given in \AA and angles in degrees.

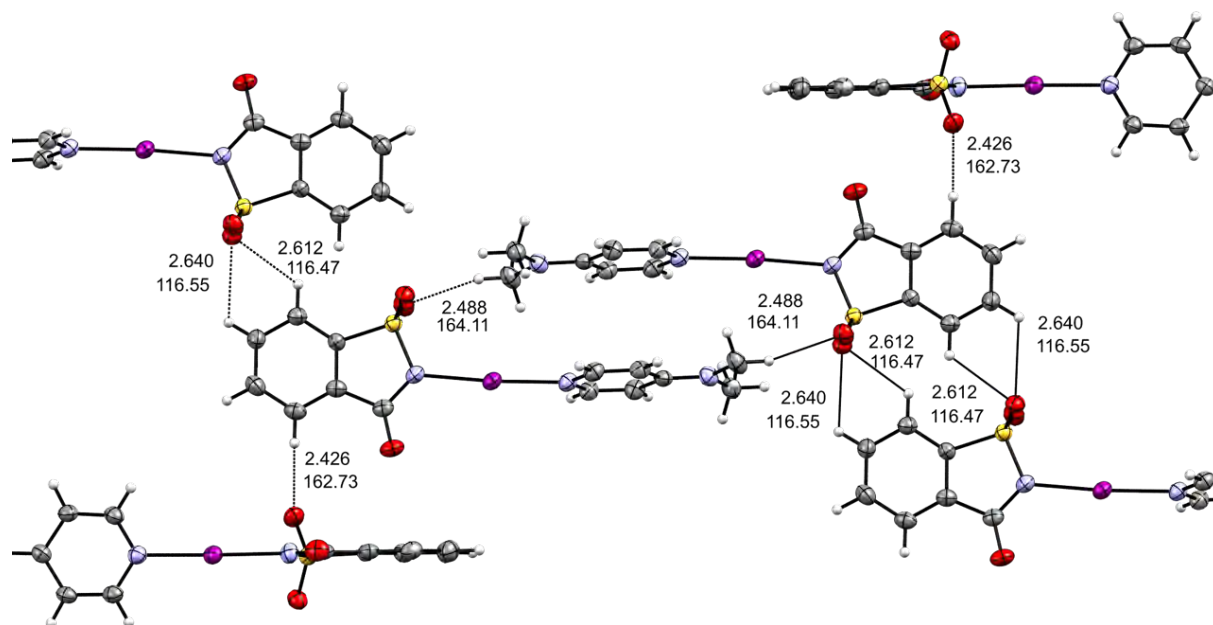


Figure S4. Cut-out of the crystal packing of XB complex **3a** with selected secondary interactions. Ellipsoids are shown at 50% probability value. Distances are given in Å and angles in degrees.

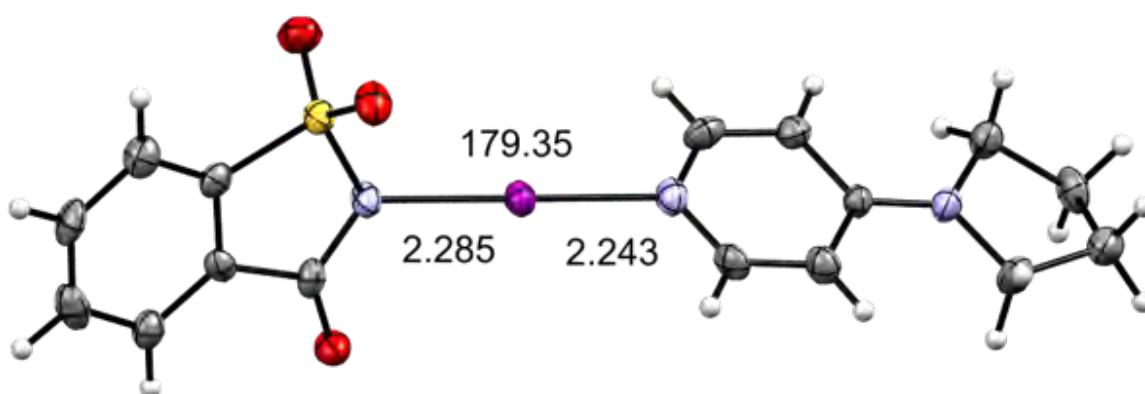


Figure S5. Displacement ellipsoid plot of XB complex **3b**. Displacement ellipsoids are drawn at the 50% probability level. Distances are given in Å and angles in degrees.

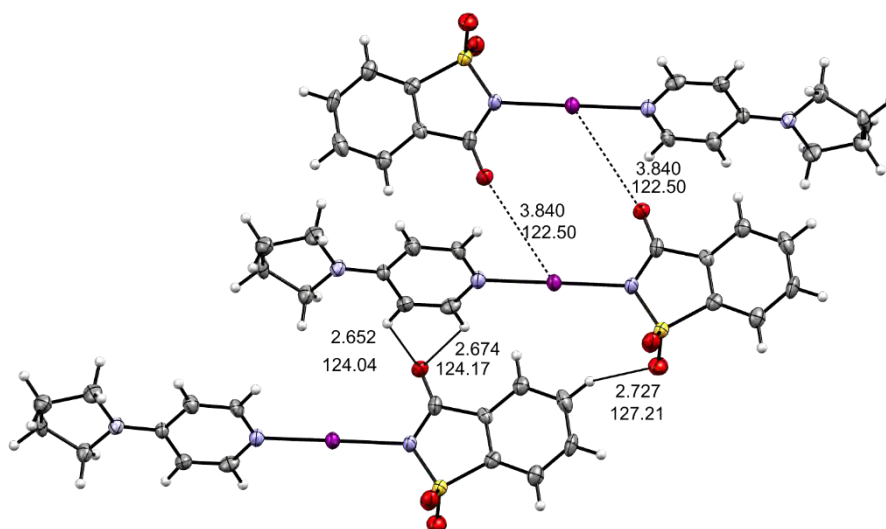


Figure S6. Cut-out of the crystal packing of XB complex **3b** with selected secondary interactions. Ellipsoids are shown at 50% probability value. Distances are given in Å and angles in degrees.

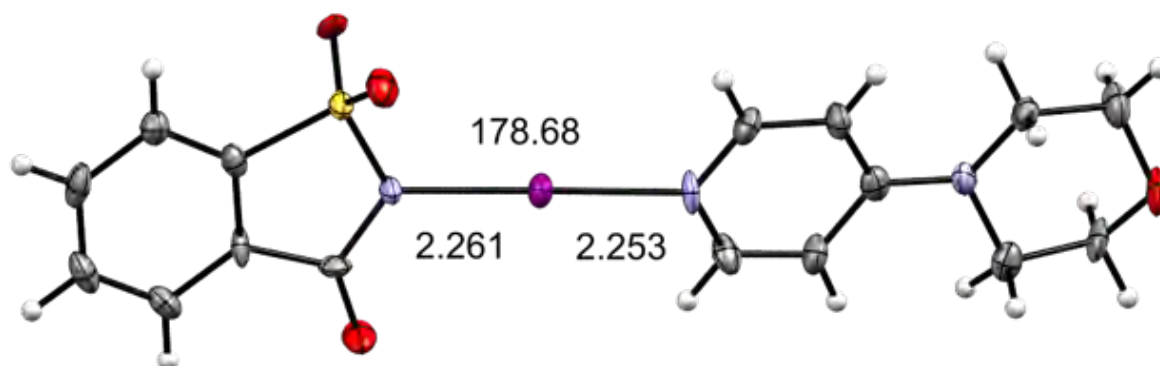


Figure S7. Displacement ellipsoid plot of XB complex **3c**. Displacement ellipsoids are drawn at the 50% probability level. Distances are given in Å and angles in degrees.

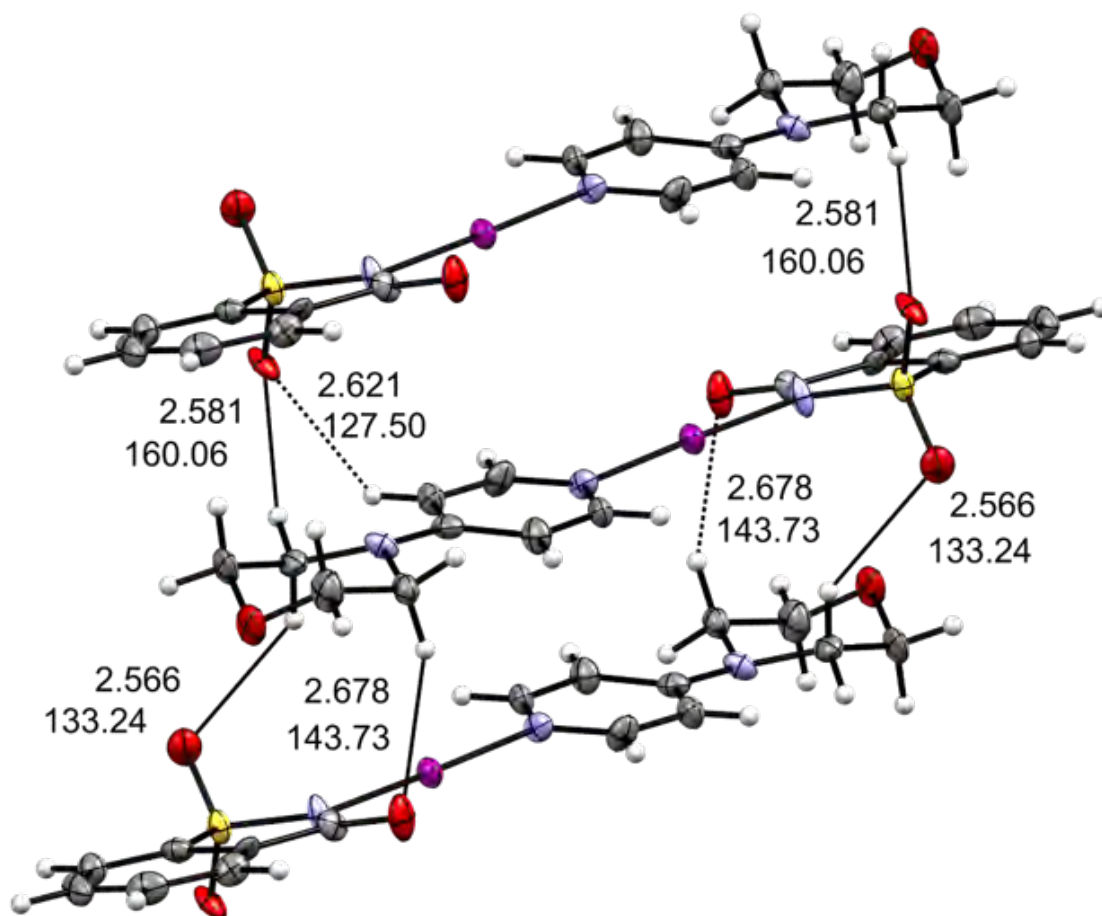


Figure S8. Cut-out of the crystal packing of XB complex **3c** with selected secondary interactions. Ellipsoids are shown at 50% probability value. Distances are given in Å and angles in degrees.

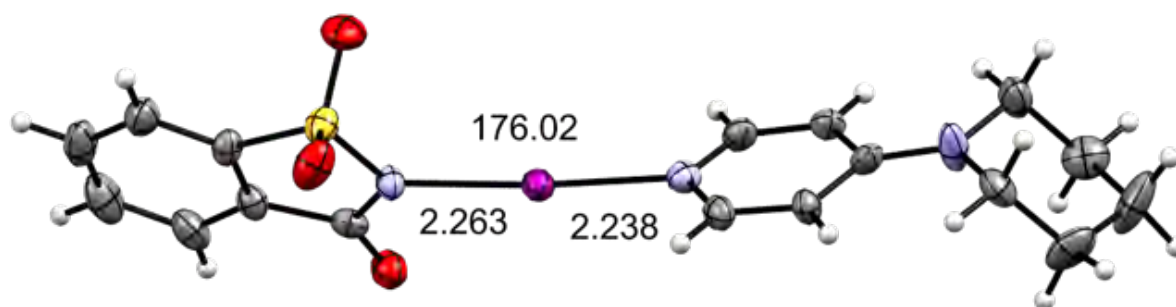


Figure S9. Displacement ellipsoid plot of XB complex **3d**. Displacement ellipsoids are drawn at the 50% probability level. Distances are given in Å and angles in degrees.

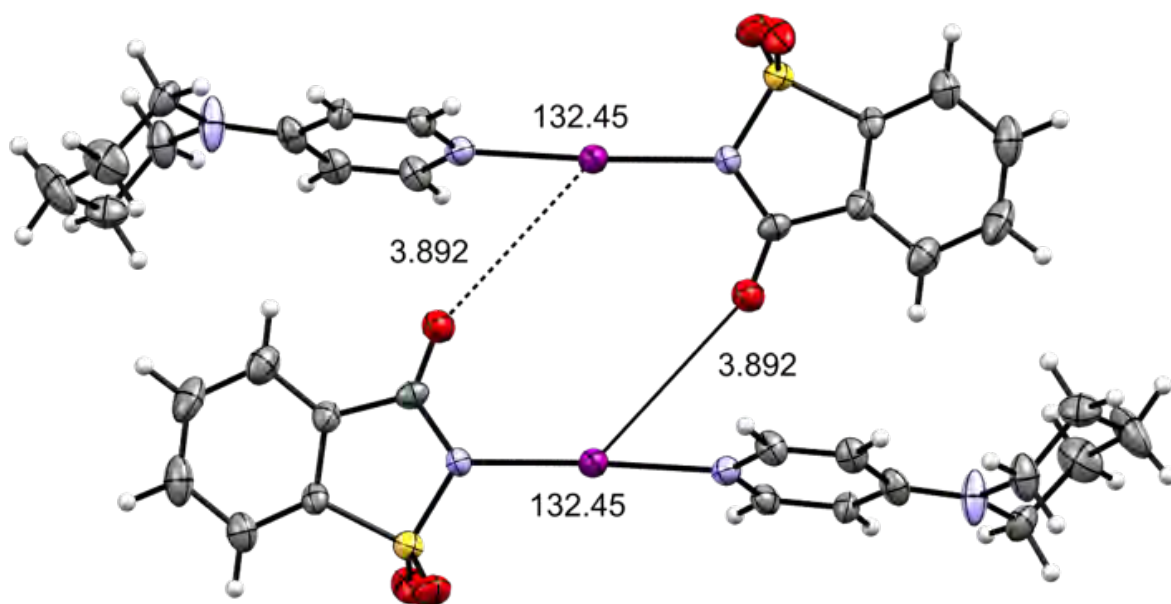


Figure S10. Cut-out of the crystal packing of XB complex **3d** with selected secondary interactions. Ellipsoids are shown at 50% probability value. Distances are given in Å and angles in degrees.

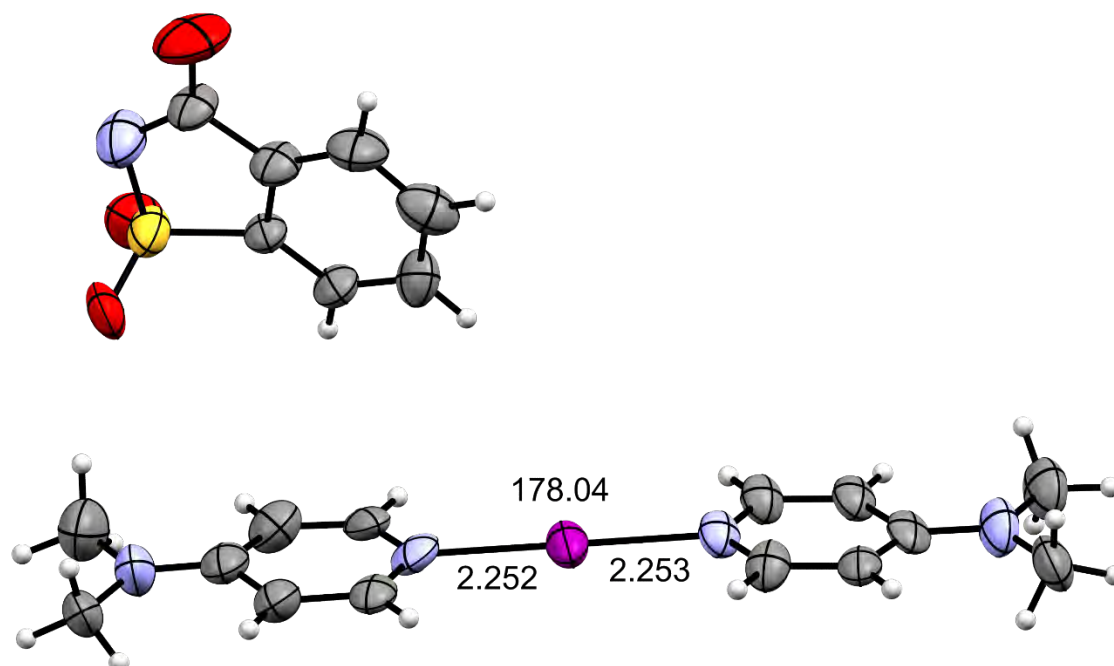


Figure S11. Displacement ellipsoid plot of symmetric iodine(I) complex **4a_1** (minor disordered positions omitted for clarity). Displacement ellipsoids are drawn at the 50% probability level. Distances are given in Å and angles in degrees.

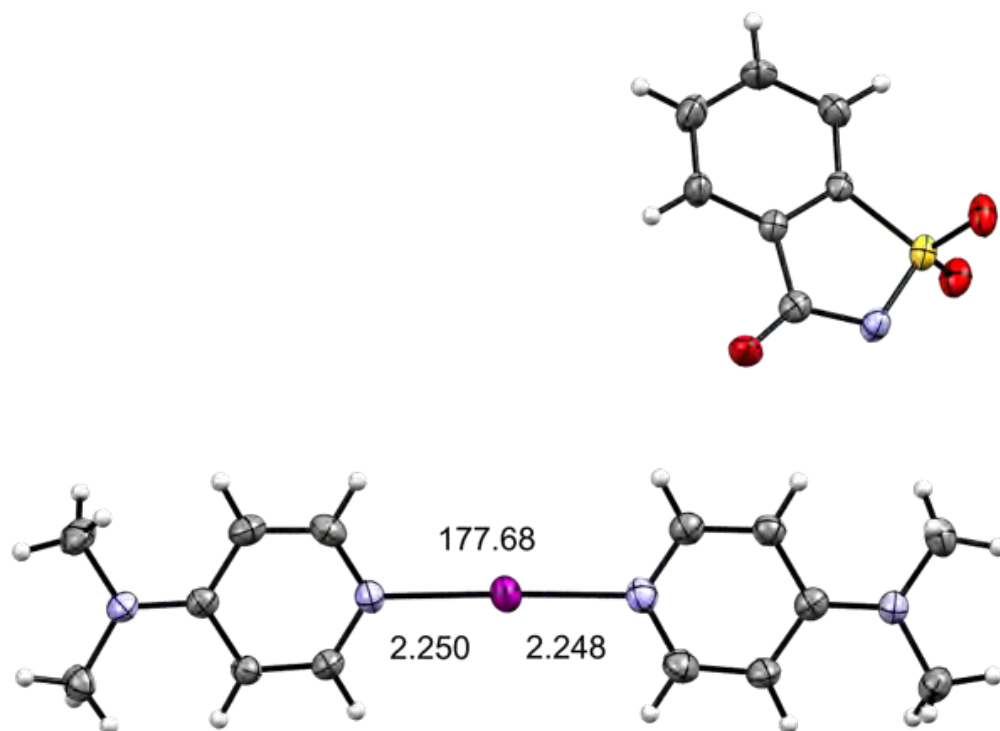


Figure S12. Displacement ellipsoid plot of symmetric iodine(I) complex **4a_2**. Displacement ellipsoids are drawn at the 50% probability level. Distances are given in Å and angles in degrees.

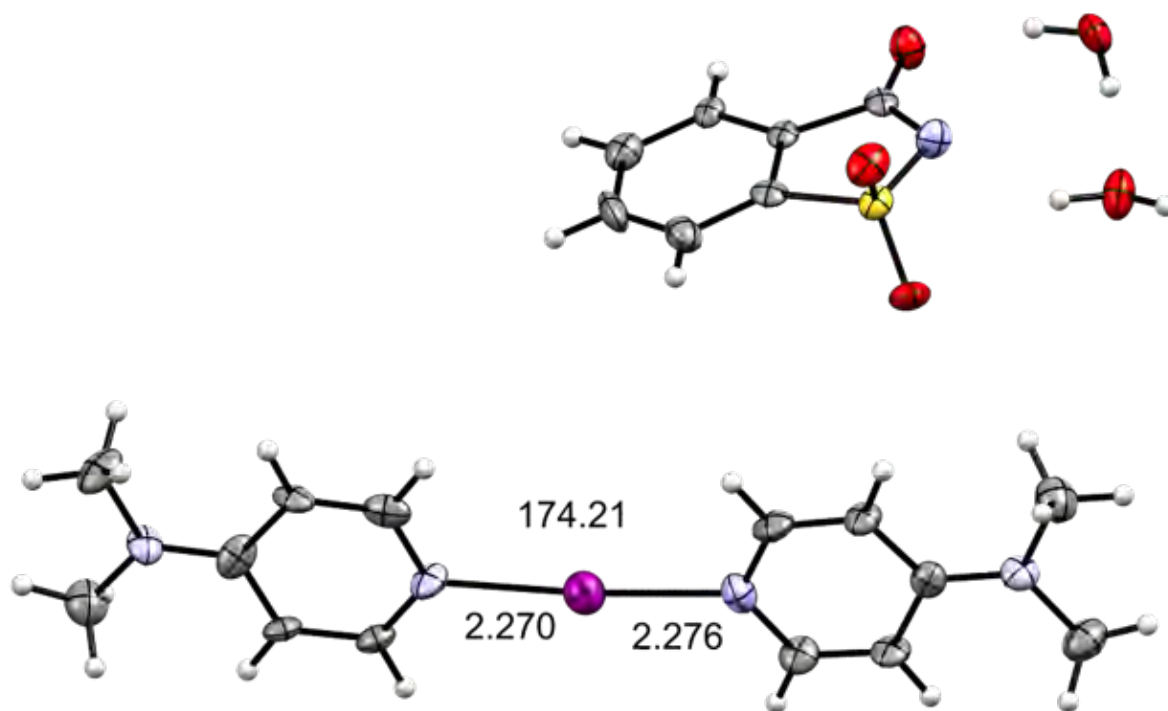


Figure S13. Displacement ellipsoid plot of symmetric iodine(I) complex **4a·H₂O**. Displacement ellipsoids are drawn at the 50% probability level. Distances are given in Å and angles in degrees.

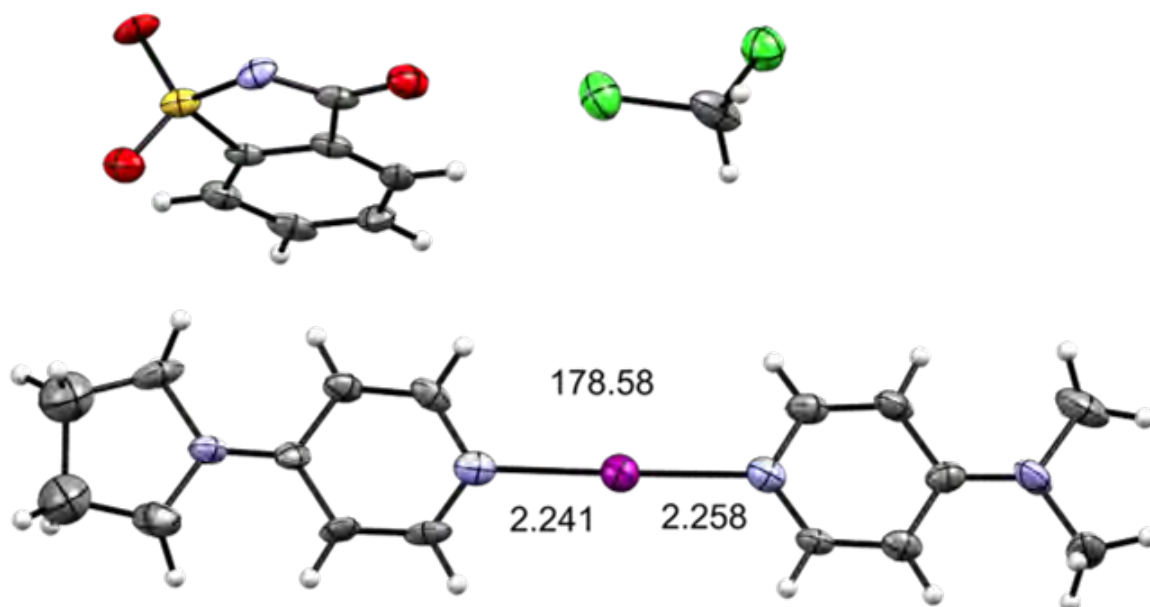


Figure S14. Displacement ellipsoid plot of asymmetric iodine(I) complex **4ab**. Displacement ellipsoids are drawn at the 50% probability level. Distances are given in Å and angles in degrees.

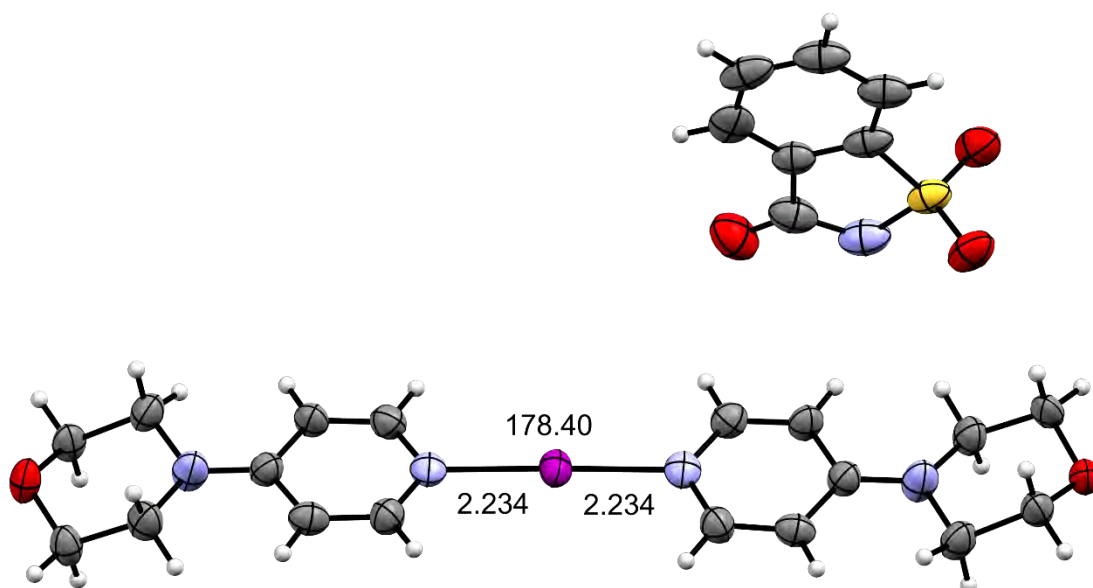


Figure S15. Displacement ellipsoid plot of asymmetric iodine(I) complex **4ac** (minor disordered positions omitted for clarity). Displacement ellipsoids are drawn at the 50% probability level. Distances are given in Å and angles in degrees.

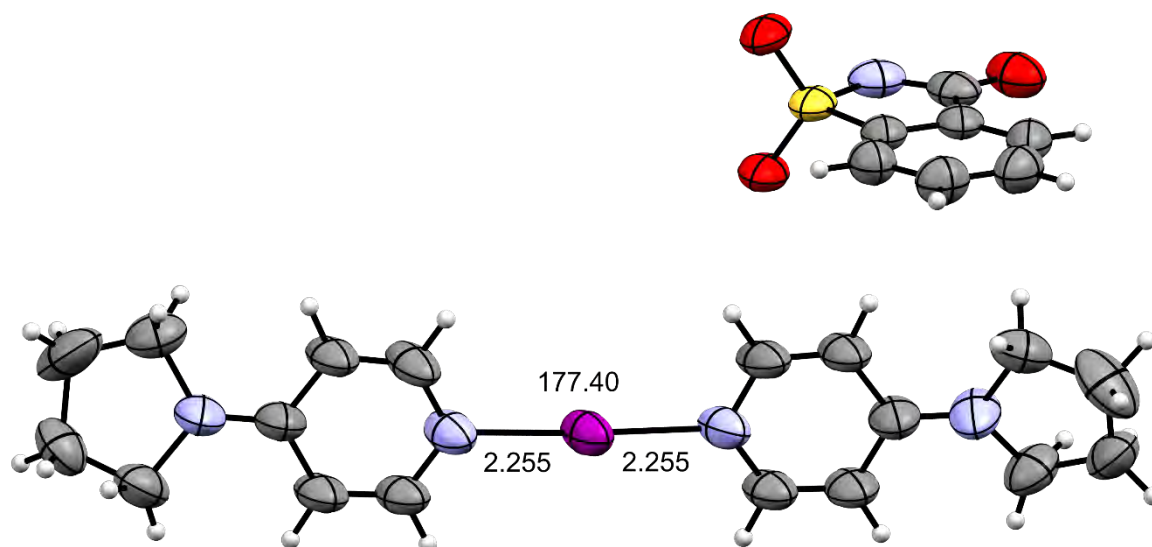


Figure S16. Displacement ellipsoid plot of asymmetric iodine(I) complex **4bd** (minor disordered positions omitted for clarity). Displacement ellipsoids are drawn at the 50% probability level. Distances are given in Å and angles in degrees.

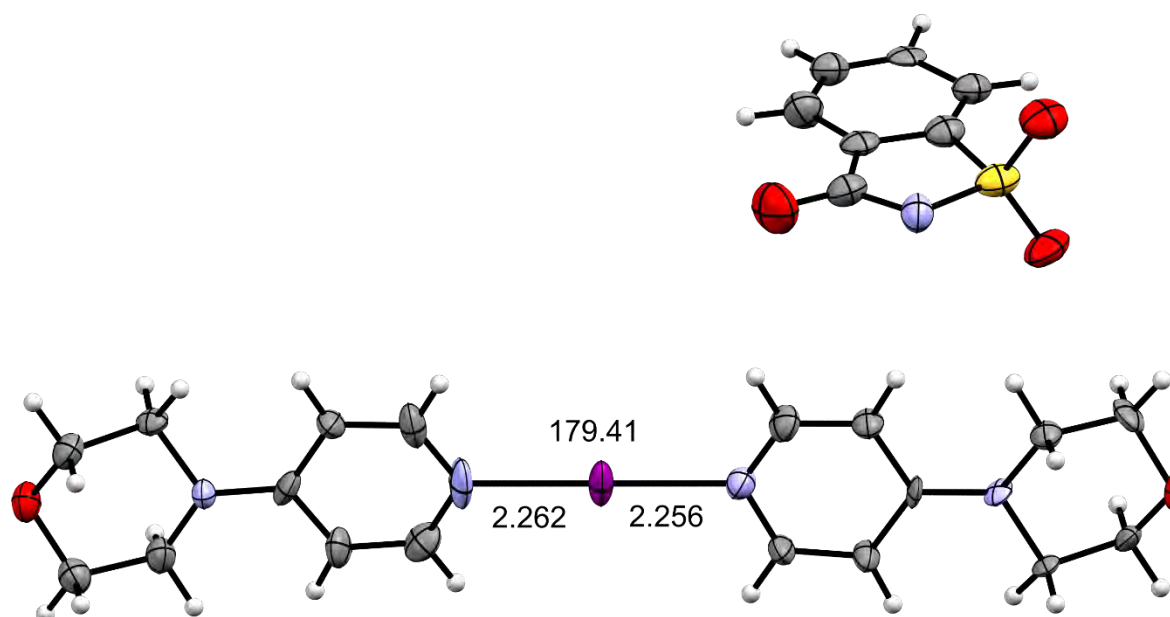


Figure S17. Displacement ellipsoid plot of symmetric iodine(I) complex **4c_1** (solvate omitted for clarity). Displacement ellipsoids are drawn at the 50% probability level. Distances are given in Å and angles in degrees.

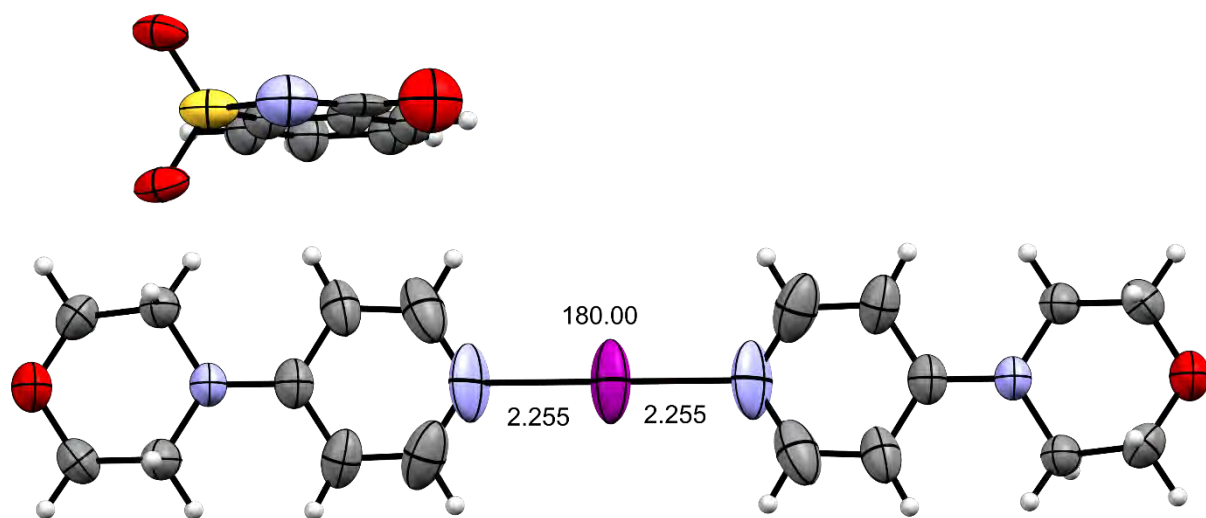


Figure S18. Displacement ellipsoid plot of the symmetric iodine(I) complex **4c_2** (minor disordered positions omitted for clarity). Displacement ellipsoids are drawn at the 50% probability level. Distances are given in Å and angles in degrees.

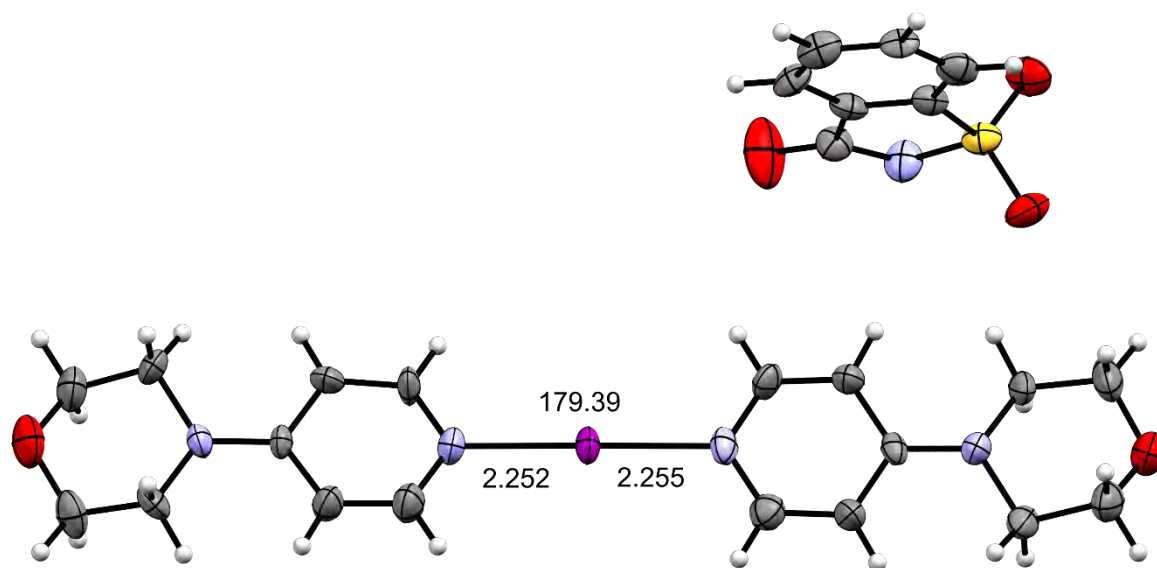


Figure S19. Displacement ellipsoid plot of the symmetric iodine(I) complex **4c_3** (solvate omitted for clarity). Displacement ellipsoids are drawn at the 50% probability level. Distances are given in Å and angles in degrees.

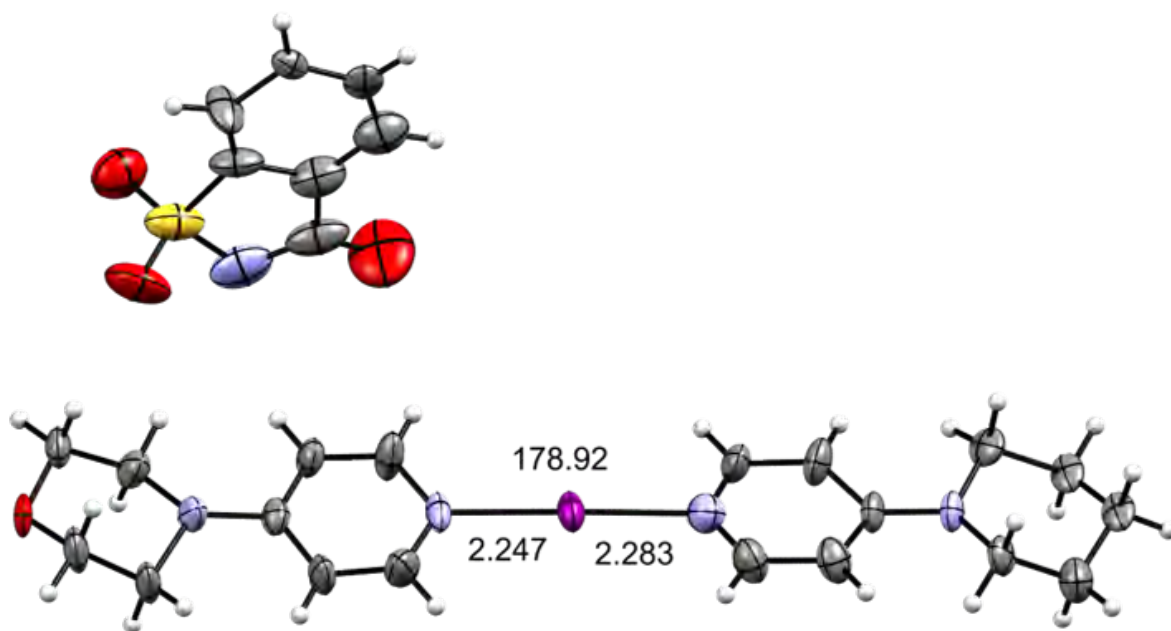


Figure S20. Displacement ellipsoid plot of asymmetric iodine(I) complex **4cd**. Displacement ellipsoids are drawn at the 50% probability level. Distances are given in Å and angles in degrees.

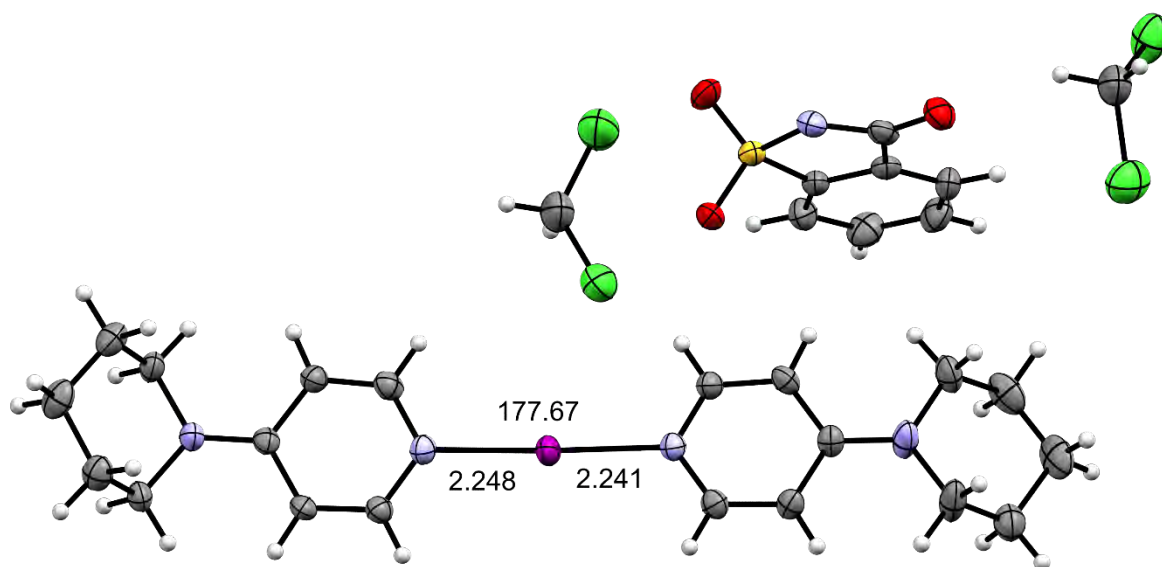


Figure S21. Displacement ellipsoid plot of symmetric iodine(I) complex **4d** (minor disordered solvate positions omitted for clarity). Displacement ellipsoids are drawn at the 50% probability level. Distances are given in Å and angles in degrees.

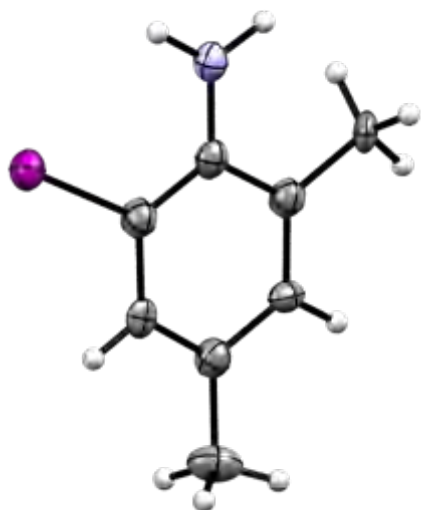


Figure S22. Displacement ellipsoid plot of 2-iodo-4,6-dimethylaniline (**8**). Displacement ellipsoids are drawn at the 50% probability level.

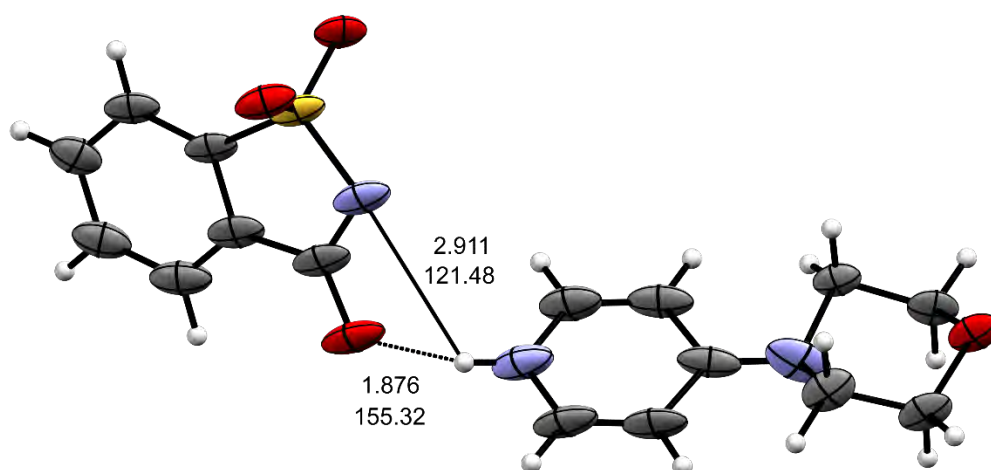


Figure S23. Displacement ellipsoid plot of the decomposition product [(MPYH)NSac]₁ (minor disordered positions omitted for clarity). Displacement ellipsoids are drawn at the 50% probability level. Distances are given in Å and angles in degrees.

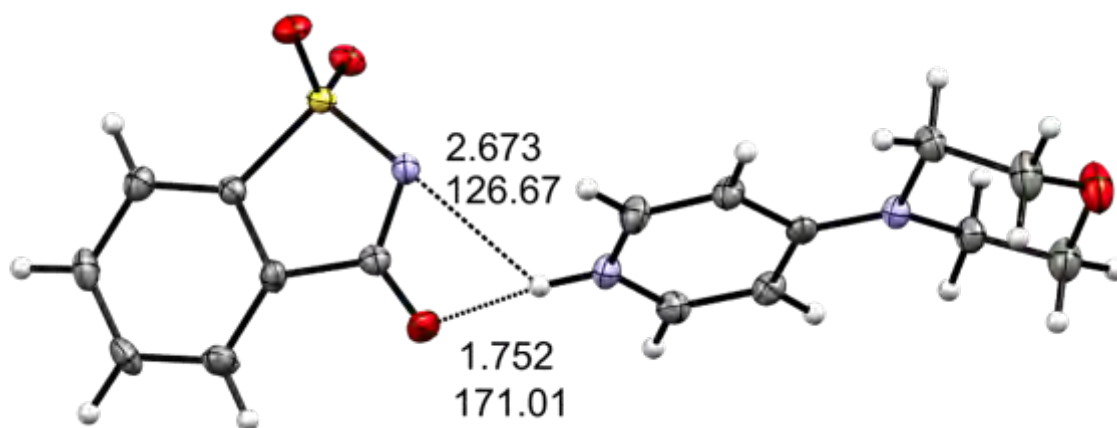


Figure S24. Displacement ellipsoid plot of the decomposition product [(MPYH)NSac]₂. Displacement ellipsoids are drawn at the 50% probability level. Distances are given in Å and angles in degrees.

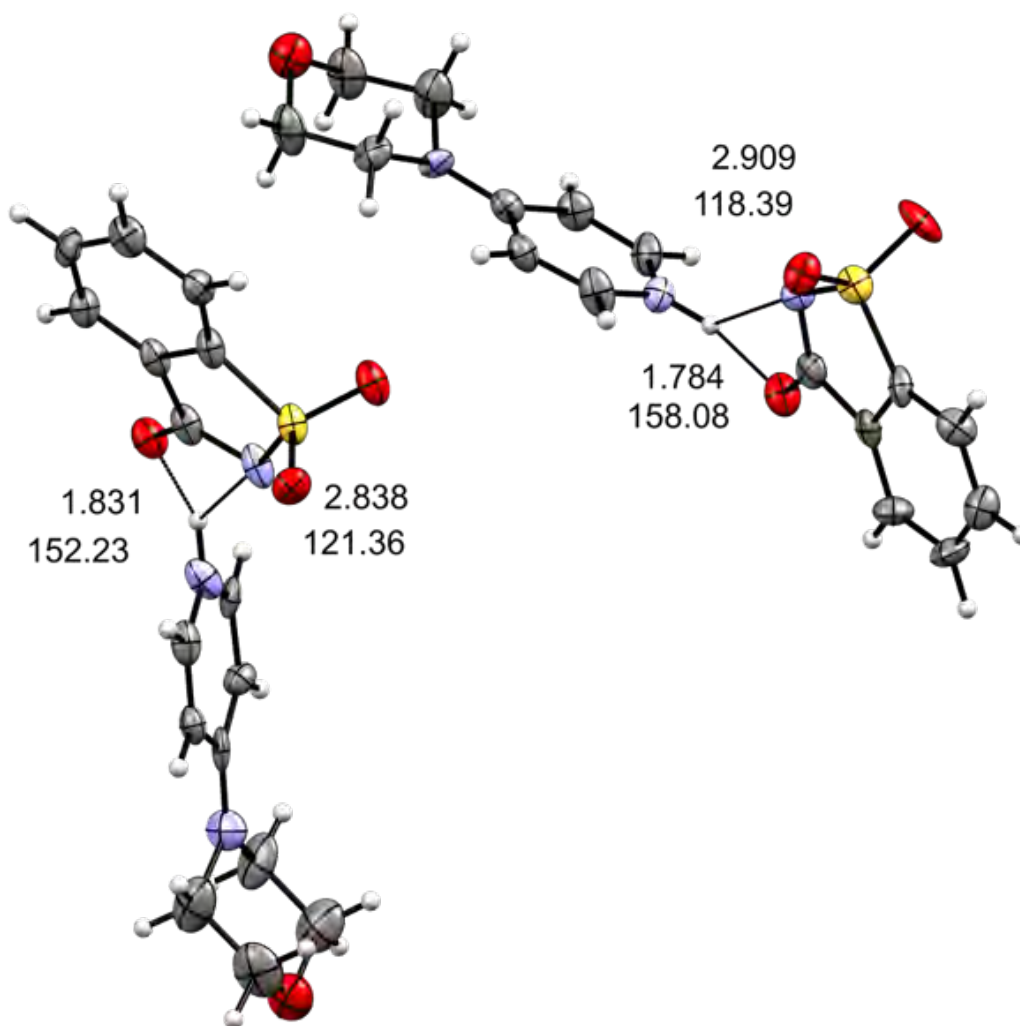


Figure S25. Displacement ellipsoid plot of the decomposition product [(MPYH)NSac]₃. Displacement ellipsoids are drawn at the 50% probability level. Distances are given in Å and angles in degrees.

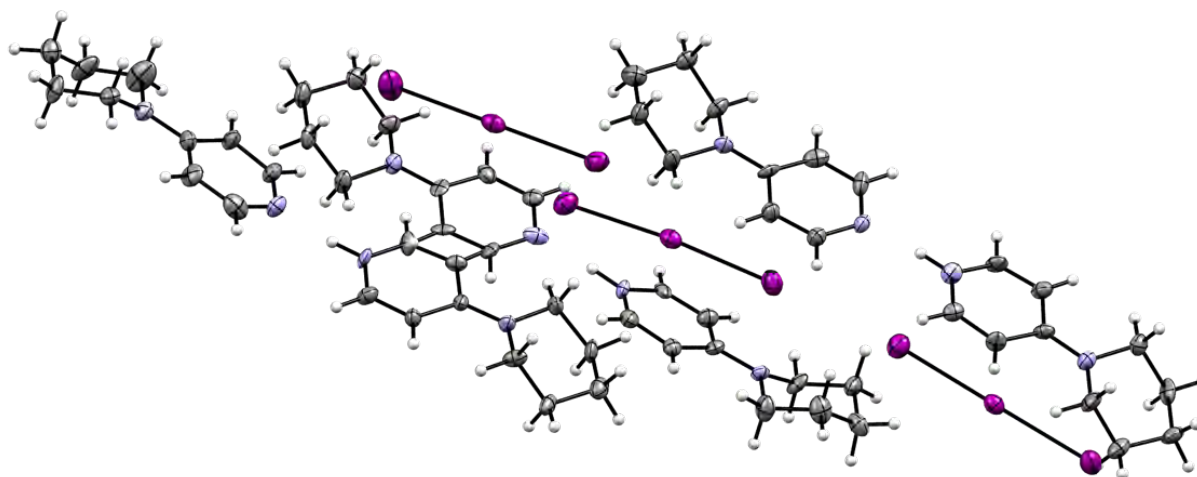


Figure S26. Displacement ellipsoid plot of the decomposition product $[(\text{PiPYH})\text{I}_3]$. Displacement ellipsoids are drawn at the 50% probability level. Distances are given in Å and angles in degrees.

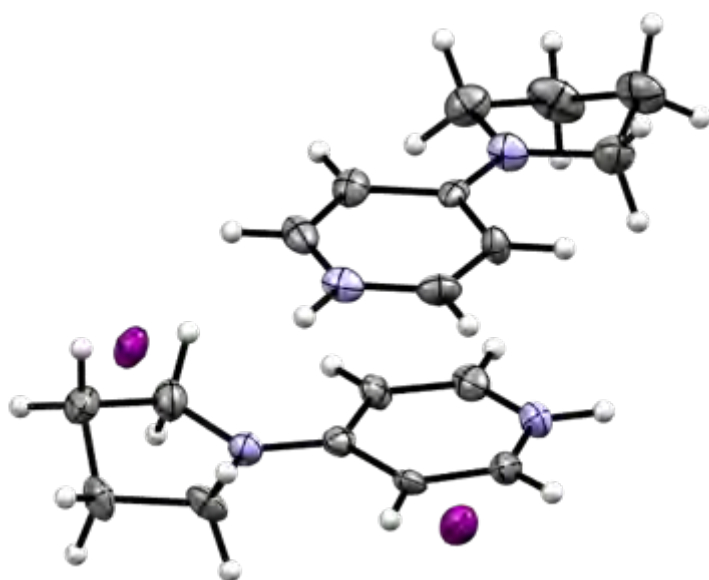


Figure S27. Displacement ellipsoid plot of the decomposition product $[(\text{PPYH})\text{I}]$. Displacement ellipsoids are drawn at the 50% probability level. Distances are given in Å and angles in degrees.

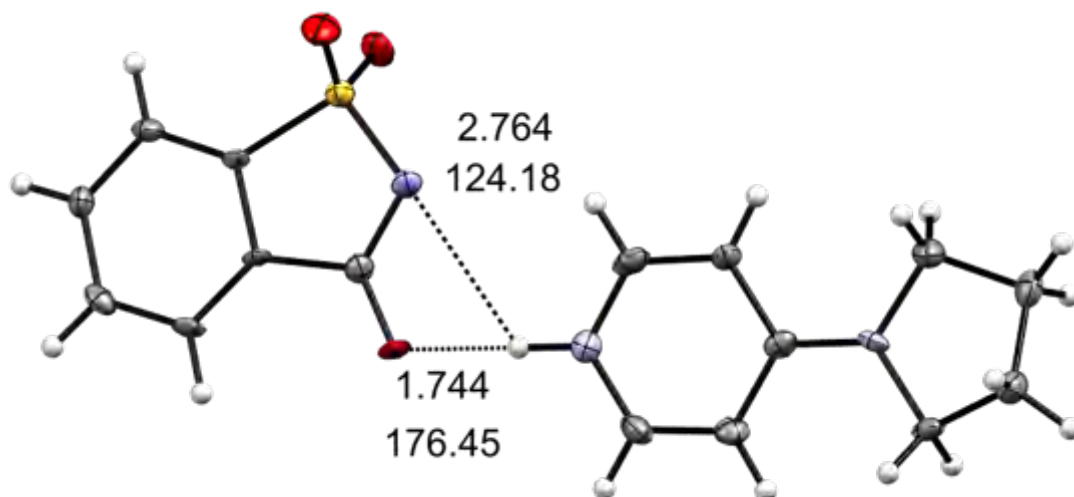


Figure S28. Displacement ellipsoid plot of the decomposition product [(PPYH)NSac]₁. Displacement ellipsoids are drawn at the 50% probability level. Distances are given in Å and angles in degrees.

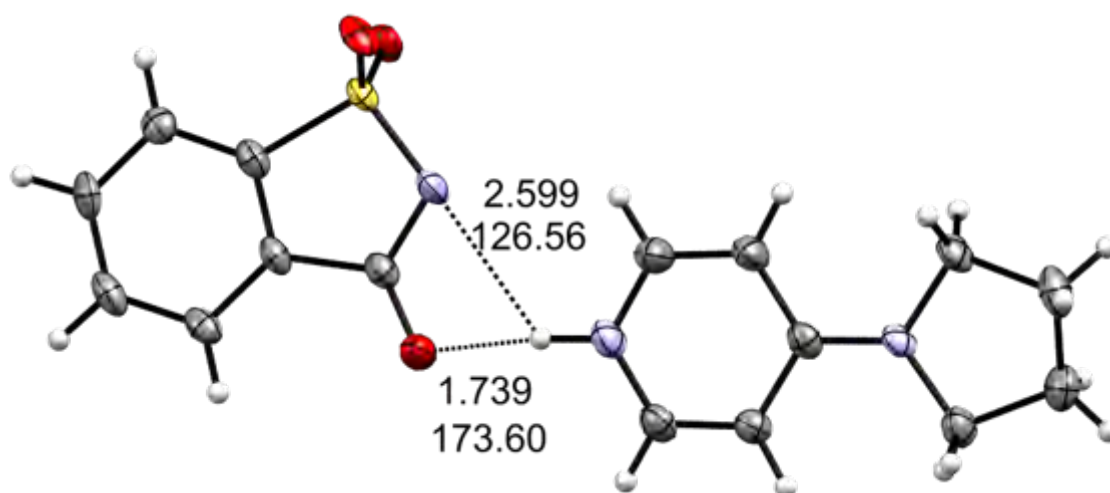


Figure S29. Displacement ellipsoid plot of the decomposition product [(PPYH)NSac]₂. Displacement ellipsoids are drawn at the 50% probability level. Distances are given in Å and angles in degrees.

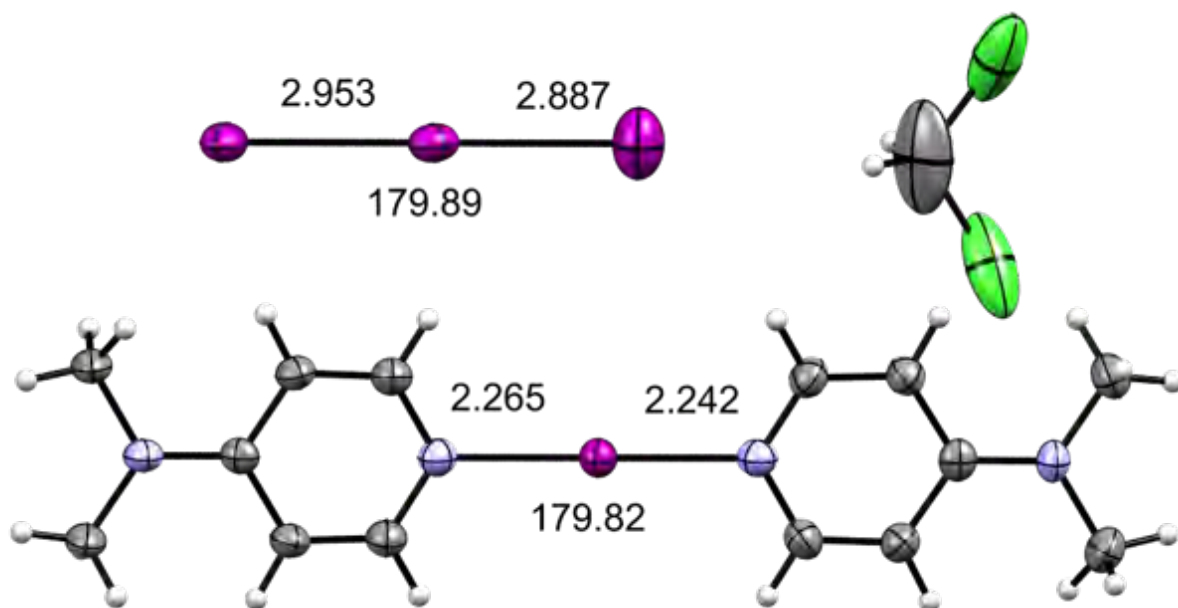


Figure S30. Displacement ellipsoid plot of $[(\text{DMAP})_2\text{I}]_3_1$. Displacement ellipsoids are drawn at the 50% probability level. Distances are given in Å and angles in degrees.

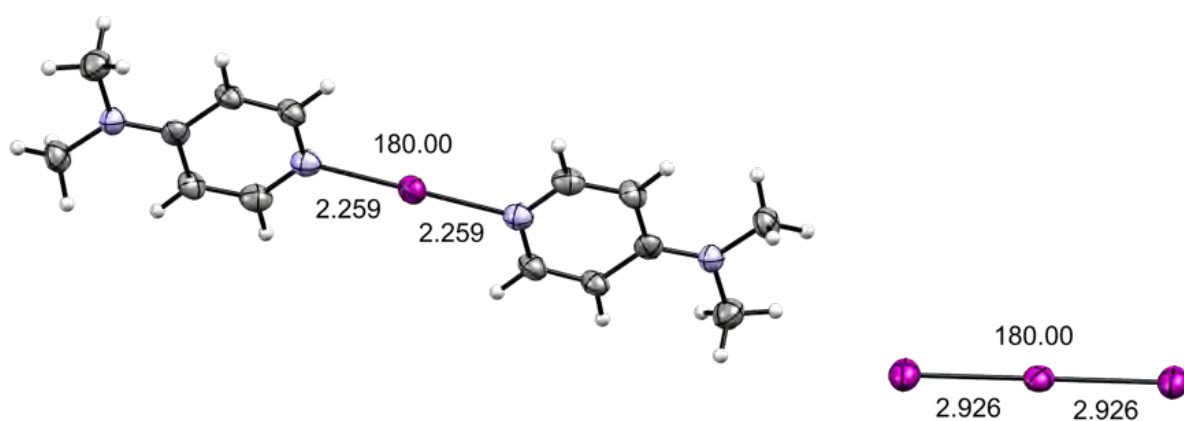


Figure S31. Displacement ellipsoid plot of $[(\text{DMAP})_2\text{I}]_3_2$. Displacement ellipsoids are drawn at the 50% probability level. Distances are given in Å and angles in degrees.

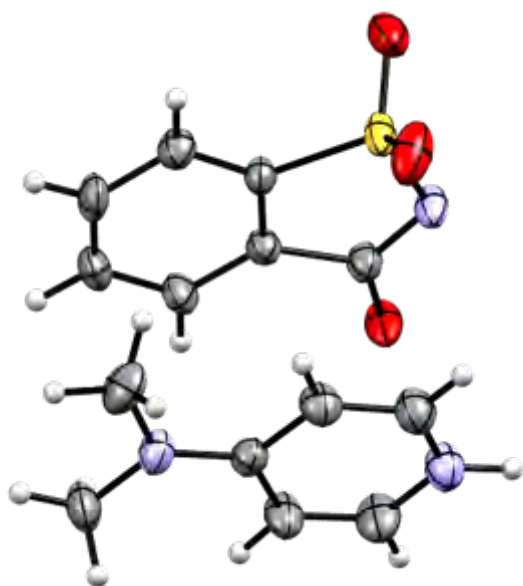


Figure S32. X-ray crystal structures of [DMAPHNSac] (CCDC817088).^{4,5}

4 IR Ex-Situ Analysis

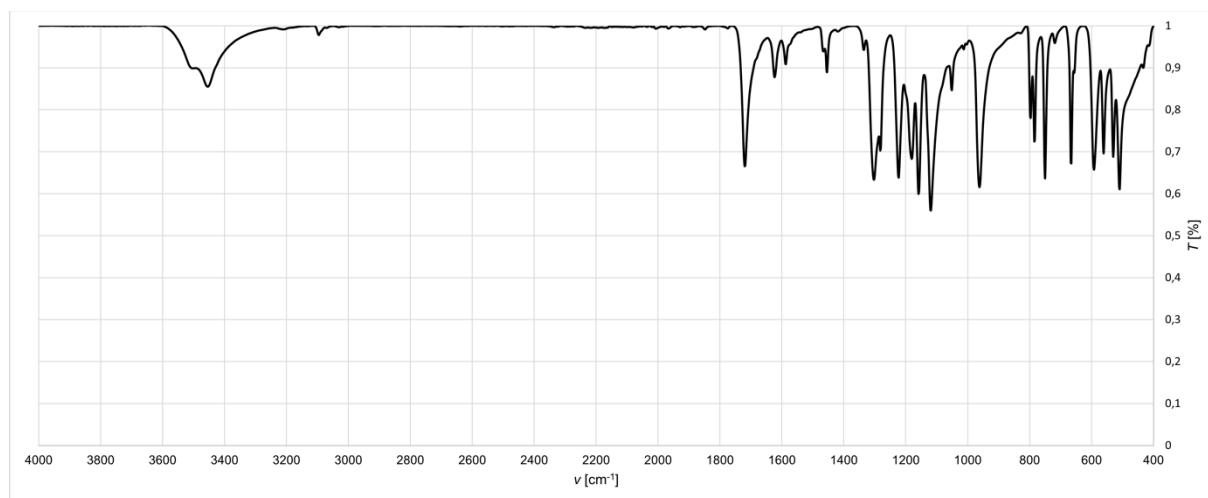


Figure S33. IR spectrum of commercially available NISac (**1**).

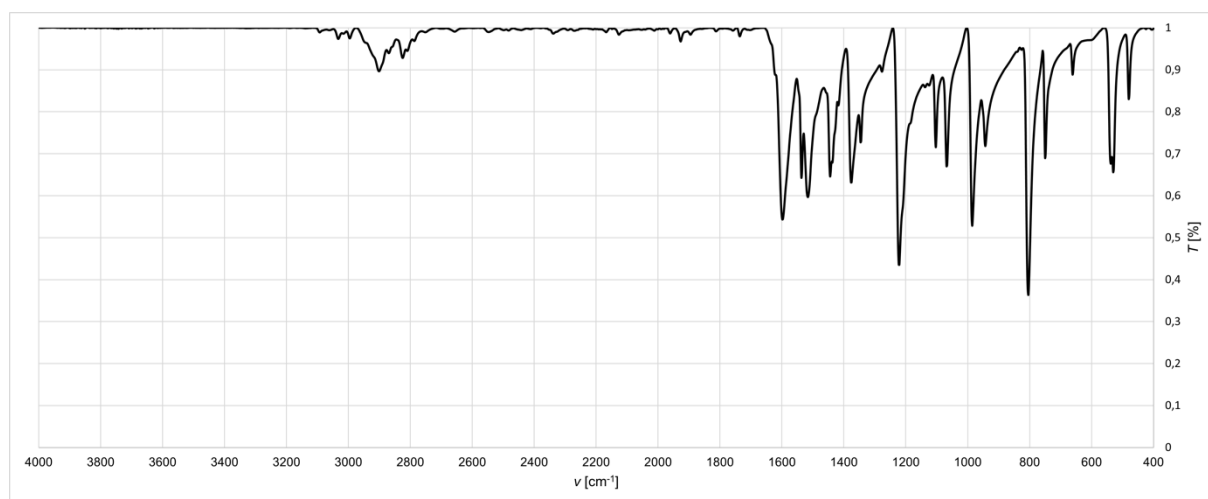


Figure S34. IR spectrum of commercially available DMAP (**2a**).

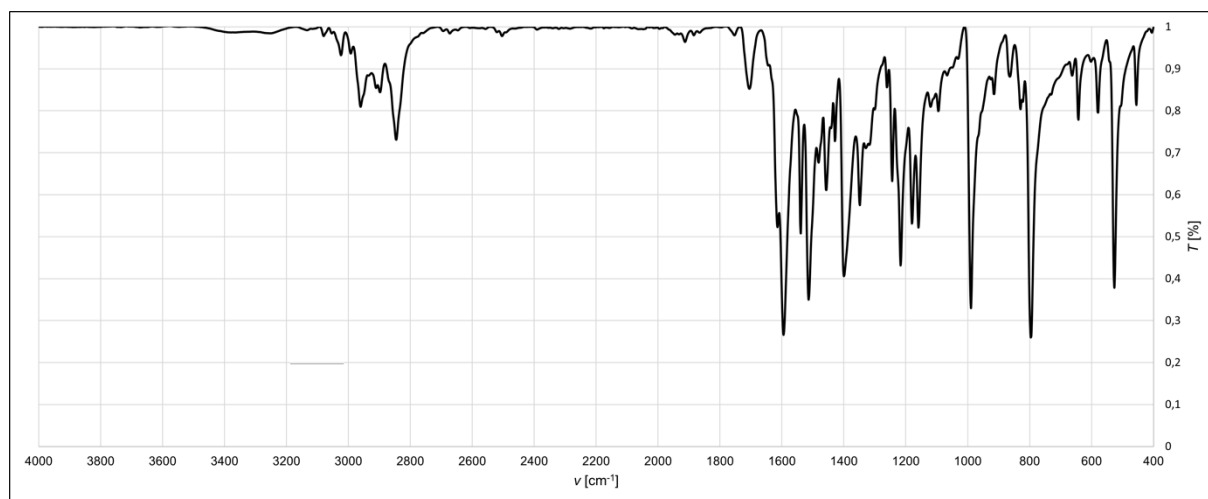


Figure S35. IR spectrum of commercially available PPY (**2b**).

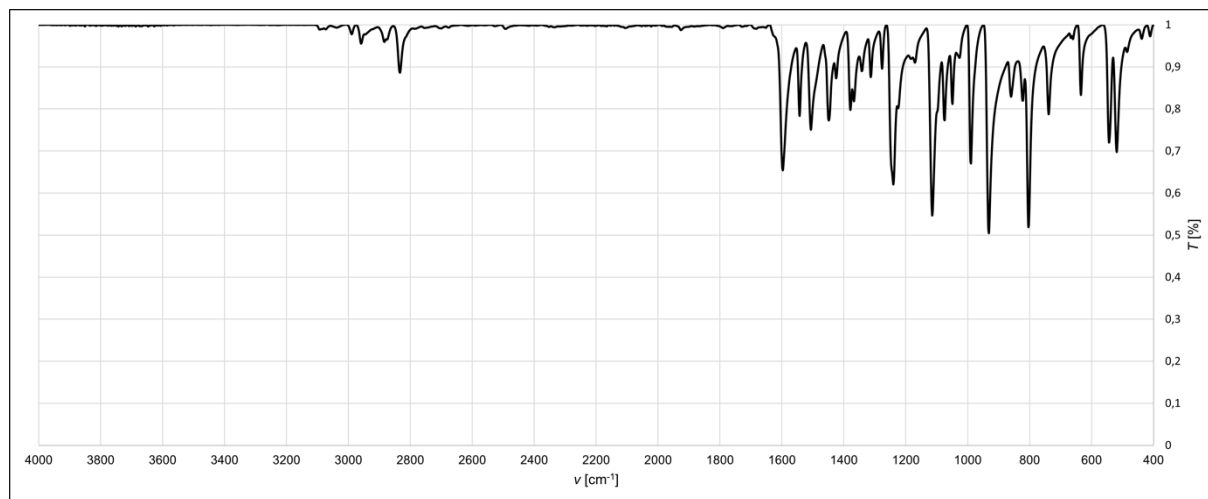


Figure S36. IR spectrum of commercially available MPY (**2c**).

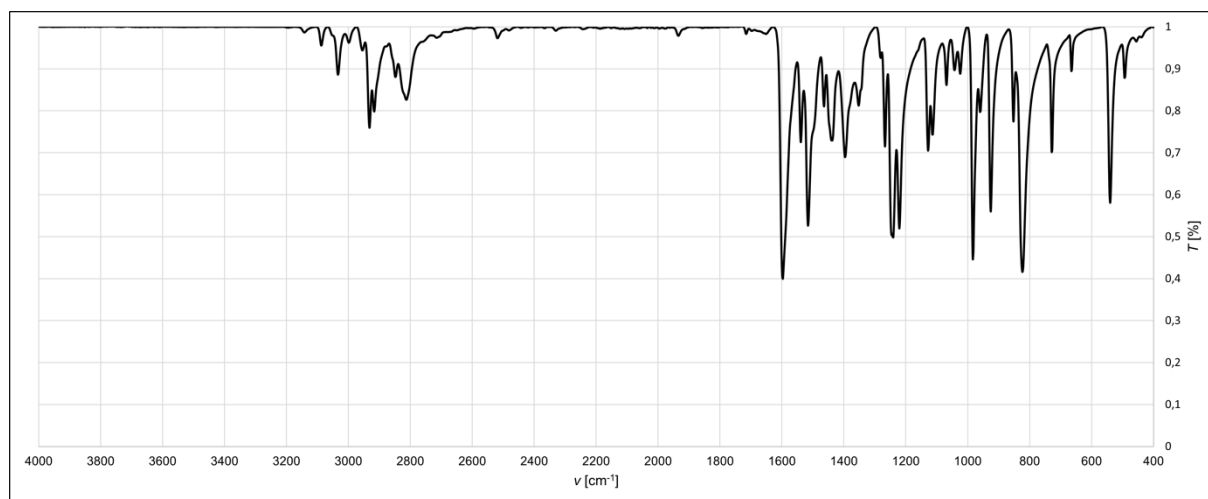


Figure S37. IR spectrum of commercially available PiPY (**2d**).

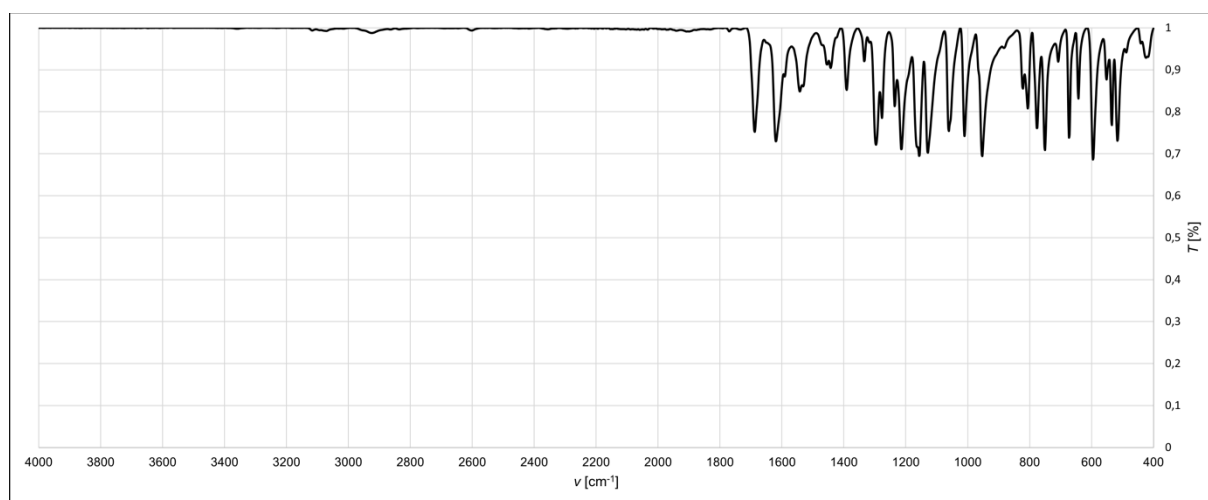


Figure S38. IR spectrum of solution prepared XB complex **3a**.

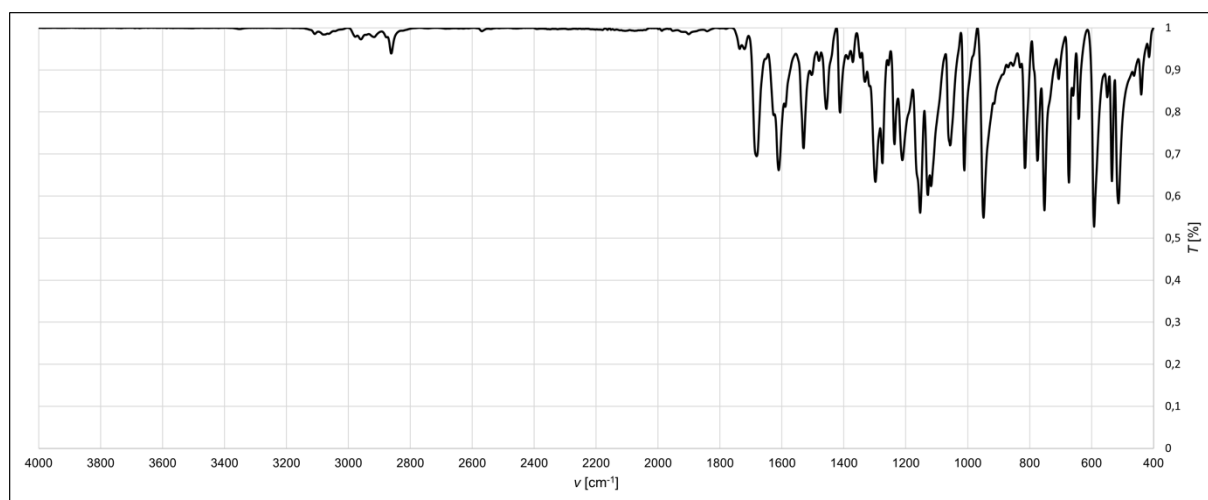


Figure S39. IR spectrum of solution prepared XB complex **3b**.

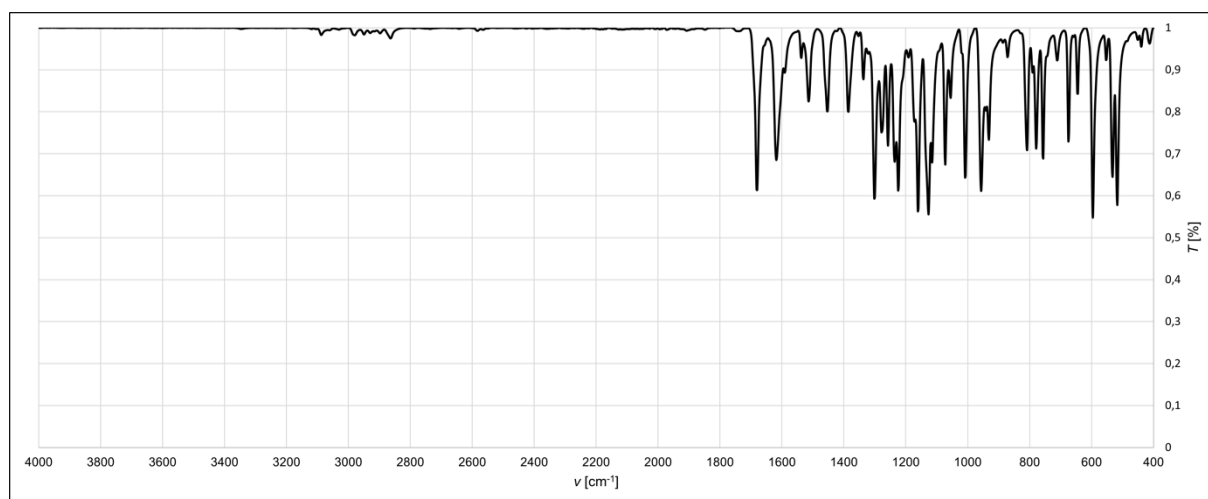


Figure S40. IR spectrum of solution prepared XB complex **3c**.

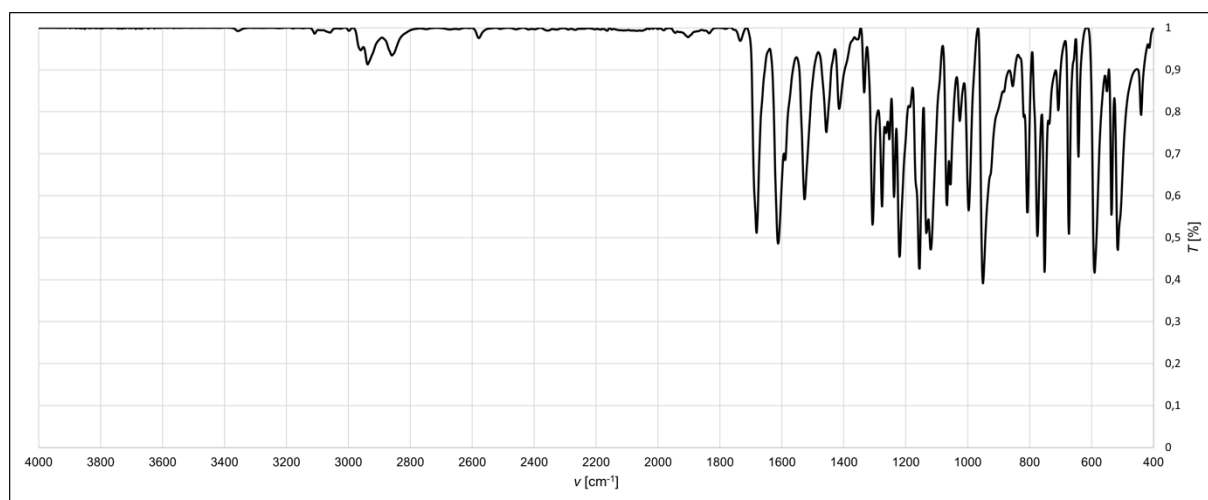


Figure S41. IR spectrum of solution prepared XB complex **3d**.

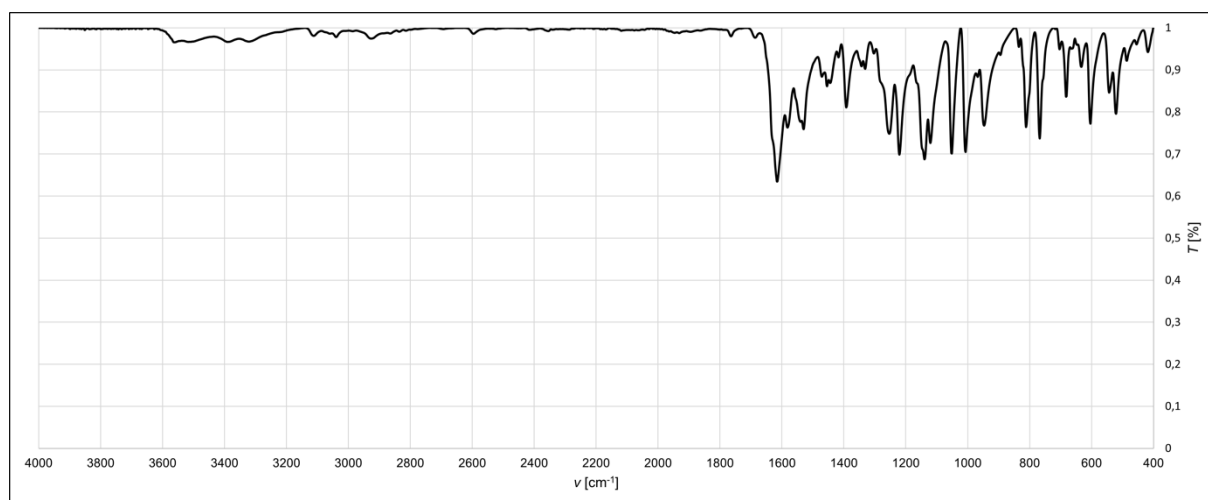


Figure S42. IR spectrum of solution prepared symmetric iodine(I) complex **4a**.

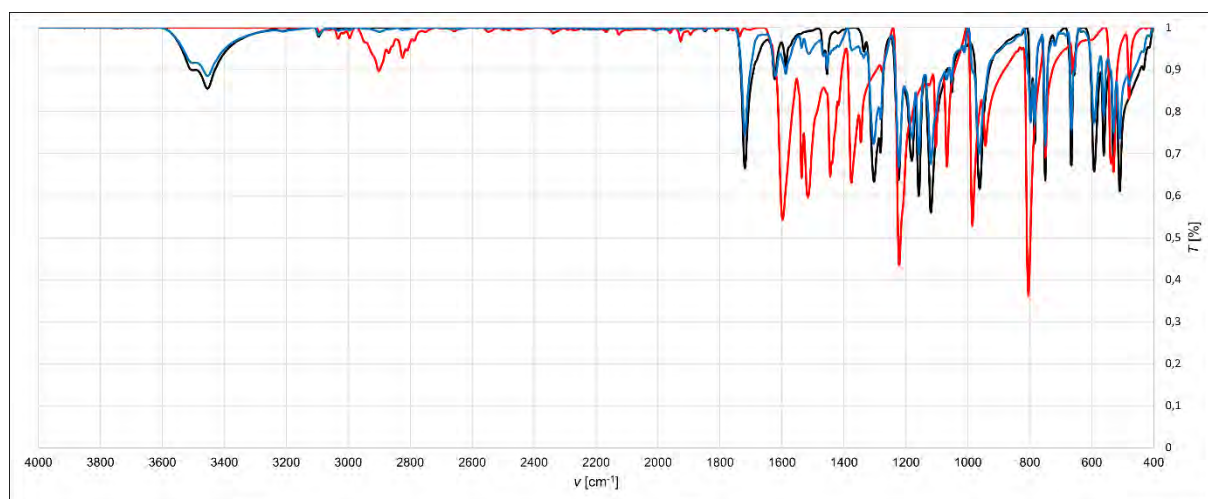


Figure S43. IR spectrum of a mixture of equal amounts of NISac and DMAP and comparison with the IR spectra of pure starting materials. Black: NISac, red: DMAP, blue: mixture.

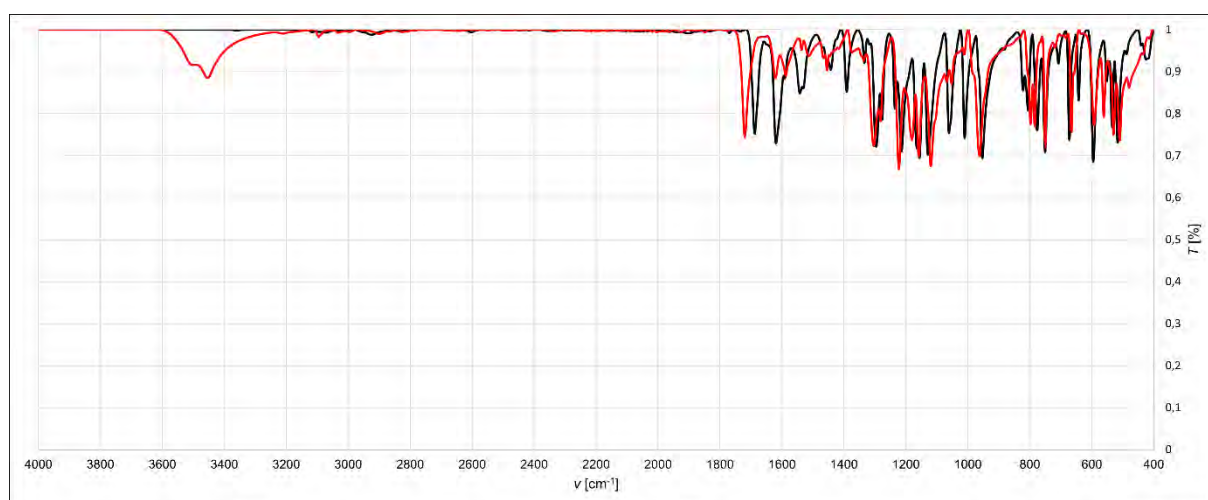


Figure S44. IR spectrum of a mixture of equal amounts of NISac and DMAP (red) and comparison with the IR spectrum of XB complex **3a** (black) obtained from solution.

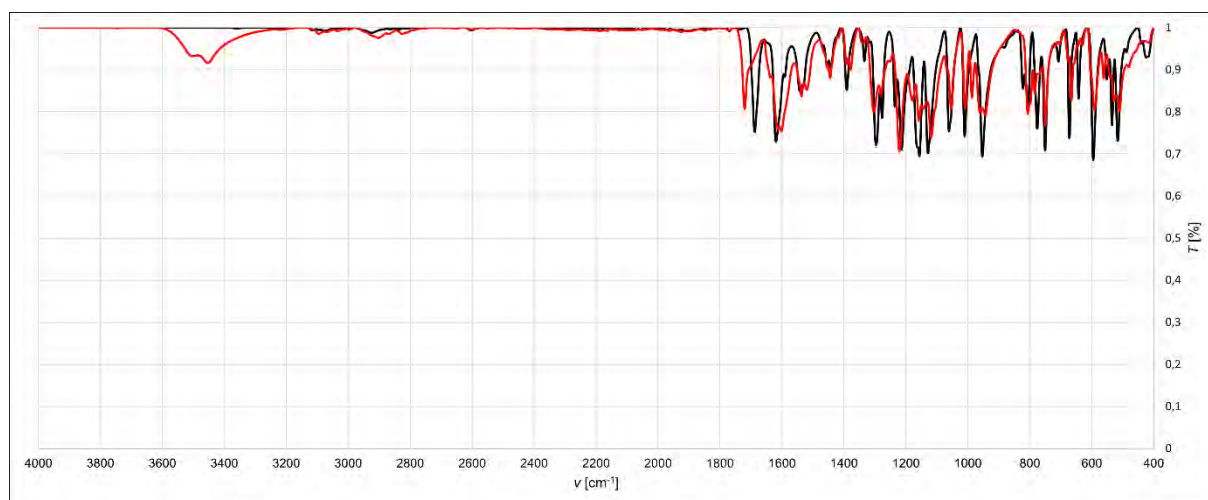


Figure S45. IR spectrum after grinding equal amounts of NISac and DMAP under neat conditions for 1 min (red) and comparison with the IR spectrum of XB complex **3a** obtained from solution (black).

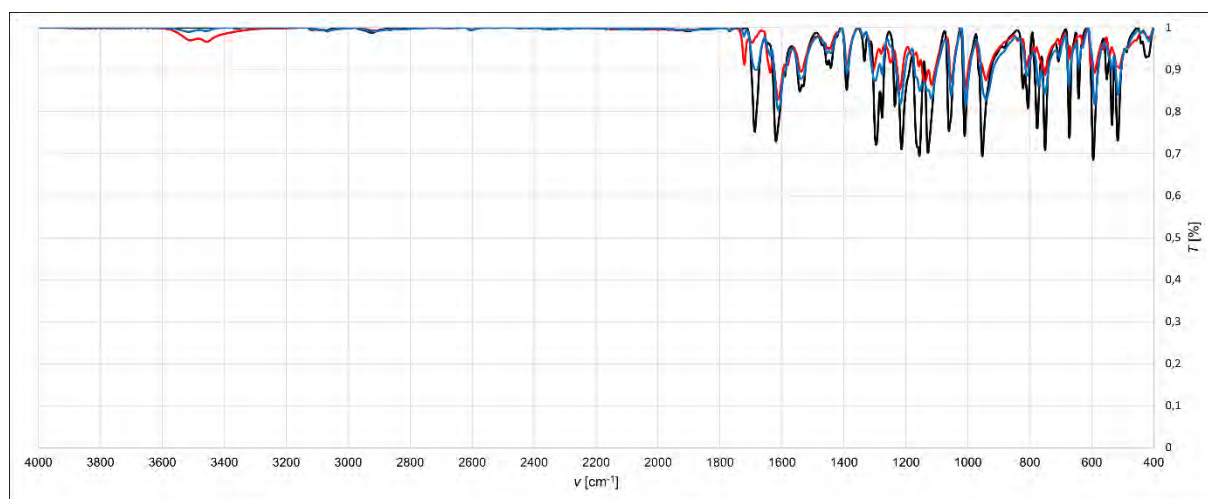


Figure S46. IR spectrum after grinding equal amounts of NISac and DMAP under neat conditions for a defined time and comparison with the IR spectrum of XB complex **3a** obtained from solution. Black: XB complex **3a**, red: 5 min grinding, blue: 10 min grinding.

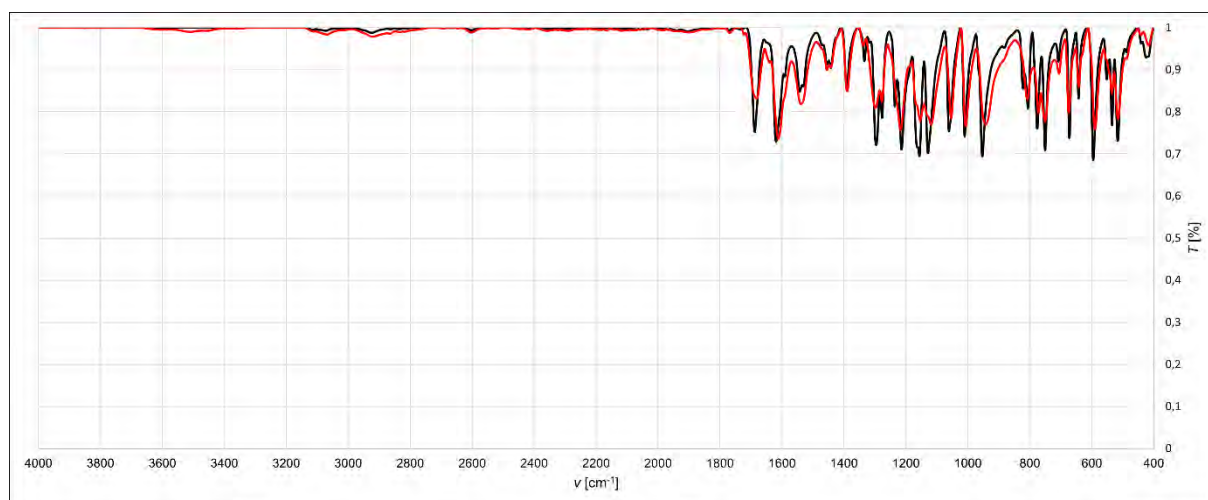


Figure S47. IR spectrum after grinding equal amounts of NISac and DMAP under neat conditions for 15 min (red) and comparison with the IR spectrum of XB complex **3a** obtained from solution (black).

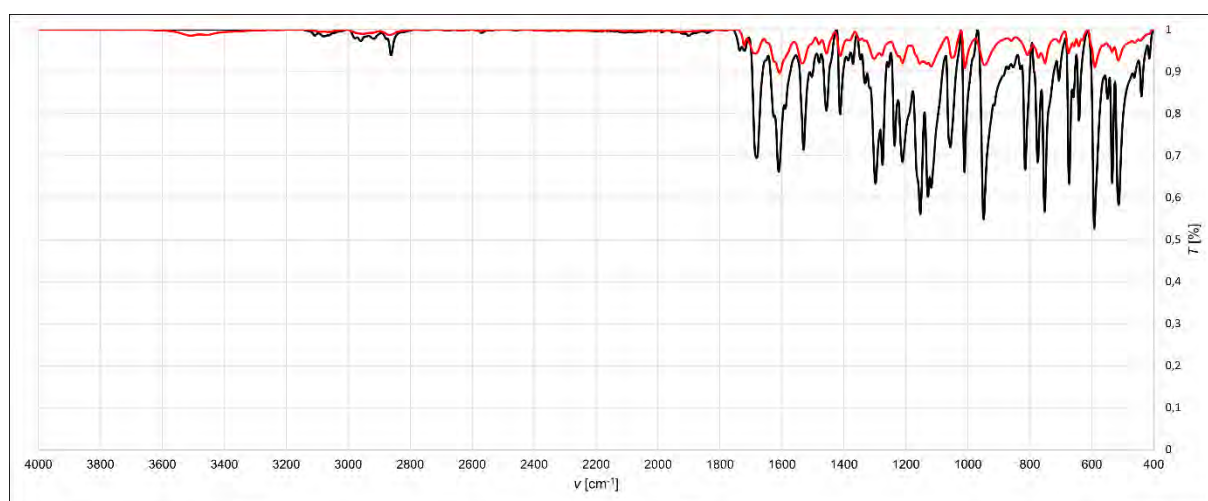


Figure S48. IR spectrum after grinding equal amounts of NISac and PPY under neat conditions for 15 min (red) and comparison with the IR spectrum of XB complex **3b** obtained from solution (black).

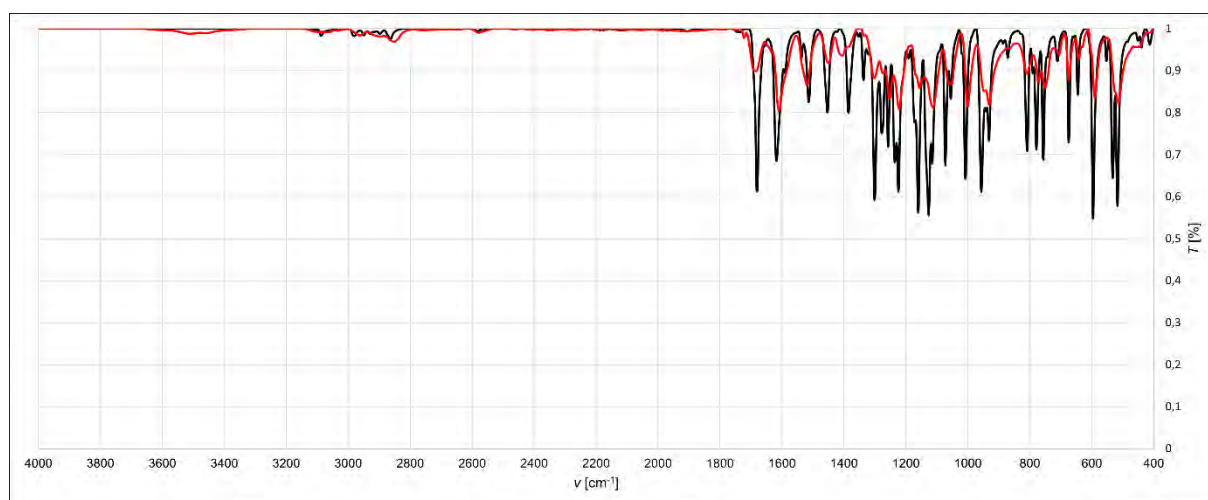


Figure S49. IR spectrum after grinding equal amounts of NISac and MPY under neat conditions for 15 min (red) and comparison with the IR spectrum of XB complex **3c** obtained from solution (black).

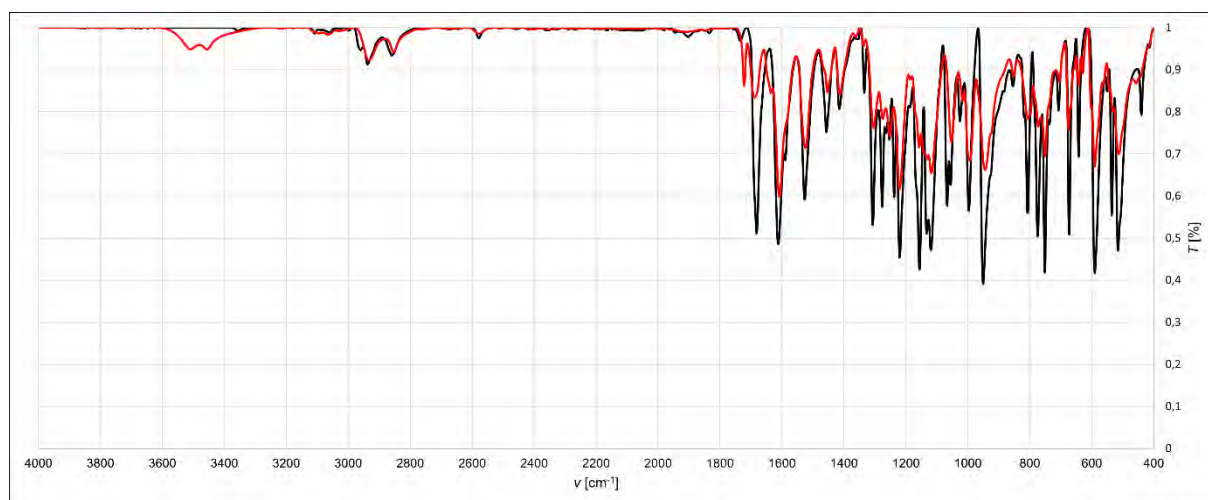


Figure S50. IR spectrum after grinding equal amounts of NISac and PiPY under neat conditions for 15 min (red) and comparison with the IR spectrum of XB complex **3d** obtained from solution (black).

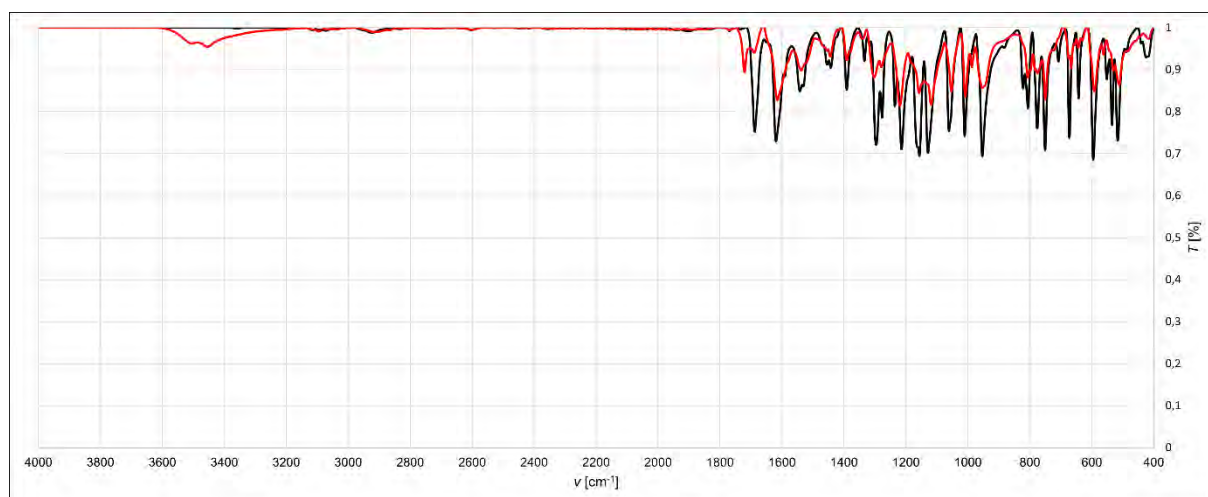


Figure S51. IR spectrum after grinding equal amounts of NISac and DMAP under LAG conditions (EtOAc) for 1 min (red) and comparison with the IR spectrum of XB complex **3a** obtained from solution (black).

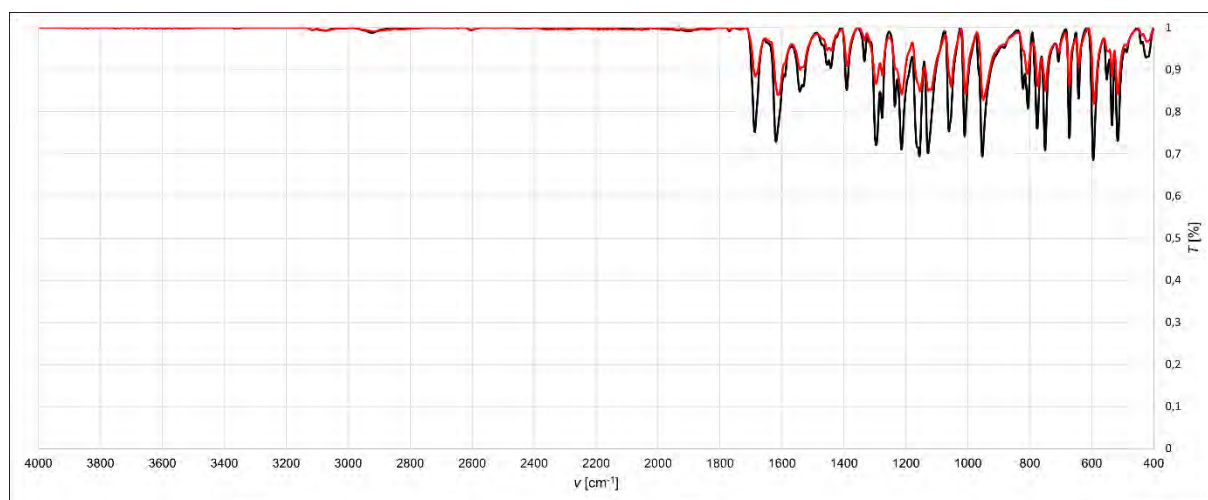


Figure S52. IR spectrum after grinding equal amounts of NISac and DMAP under LAG conditions (EtOAc) for 5 min (red) and comparison with the IR spectrum of XB complex **3a** obtained from solution (black).

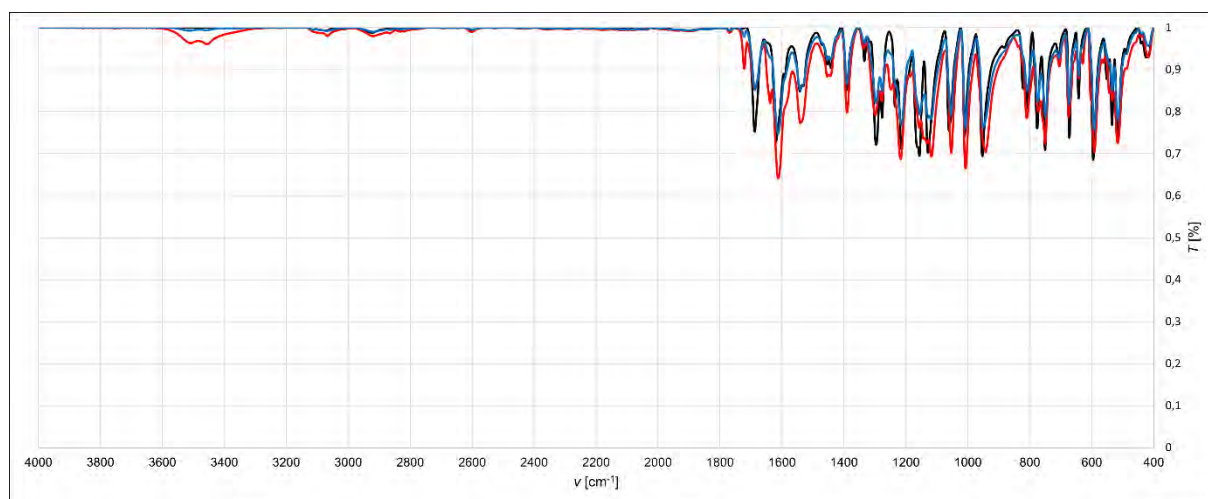


Figure S53. IR spectrum after grinding equal amounts of NISac and DMAP under different LAG conditions (EtOAc) and comparison with the IR spectrum of XB complex **3a** obtained from solution. Black: XB complex **3a**, red: only 1 drop EtOAc, 3 min grinding, blue: 3 drops EtOAc in the beginning, 3 min grinding.

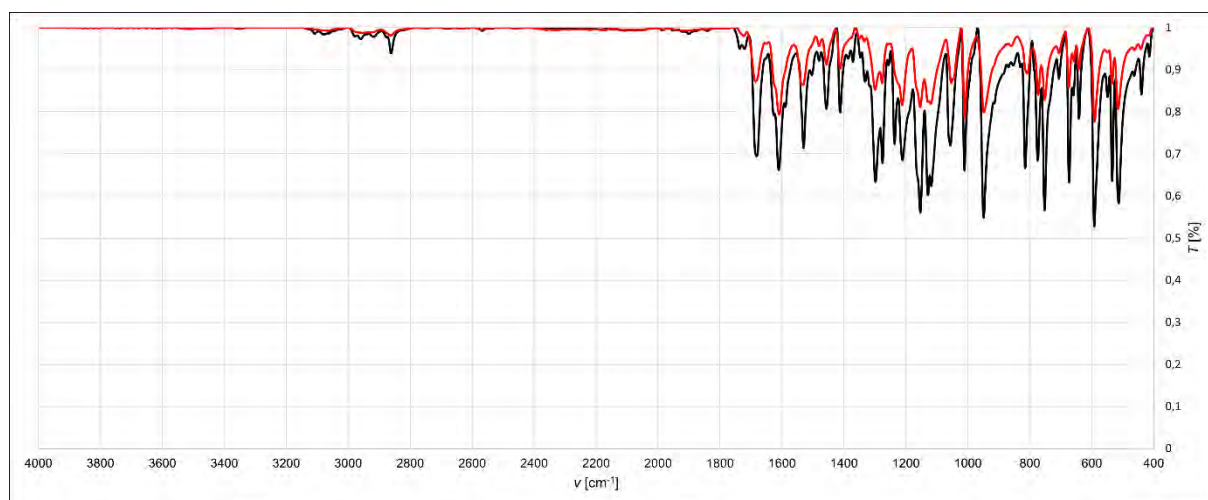


Figure S54. IR spectrum after grinding equal amounts of NISac and PPY under LAG conditions (EtOAc) for 5 min (red) and comparison with the IR spectrum of XB complex **3b** obtained from solution (black).

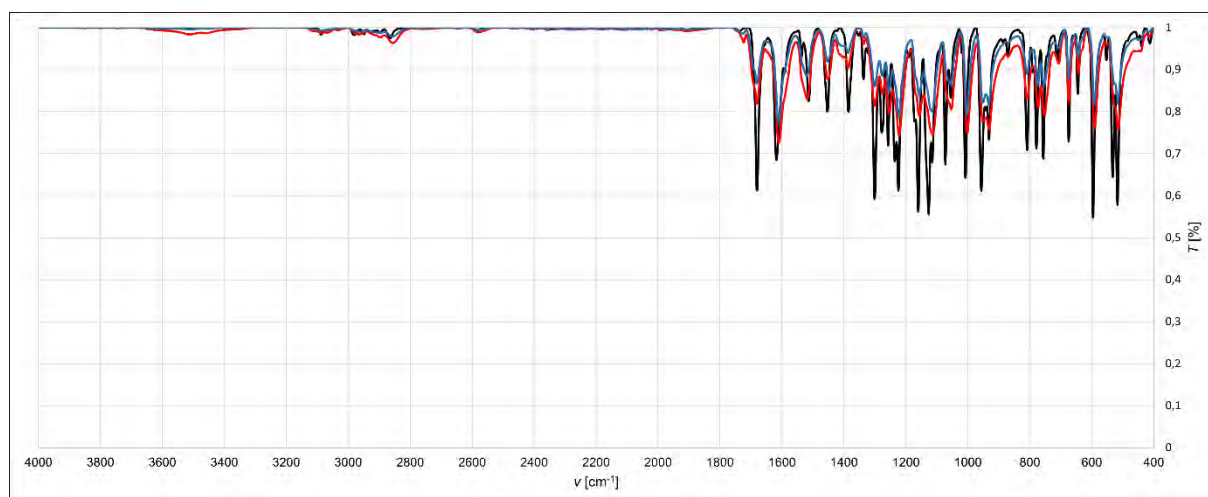


Figure S55. IR spectrum after grinding equal amounts of NISac and MPY under LAG conditions (EtOAc) for 5-6 min and comparison with the IR spectrum of XB complex **3c** obtained from solution. Black: XB complex **3c**, red: 5 min grinding, blue: 6 min grinding.

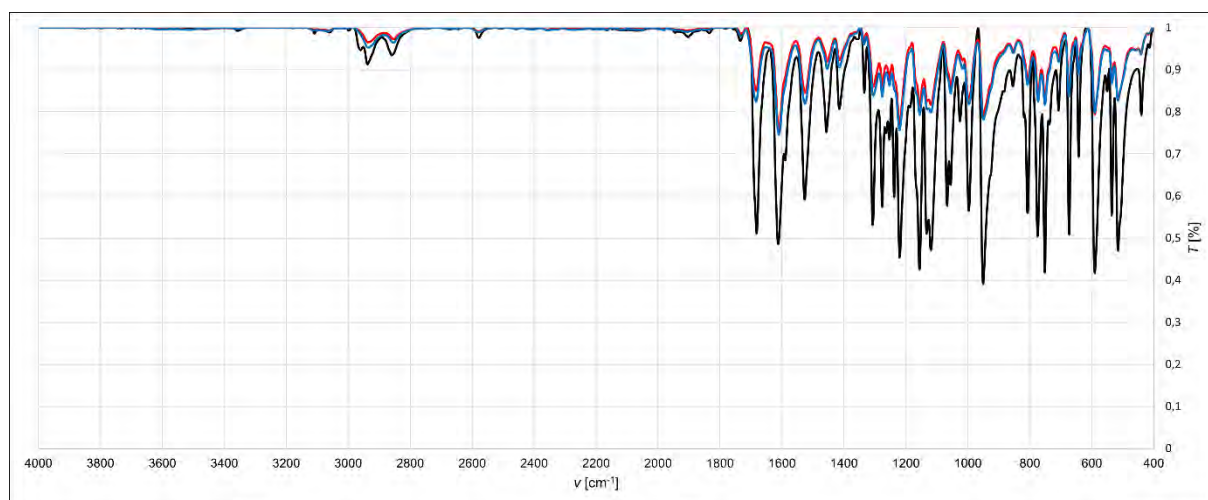


Figure S56. IR spectrum after grinding equal amounts of NISac and PiPY under LAG conditions (EtOAc) for 5-6 min and comparison with the IR spectrum of XB complex **3d** obtained from solution. Black: XB complex **3d**, red: 5 min grinding, blue: 6 min grinding.

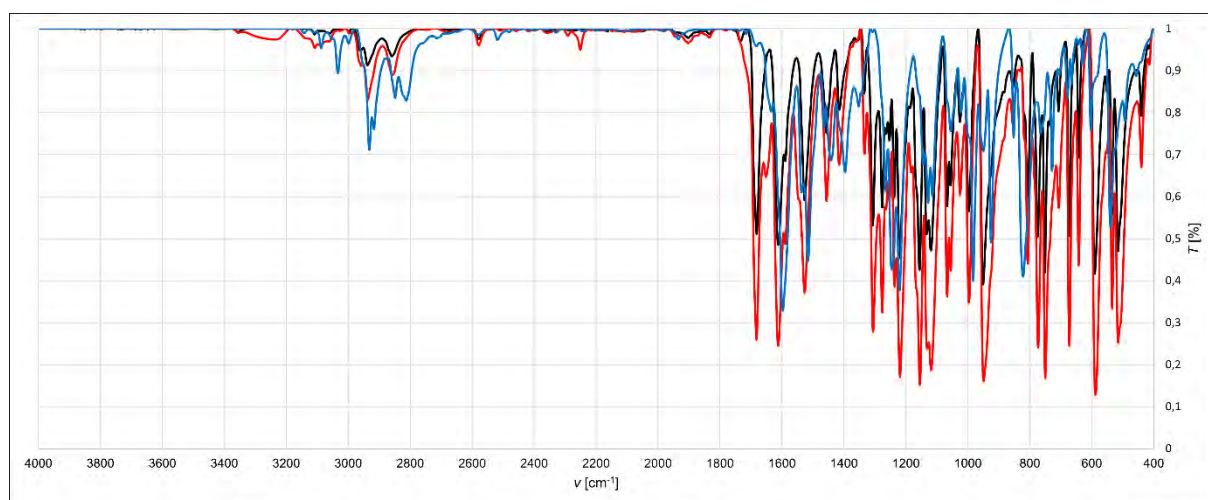


Figure S57. IR spectrum after grinding equal amounts of NISac and PiPY under LAG conditions (MeCN) for 2 min and comparison with the IR spectrum of XB complex **3d** obtained from solution. Black: XB complex **3d**, red: 1 min grinding, blue: 2 min grinding.

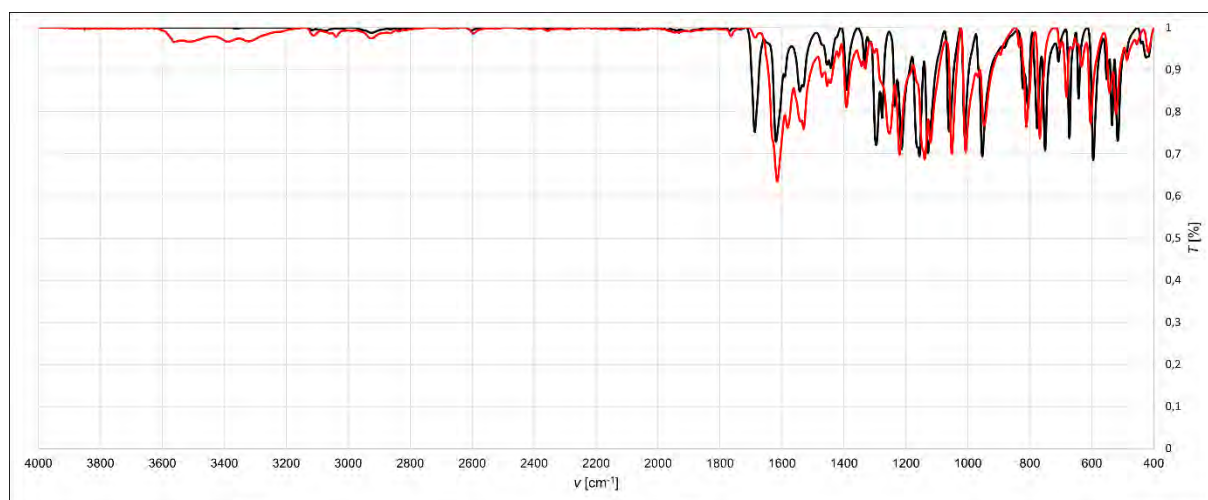


Figure S58. Comparison of the IR spectra of XB complex **3a** obtained from solution (black) and symmetric iodine(I) complex **4a** obtained from solution (red).



Figure S59. IR spectrum after grinding equal amounts of DMAP and XB complex **3a** under neat conditions for 2 min (red) and comparison with the IR spectrum of symmetric iodine(I) complex **4a** obtained from solution (black).

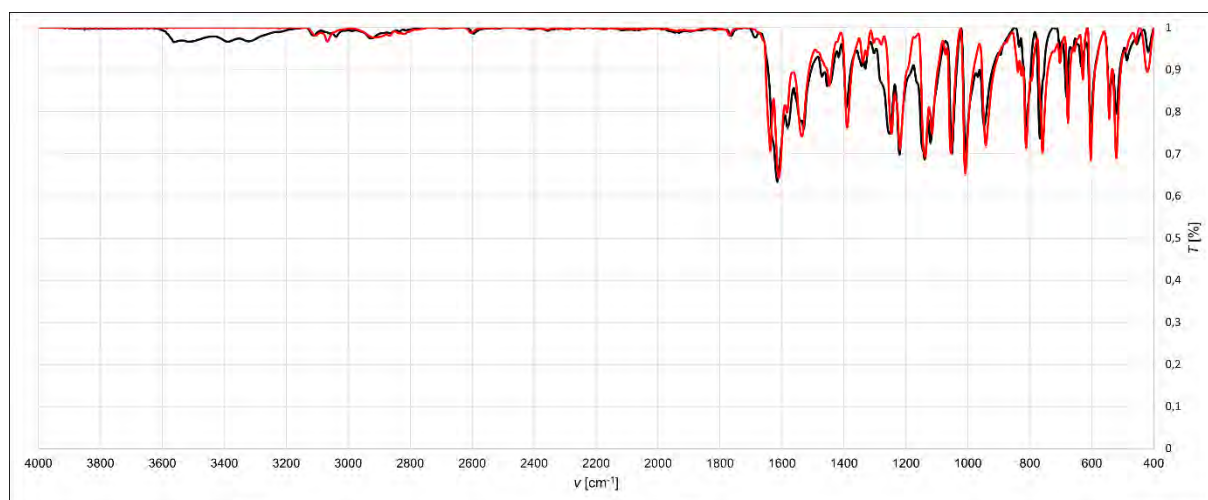


Figure S60. IR spectrum after grinding equal amounts of DMAP and XB complex **3a** under neat conditions for 10 min (red) and comparison with the IR spectrum of symmetric iodine(I) complex **4a** obtained from solution (black).

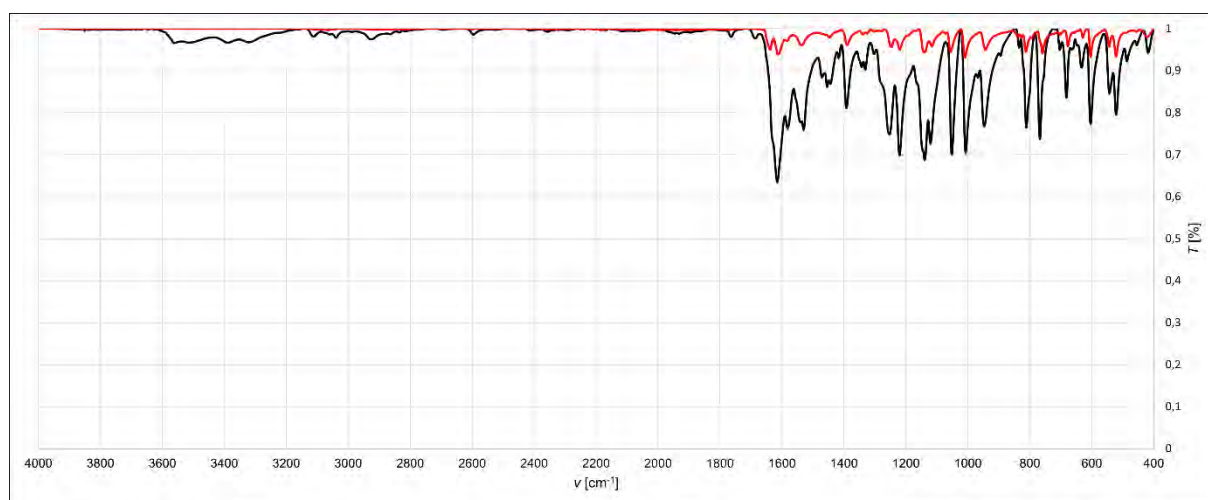


Figure S61. IR spectrum after grinding equal amounts of DMAP and XB complex **3a** under LAG conditions (EtOAc) for 5 min (red) and comparison with the IR spectrum of symmetric iodine(I) complex **4a** obtained from solution (black).

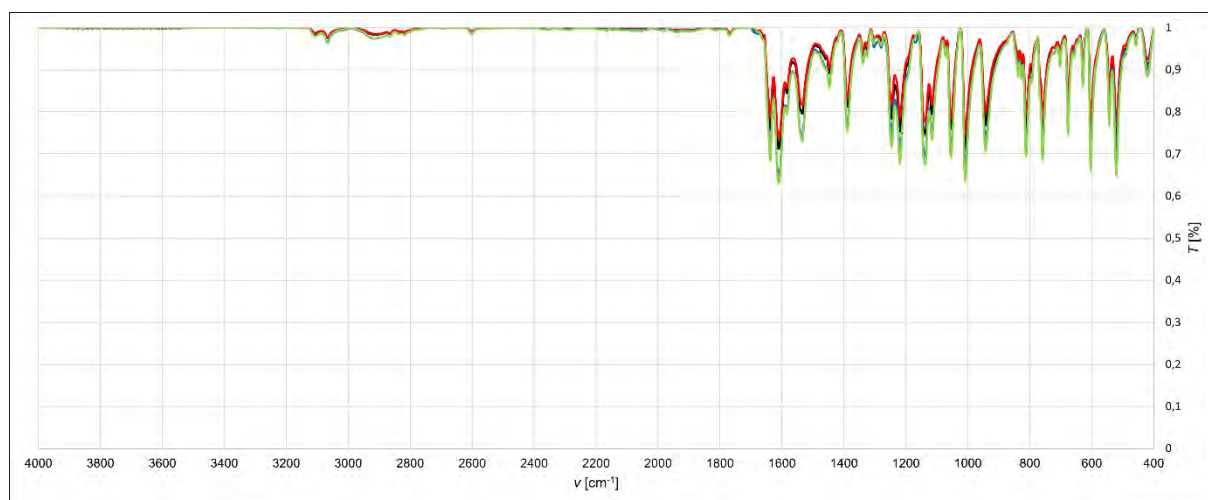


Figure S62. IR spectrum after grinding equal amounts of DMAP and XB complex **3a** under LAG conditions (chosen solvent) for 5 min. Black: DCM, red: CHCl_3 , blue: acetone, green: MeCN.

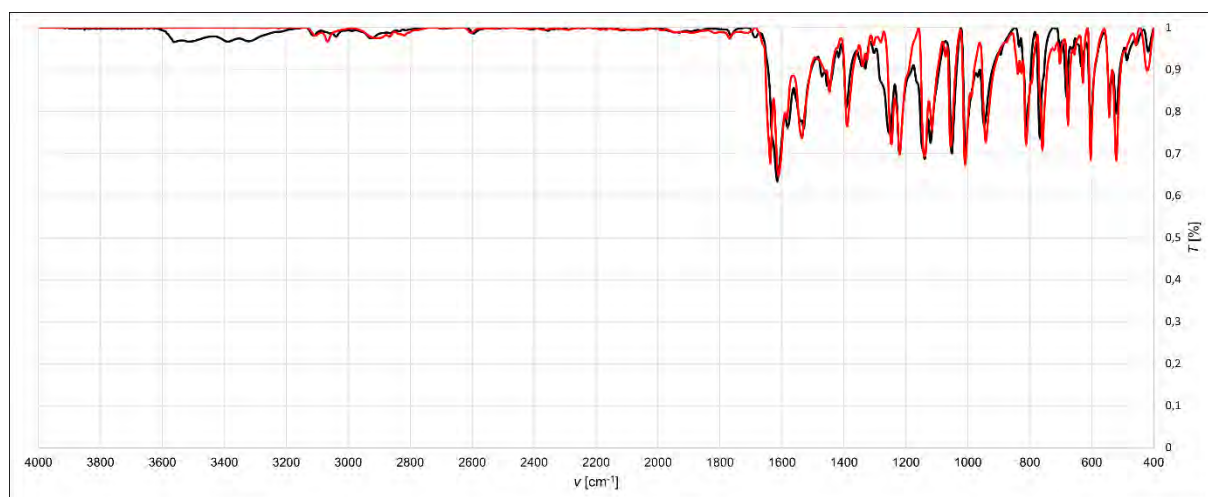


Figure S63. IR spectrum after grinding equal amounts of NISac and DMAP under LAG conditions (EtOAc) for 5 min, then adding another equivalent of DMAP and another grinding for 5 min under LAG (EtOAc) conditions (red) and comparison with IR spectrum of symmetric iodine(I) complex **4a** (black).

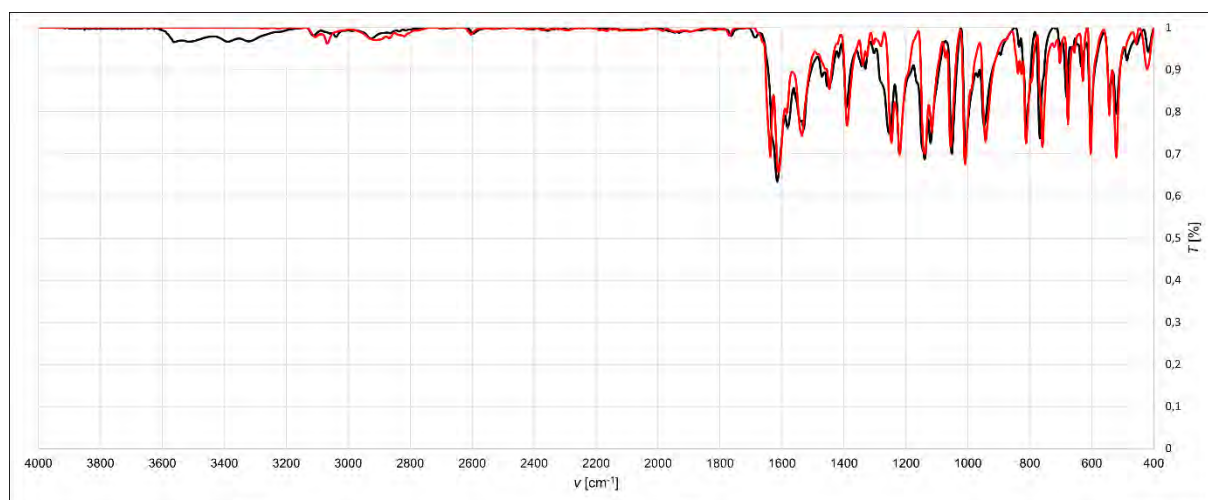


Figure S64. IR spectrum after grinding 1 equivalent of NISac and 2 equivalents of DMAP under LAG conditions (EtOAc) for 5 min (red) and comparison with IR spectrum of symmetric iodine(I) complex **4a** (black).

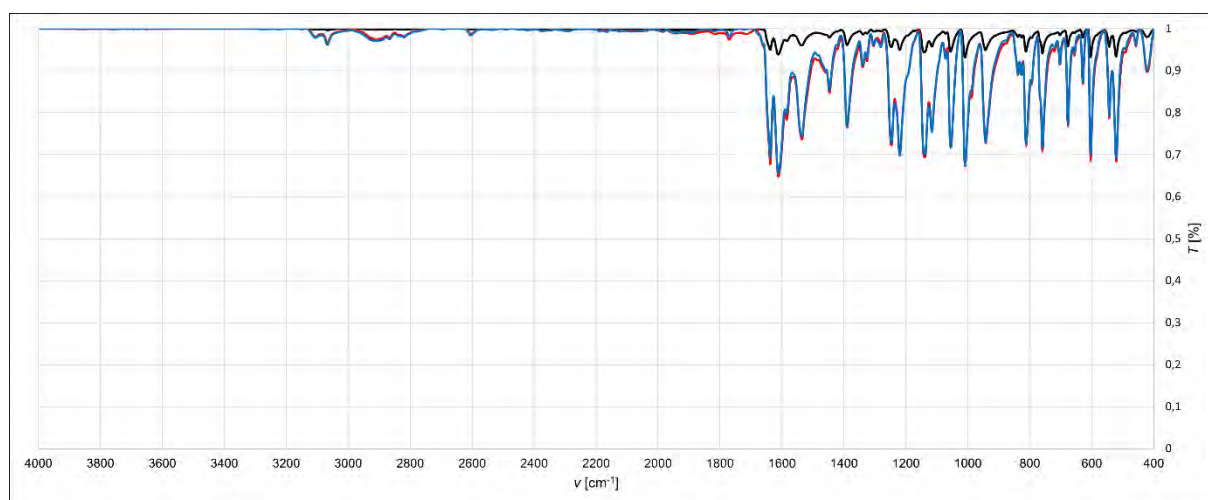


Figure S65. Comparison of the IR spectra of the developed methods for the mechanochemical preparation of symmetric iodine(I) complex **4a**. Black: Grinding of solution made XB complex **3a** and DMAP, red: two-step synthesis, blue: one-pot synthesis.

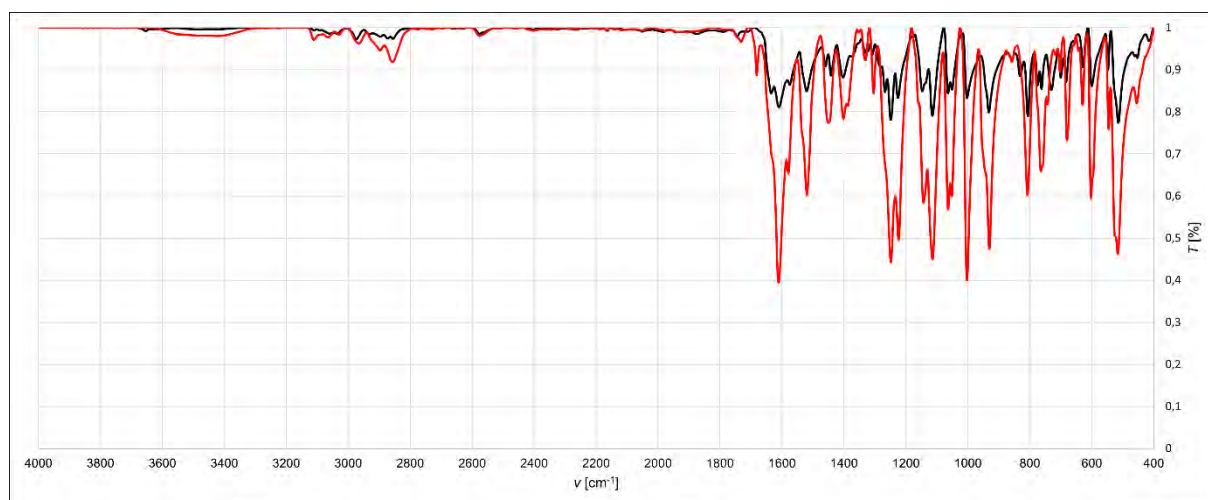


Figure S66. IR spectrum after grinding equal amounts of MPY and XB complex **3c** under LAG conditions (EtOAc) for 5 min (red) and comparison with the IR spectrum of symmetric iodine(I) complex **4c** (black) obtained from solution.

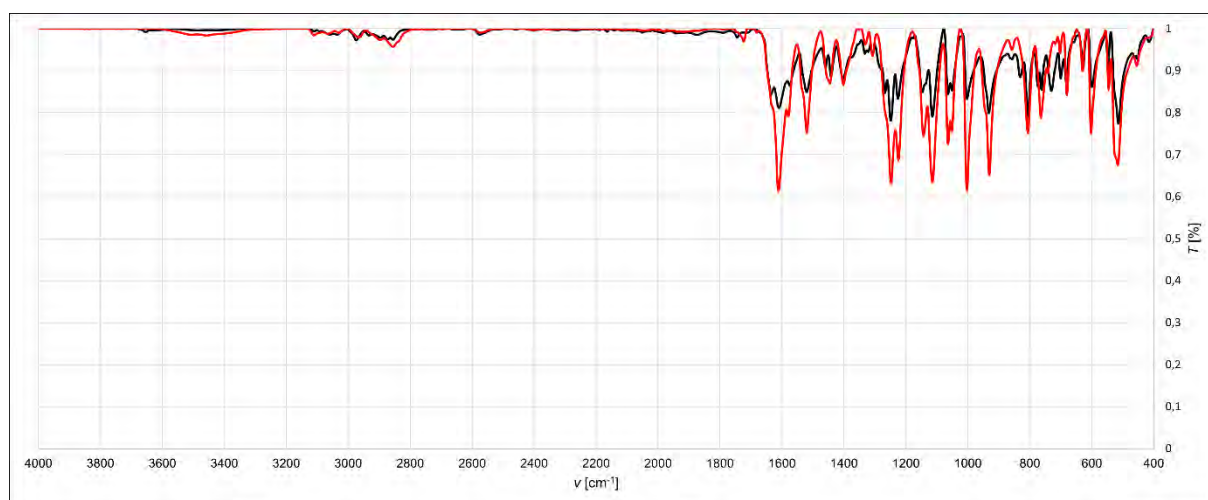


Figure S67. IR spectrum after grinding 1 equivalent of NISac and 2 equivalents of MPY under LAG conditions (EtOAc) for 5 min (red) and comparison with IR spectrum of symmetric iodine(I) complex **4c** (black) obtained from solution.

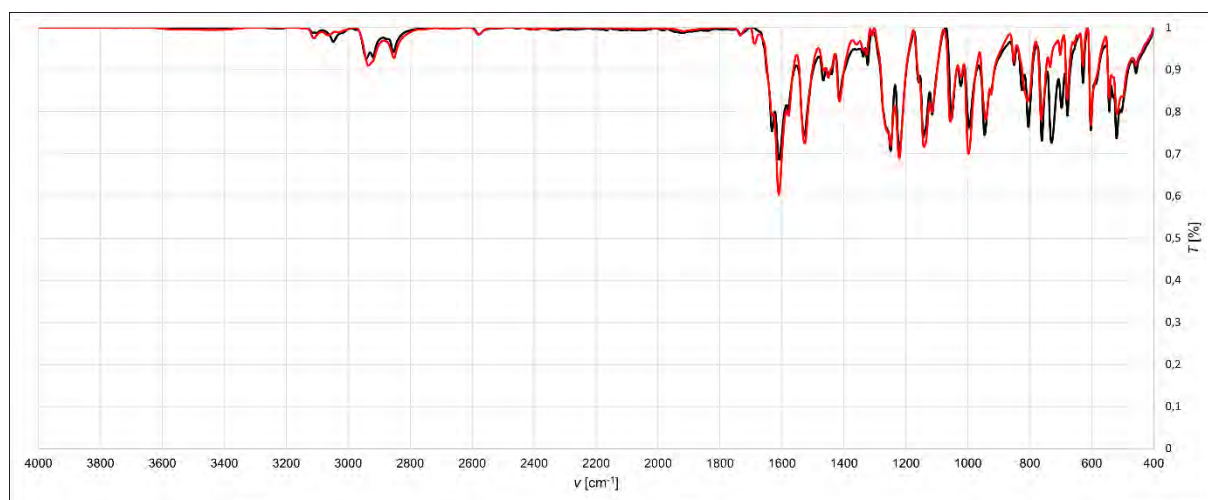


Figure S68. IR spectrum after grinding equal amounts of PiPY and XB complex **3c** under LAG conditions (EtOAc) for 5 min (red) and comparison with the IR spectrum of symmetric iodine(I) complex **4d** (black) obtained from solution.

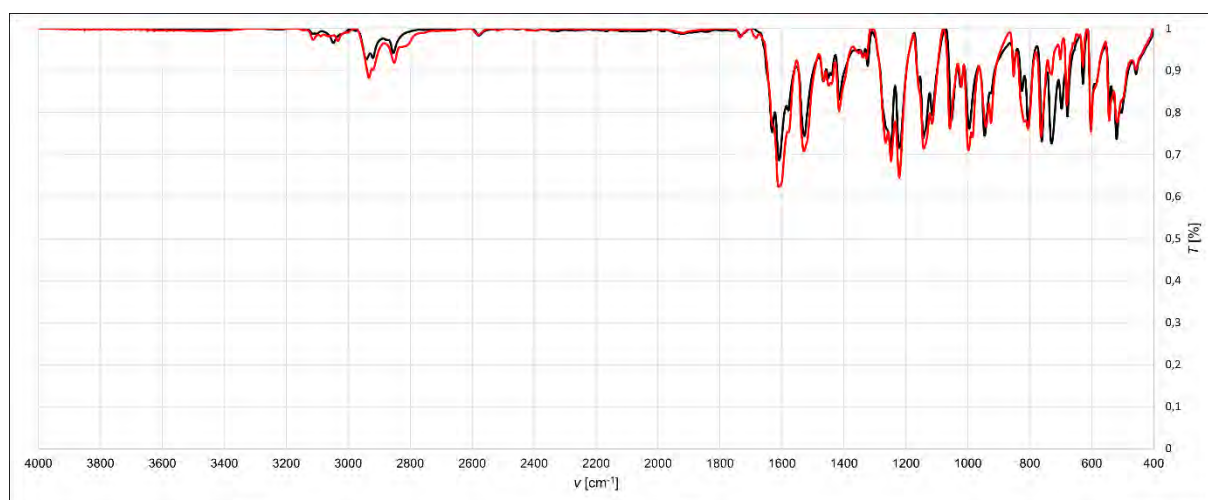


Figure S69. IR spectrum after grinding 1 equivalent of NISac and 2 equivalents of PiPY under LAG conditions (EtOAc) for 5 min (red) and comparison with IR spectrum of symmetric iodine(I) complex **4d** (black) obtained from solution.

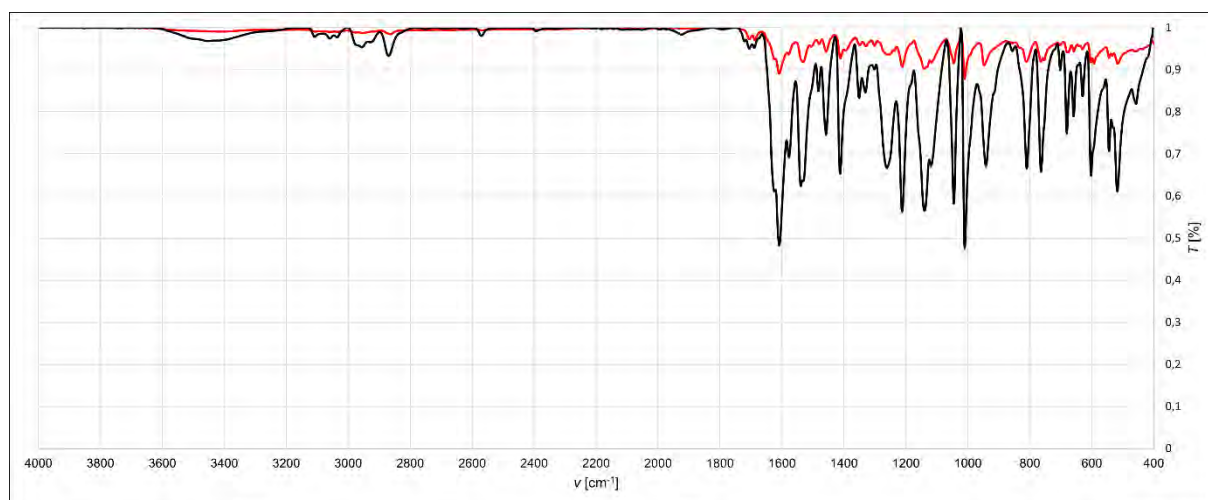


Figure S70. Comparison of the IR spectra after grinding equal amounts of PiPY and XB complex **3c** under LAG conditions (EtOAc) for 5 min (red) and after grinding 1 equivalent of NISac and 2 equivalents of PPY under LAG conditions (EtOAc) for 5 min (black).

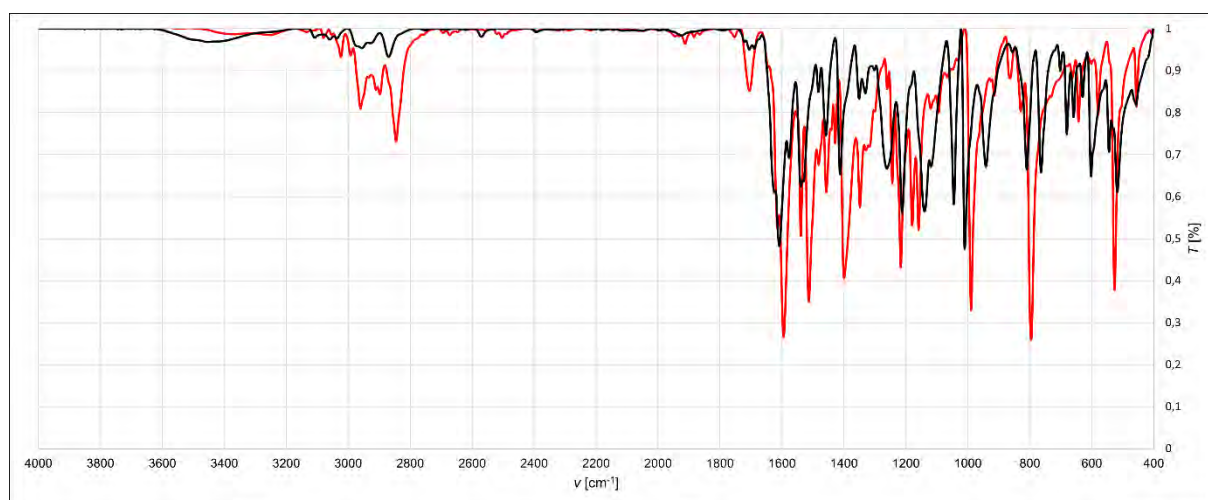


Figure S71. Comparison of the IR spectra after grinding 1 equivalent of NISac and 2 equivalents of PPY under LAG conditions (EtOAc) for 5 min (black) and PPY (red).

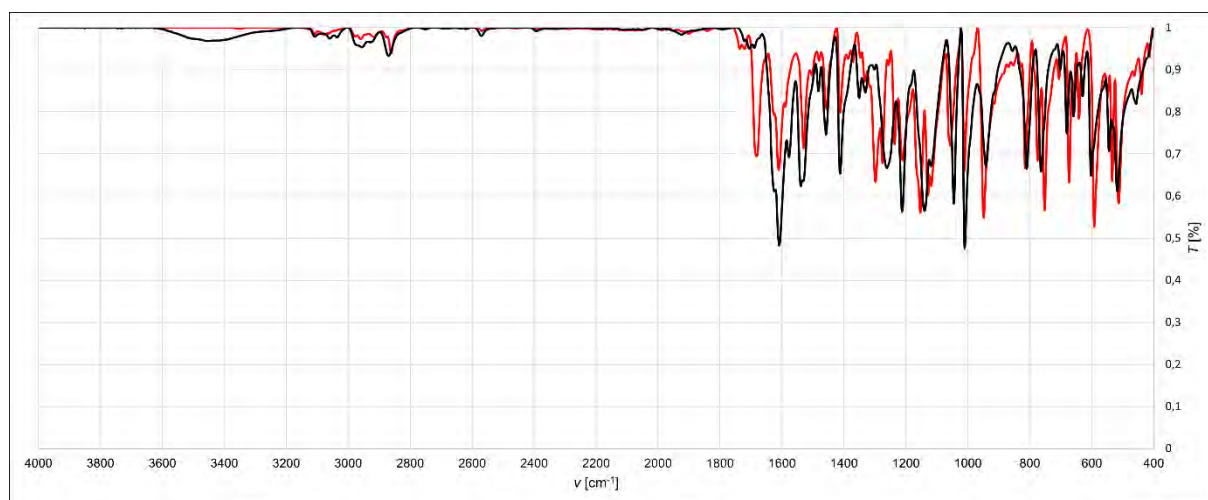


Figure S72. Comparison of the IR spectra after grinding 1 equivalent of NISac and 2 equivalents of PPY under LAG conditions (EtOAc) for 5 min (black) and solution made XB complex **3b** (red).

5 PXRD Ex-Situ Analysis

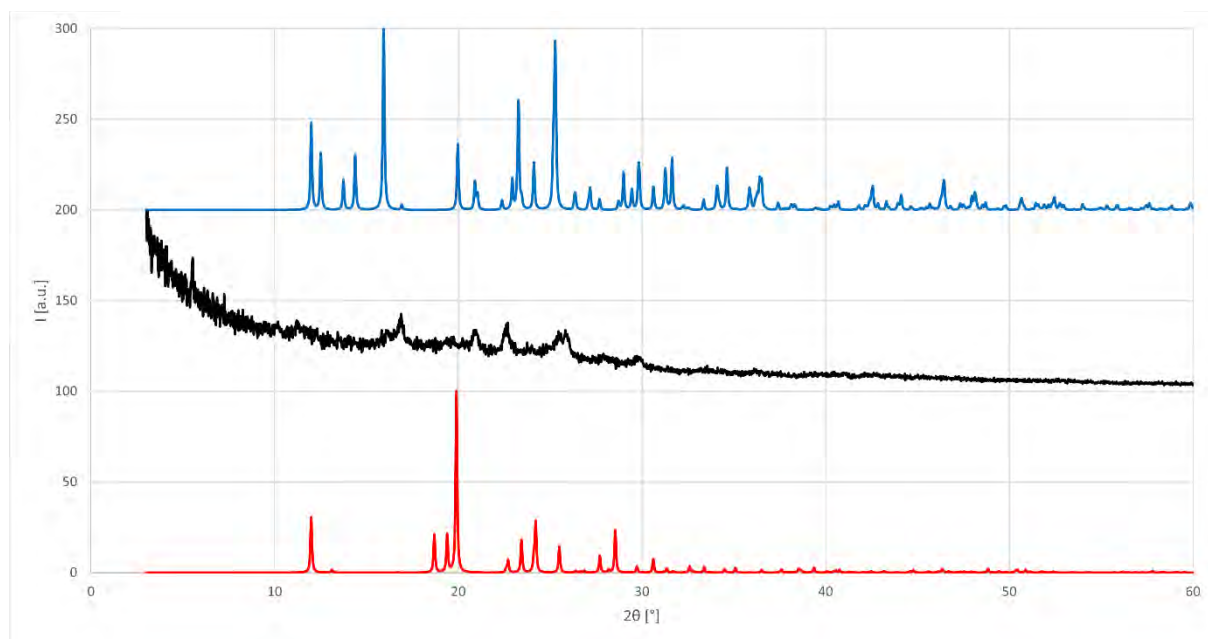


Figure S73. PXRD pattern after grinding equal amounts of NISac and DMAP under neat conditions for 15 min (black) and comparison with simulated PXRD patterns of NISac (blue) and DMAP (red).

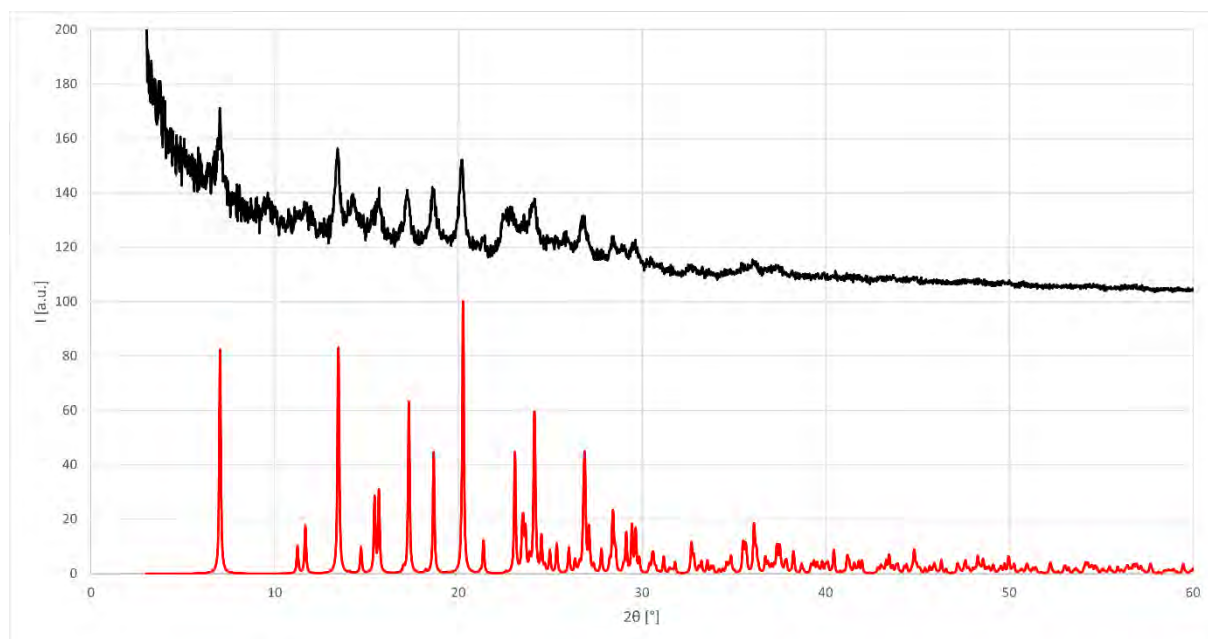


Figure S74. PXRD pattern after grinding equal amounts of NISac and DMAP under LAG conditions (EtOAc) for 5 min (black) and comparison with simulated PXRD patterns of XB complex **3a** obtained from solution (red). CCDC1060261 was used for the simulation.^{5,6}

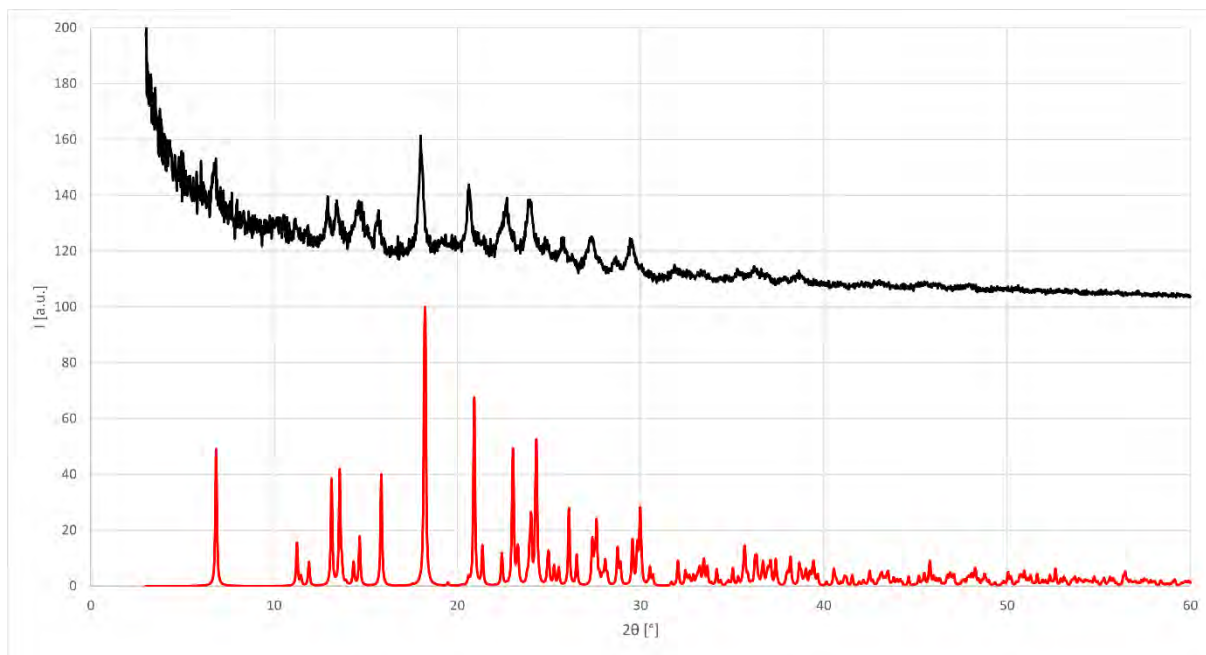


Figure S75. PXRD pattern after grinding equal amounts of NISac and PPY under LAG conditions (EtOAc) for 5 min (black) and comparison with simulated PXRD patterns of XB complex **3b** obtained from solution (red).

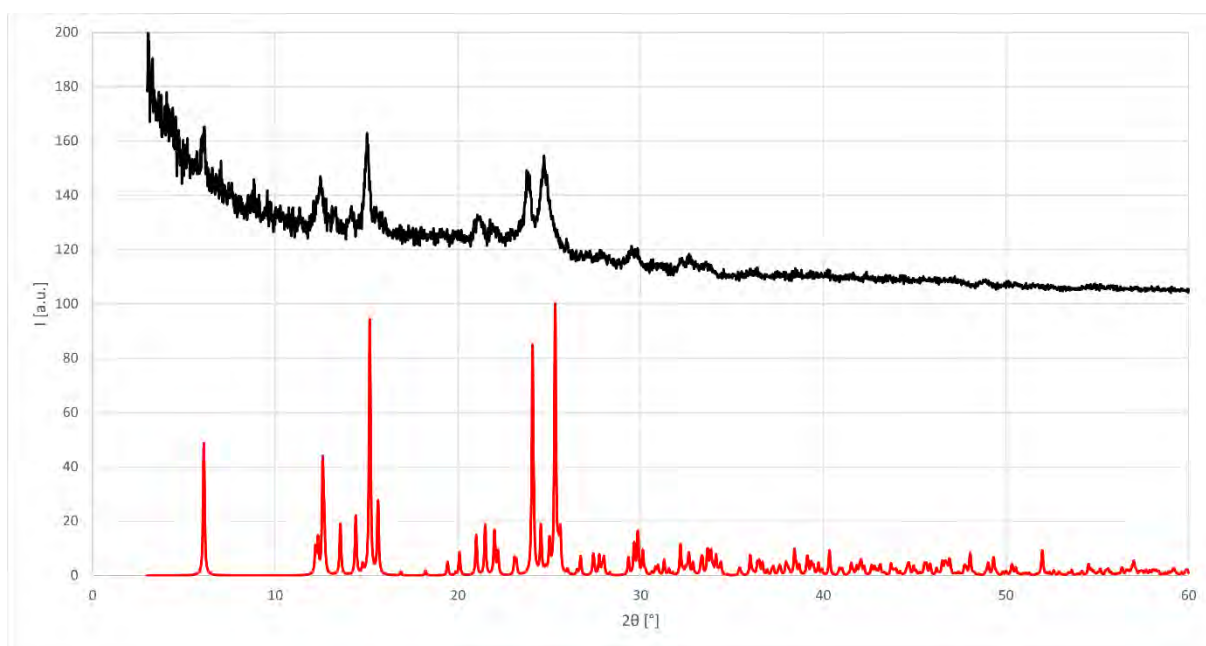


Figure S76. PXRD pattern after grinding equal amounts of NISac and MPY under LAG conditions (EtOAc) for 5 min (black) and comparison with simulated PXRD patterns of XB complex **3c** obtained from solution (red).

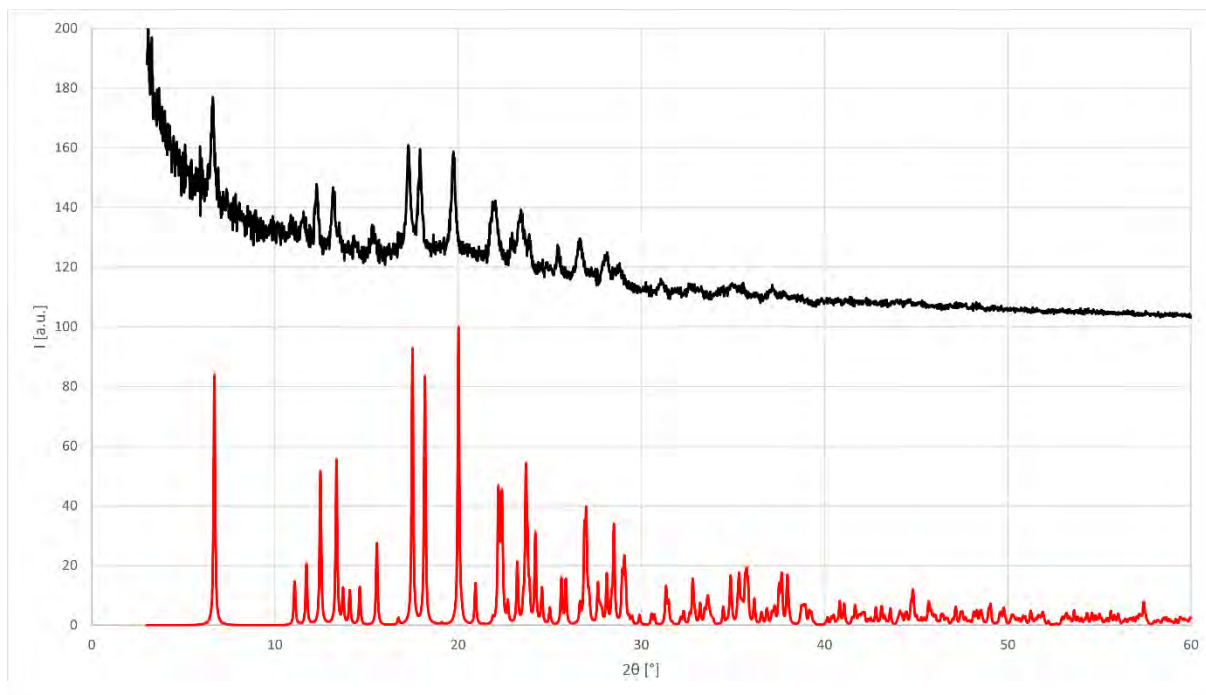


Figure S77. PXRD pattern after grinding equal amounts of NISac and PiPY under LAG conditions (EtOAc) for 5 min (black) and comparison with simulated PXRD patterns of XB complex **3d** obtained from solution (red).

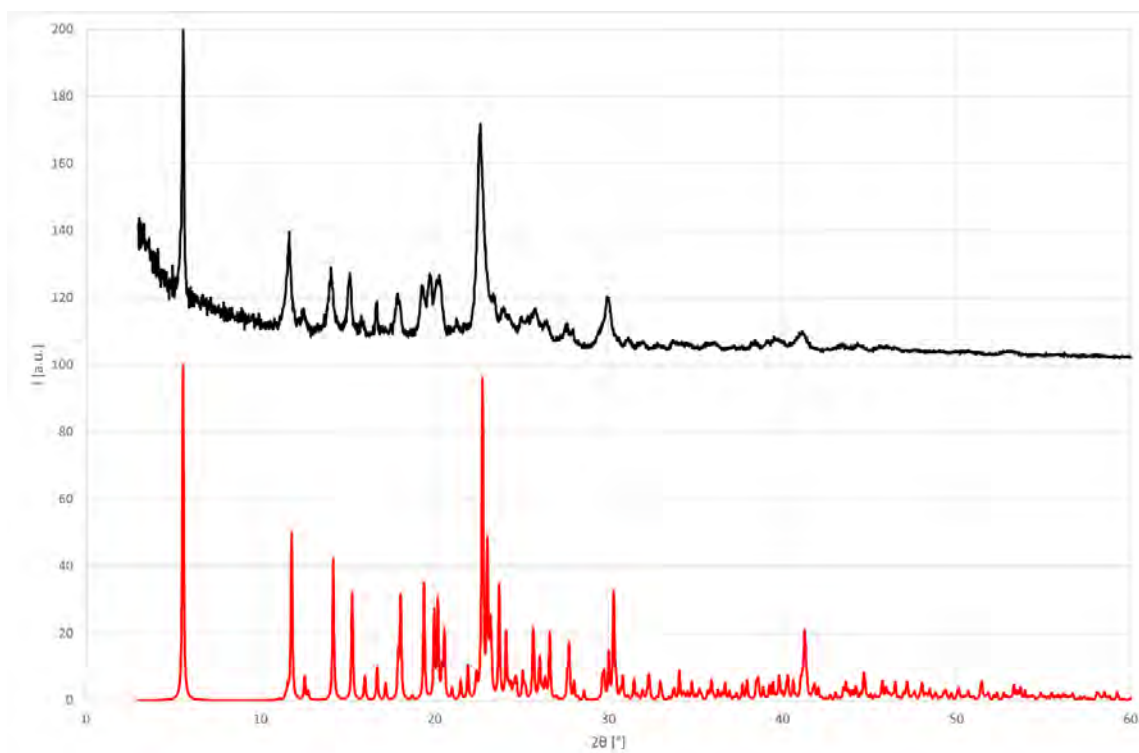


Figure S78. PXRD pattern after grinding equal amounts of DMAP and solution prepared XB complex **3a** under LAG conditions (EtOAc) for 5 min (black) and comparison with simulated PXRD patterns of symmetric iodine(I) complex **4a** obtained from solution (red).

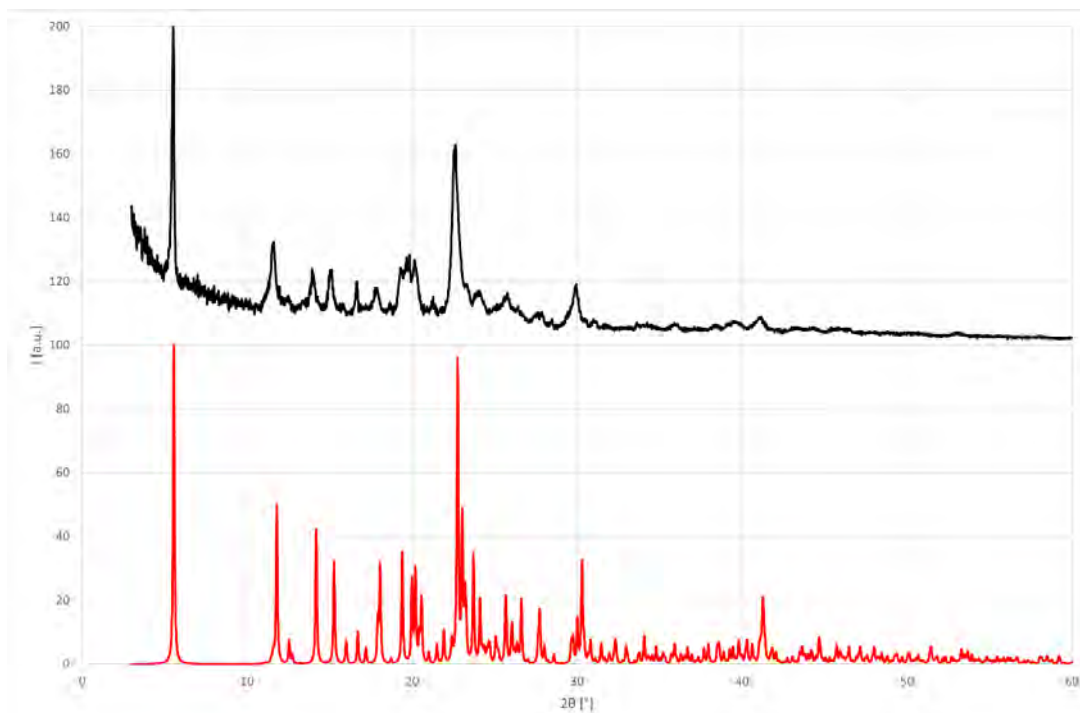


Figure S79. PXRD pattern after grinding equal amounts of NISac and DMAP under LAG conditions (EtOAc) for 5 min, then adding another equivalent of DMAP and another grinding for 5 min under LAG (EtOAc) conditions (black) and comparison with simulated PXRD patterns of symmetric iodine(I) complex **4a** obtained from solution (red).

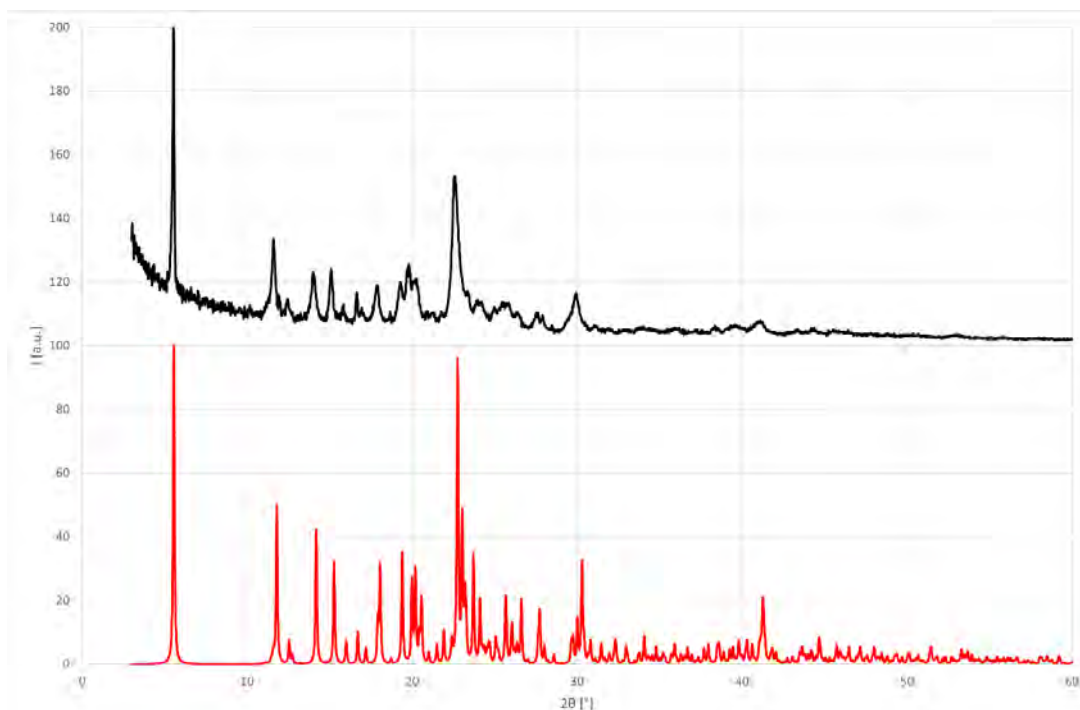


Figure S80. PXRD pattern after grinding 1 equivalent of NISac and 2 equivalents of DMAP under LAG conditions (EtOAc) for 5 min (black) and comparison with simulated PXRD patterns of symmetric iodine(I) complex **4a** obtained from solution (red).

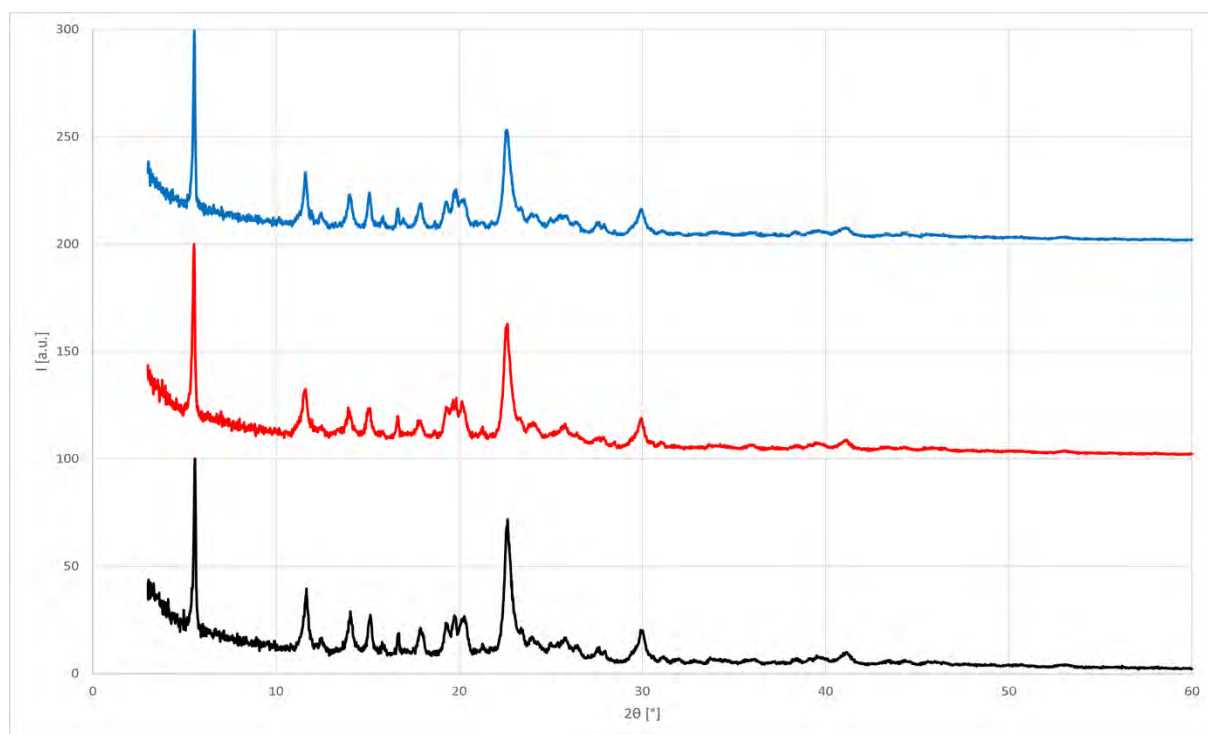


Figure S81. Comparison of the PXRD pattern of the developed methods for the preparation of symmetric iodine(I) complex **4a**. Black: Grinding solution made XB complex **3a** and DMAP, red: two step synthesis, blue: one-pot synthesis.

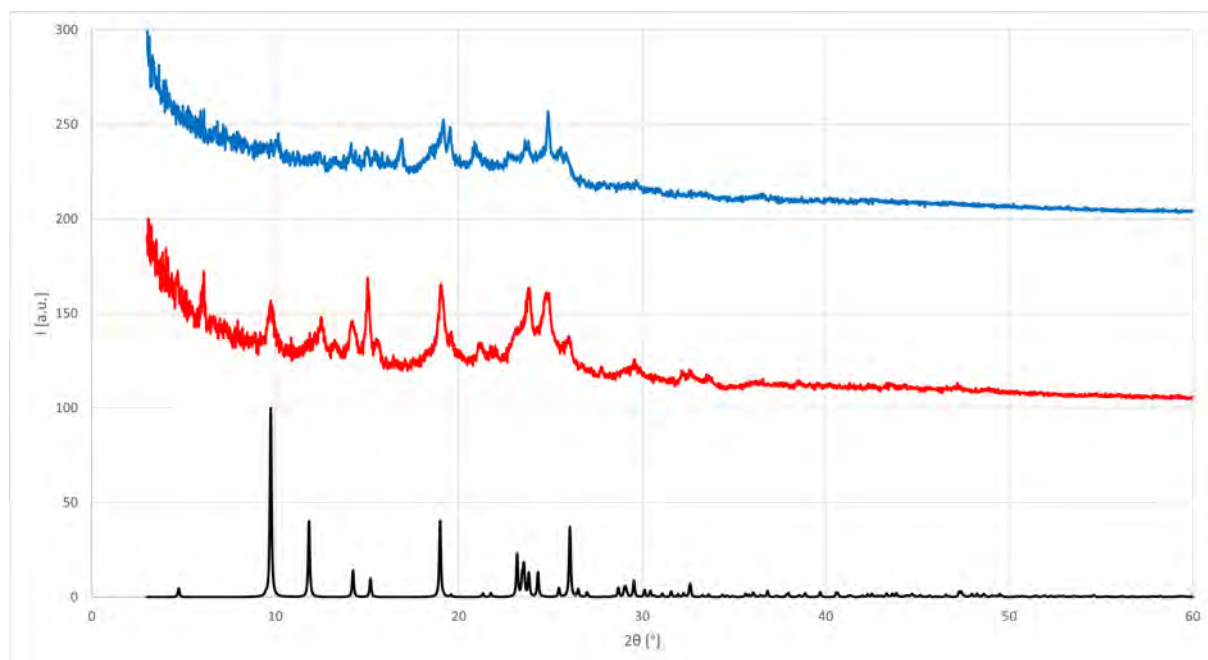


Figure S82. PXRD pattern after grinding equal amounts of MPY and solution prepared XB complex **3c** under LAG conditions (EtOAc) for 5 min (red), after grinding 1 equivalent of NISac and 2 equivalents of MPY under LAG conditions (EtOAc) for 5 min (blue), and comparison with simulated PXRD pattern of symmetric iodine(I) complex **4c** obtained from solution (black).

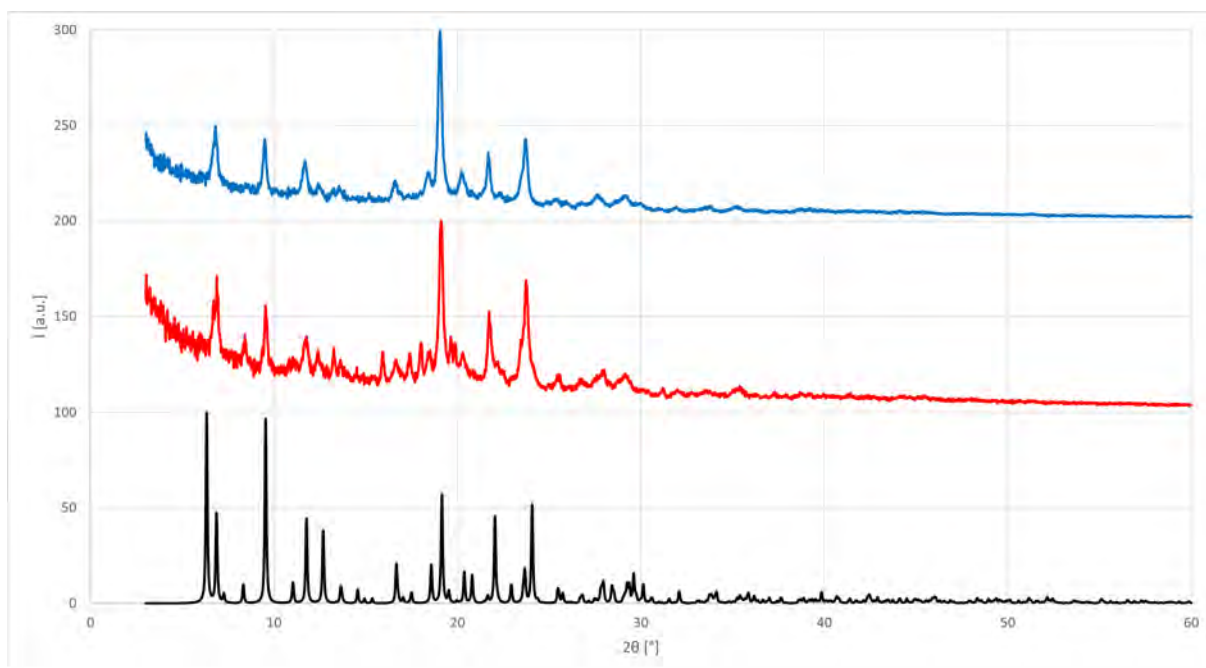


Figure S83. PXR D pattern after grinding equal amounts of PiPY and solution prepared XB complex **3d** under LAG conditions (EtOAc) for 5 min (red), after grinding 1 equivalent of NISac and 2 equivalents of PiPY under LAG conditions (EtOAc) for 5 min (blue), and comparison with simulated PXR D pattern of symmetric iodine(I) complex **4d** obtained from solution (black).

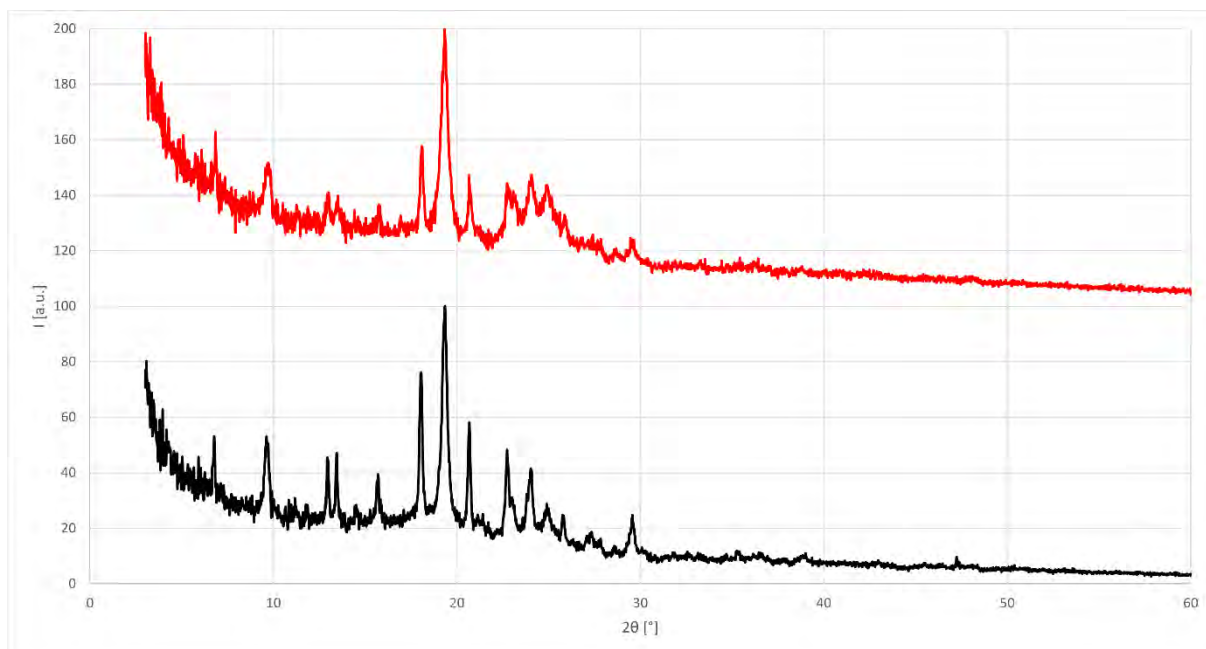


Figure S84. PXR D pattern after grinding equal amounts of PPY and solution prepared XB complex **3b** under LAG conditions (EtOAc) for 5 min (red), after grinding 1 equivalent of NISac and 2 equivalents of PPY under LAG conditions (EtOAc) for 5 min (black).

6 General Synthetic Procedures and Scale-Up Experiments

6.1 General Procedure 1 (GP1) – Microwave-assisted Synthesis of 4-Substituted Pyridines

A literature adjusted procedure was used.⁷ A 10 mL microwave tube equipped with a magnetic stirring bar was charged with 4-chloropyridine hydrochloride (225.0 mg, 1.50 mmol, 1.00 equiv.) and the chosen secondary amine (9.00 mmol, 6.00 equiv.). Then, water (1 mL) was added, and the reaction mixture was irradiated with 150 W for 30 min at 130 °C. After cooling down to rt, the resulting mixture was partitioned between DCM (50 mL) and 2M Na₂CO₃ solution (10 mL). The organic phase was dried over MgSO₄, filtered and the pyridine derivative was purified by running a dry loaded column chromatography.

6.2 General Procedure 2 (GP2) – Solution Synthesis of XB Complexes using DMAP, MPY, PiPY

A 4 mL vial was charged with NISac (100.0 mg, 0.324 mmol, 1.00 equiv.), which was dissolved in EtOAc (1.5 mL). A second 4 mL vial was charged with the chosen pyridine derivative (0.324 mmol, 1.00 equiv.), which was dissolved in EtOAc (1.5 mL). Then, the solutions were combined, shaken and the precipitate was collected on a Büchner filter. The solid was washed with cold Et₂O and dried in a stream of air to yield the desired XB complex.

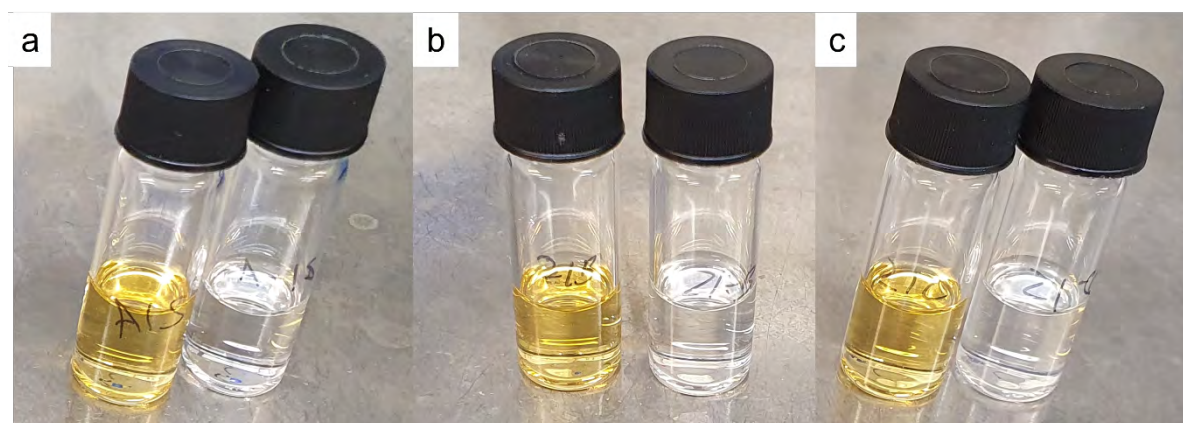


Figure S85. Solutions of NISac (always left side, clear yellow) and pyridine derivatives: a) DMAP, b) MPY, c) PiPY in EtOAc before they were combined.

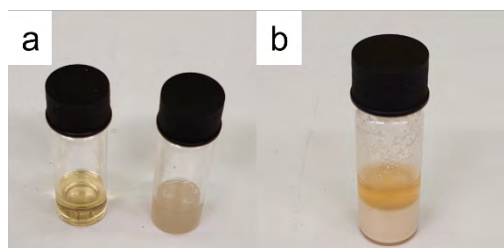


Figure S86. Solution of a) NISac (left side, clear yellow) and PPY (self-made, right side, slightly cloudy), b) precipitated [NISac-PPY] after the solutions were combined.

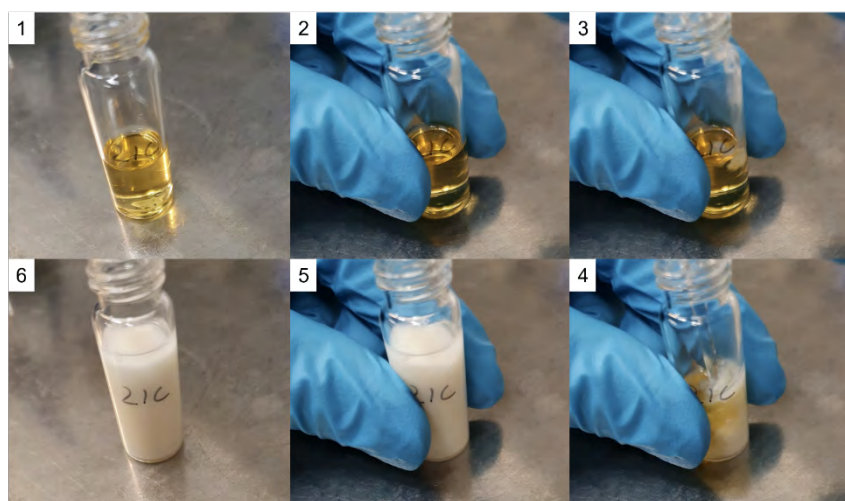


Figure S87. Time leap of the XB complex formation exemplified for [NISac-PiPY] (1: NISac solution (EtOAc), 2–5: addition of MPY solution (EtOAc), 6: precipitated XB complex).

6.3 Scale-Up Experiments

Using DMAP (1 mmol Approach)

A 50 mL round bottom flask equipped with a magnetic stirring bar was charged with NISac (309.0 mg, 1.00 mmol, 1.00 equiv.), which was dissolved in EtOAc (25 mL) under stirring at rt. A 10 mL screw cap vial equipped with a magnetic stirring bar was charged with DMAP (122.0 mg, 1.00 mmol, 1.00 equiv.) and dissolved in EtOAc (2 mL) under stirring at rt. Then, the DMAP solution was added in one portion to the NISac solution. The reaction mixture was heavily stirred and the XB complex precipitated immediately. After 5 min, the precipitate was filtered off using a Büchner filter, washed with cold Et₂O and dried in a stream of air to yield the desired XB complex as a white solid (376.2 mg, 0.872 mmol, 87%).

Using PPY

A 100 mL round bottom flask equipped with a magnetic stirring bar was charged with PPY (commercial source, 94.5 mg, 0.638 mmol, 1.00 equiv.) and DCM (10 mL). The reaction mixture was stirred at rt

until everything was dissolved. Then, it was filtered over a short plug of cotton into a 15 mL vial. Next, a 4 mL vial was charged with NISac (197.1 mg, 0.638 mmol, 1.00 equiv.), which was dissolved in EtOAc (2 mL). The solutions were combined, shaken and stored at rt overnight for precipitation. The next day, the precipitate was filtered off using a Büchner funnel, washed with cold Et₂O and dried in a stream of air to yield the desired XB complex as yellow crystals. (73.9 mg, 0.171 mmol, 68%).

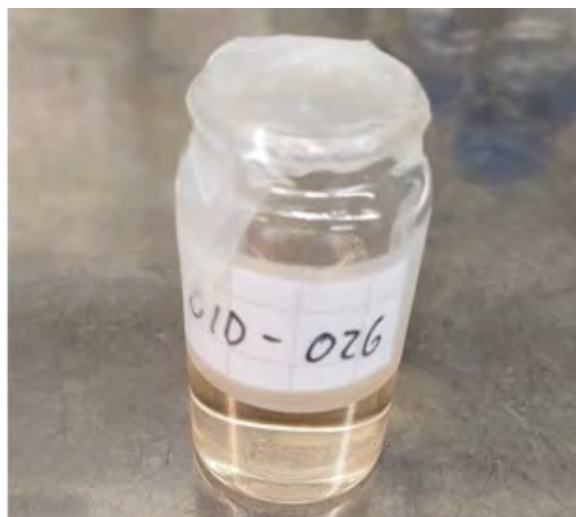


Figure S88. Starting XB complex precipitation of [NISac-PPY] 5 min after combination of the solutions.

6.4 General Procedure 3 (GP3) – Ex-situ Analysis of the XB Complex Formation by IR and PXRD Analysis

An agate mortar was charged with the NISac (25.3 mg, 0.082 mmol, 1.00 equiv.) and the corresponding pyridine derivative (0.082 mmol, 1.00 equiv.). The reaction mixture was ground for *n* cycles of 1 min. If used, one drop of the chosen solvent was added before each grinding cycle. Aliquots were taken for IR and PXRD analysis after the indicated time.

6.5 General Procedure 4 (GP4) – Mechanochemical Synthesis of the XB Complexes (Mortar and Pestle)

An agate mortar was charged with the NISac (25.3 mg, 0.082 mmol, 1.00 equiv.) and the corresponding pyridine derivative (0.082 mmol, 1.00 equiv.). A drop of EtOAc was added and the reaction mixture ground for 1 min. This was repeated 5 times to yield the desired XB complex quantitatively.

6.6 General Procedure 5 (GP5) – Mechanochemical Synthesis of XB Complex [NISac-DMAP] (Planetary Mill)

A 12 mL agate milling vessel equipped with 3 balls (10 mm in Ø) of the same material was charged with NISac (61.8 mg, 0.2 mmol, 1.00 equiv.) and DMAP (24.4 mg, 0.2 mmol, 1.00 equiv.). Then, a drop

of EtOAc was added, the jar was closed and milled for 1 min at 400 rpm. This cycle was repeated 5 times to yield the corresponding XB complex quantitatively.

If the same conditions were applied using a neat grinding approach the product was observed, but not quantitatively.

6.7 General Procedure 6 (GP6) – Ex-situ Analysis of the Iodonium Complex Formation by IR and PXRD Analysis

A: Starting from Solution Made XB Complex

An agate mortar was charged with the [NISac-DMAP] (20.0 mg, 0.046 mmol, 1.00 equiv.) and DMAP (5.7 mg, 0.046 mmol, 1.00 equiv.). The reaction mixture was ground for n cycles of 1 min. If used, one drop of the chosen solvent was added before each grinding cycle. Aliquots were taken for IR and PXRD analysis.

Note: The same procedure and stoichiometries apply for the complexes based on the other pyridine derivatives PPY, MPY, and PiPY. For MPY and PiPY the successful synthesis is shown by the comparison of IR spectra and PXRD pattern of the crystals obtained in the crystallization approaches.

B: Starting from Mechanochemically Made XB Complex

An agate mortar was charged with NISac (25.3 mg, 0.082 mmol, 1.00 equiv.) and DMAP (10.0 mg, 0.082 mmol, 1.00 equiv.). The reaction mixture was ground for 5 cycles of 1 min adding a drop of EtOAc prior to each cycle to obtain the desired XB complex quantitatively. Then, DMAP (10.0 mg, 0.082 mg, 1.00 equiv.) was added, and the reaction mixture was ground for n cycles of 1 min. If used, one drop of the chosen solvent was added before each grinding cycle. Aliquots were taken for IR and PXRD analysis.

Note: This was only demonstrated for DMAP as proof-of-concept.

C: Starting from NISac and DMAP

An agate mortar was charged with the NISac (25.3 mg, 0.082 mmol, 1.00 equiv.) and DMAP (20.0 mg, 0.164 mmol, 2.00 equiv.). The reaction mixture was ground for n cycles of 1 min. If used, one drop of the chosen solvent was added before each grinding cycle. Aliquots were taken for IR and PXRD analysis.

Note: The same procedure and stoichiometries apply for the complexes based on the other pyridine derivatives PPY, MPY, and PiPY. For MPY and PiPY the successful synthesis is shown by the comparison of IR spectra and PXRD pattern of the crystals obtained in the crystallization approaches.

6.8 General Procedure 7 (GP7) – Mechanochemical Synthesis of [I(DMAP)₂]NSac

A 12 mL agate vessel equipped with 3 balls (10 mm in Ø) of the same material was charged with NISac (61.8 mg, 0.20 mmol, 1.00 equiv.) and DMAP (48.9 mg, 0.40 mmol, 2.00 equiv.). Then, a drop of EtOAc was added, the jar was closed and milled for 1 min at 400 rpm. This cycle was repeated 5 times to yield the corresponding iodonium complex quantitatively.

1 mmol Approach:

The same protocol can be applied for a larger synthesis using NISac (309.1 mg, 1.00 mmol, 1.00 equiv.) and DMAP (244.3 mg, 2.00 mmol, 2.00 equiv.) to yield the desired iodonium complex quantitatively.

6.9 General Procedure 8 (GP8) – Iodination of Antipyrine (Solution)

A 10 mL screw cap vial equipped with a magnetic stirring bar was charged with antipyrine (37.6 mg, 0.2 mmol, 1.00 equiv.), which was dissolved in DCM (3 mL). Then, the electrophilic iodination reagent (0.2 mmol, 1.00 equiv.) was added, the vial closed, and the reaction mixture was stirred for 1 h at rt. Afterwards, the reaction mixture was separated between DCM and an aqueous (aq.) saturated (sat.) NaHCO₃ solution (each 10 mL). After phase separation, the aq. phase was extracted twice with DCM (20 mL), the organic phases combined, and dried over Na₂SO₄. The product was purified by column chromatography.

6.10 General Procedure 9 (GP9) – Iodination of Antipyrine (Planetary Mill)

A 12 mL agate vessel equipped with 10 milling balls (5 mm in Ø) of the same material was charged with the electrophilic iodination reagent (0.2 mmol, 1.00 equiv.) and antipyrine (37.6 mg, 0.20 mmol, 1.00 equiv.). Then, the reaction mixture was milled for 4 cycles consisting of 15 min milling time, a break of 5 min and reversing the milling direction with each cycle. The reaction mixture was separated between DCM and an aq. sat. NaHCO₃ solution (each 10 mL). After phase separation, the aq. phase was extracted twice with DCM (20 mL), the organic phases combined, and dried over Na₂SO₄. The product was purified by column chromatography.

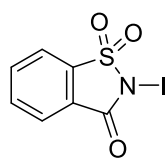
1 mmol Approach:

The same protocol can be applied for a larger synthesis using antipyrine (188 mg, 1.00 mmol, 1.00 equiv.) and 1.00 mmol of the selected iodination reagent.

7 Analytical Data

7.1 Starting Materials

N-Iodosaccharin (1)



A 100 mL round bottom flask wrapped in aluminum foil, equipped with a magnetic stirring bar was charged with saccharin (1000 mg, 5.46 mmol, 1.00 equiv.), PIDA (1088 mg, 3.28 mmol, 0.60 equiv.), and iodine (901 mg, 3.55 mmol, 0.65 equiv.) in the given order. Then, CHCl_3 (20 mL) were added at the reaction mixture was stirred at ambient temperature for 6 h followed by another hour at 0 °C using an ice bath. The precipitate was filtered off using a Büchner filter funnel (porosity 3 glass frit) with a 125 mL capacity. It was washed with cold CHCl_3 until colorless and dried in a stream of air. The mother lye was stored in the freezer to precipitate more product, which was treated as above. The precipitates were combined and further dried in vacuo at 40 °C using a rotary evaporator to yield the product as colorless solid (1259 mg, 4.07 mmol, 75%).

mp: turned yellow during heating, orange around 175 °C, 190.0°C (decomp.).

^1H NMR (600 MHz, CDCl_3) δ (ppm): 8.11 (d, $J = 7.7$ Hz, 1H), 8.05 (d, $J = 7.5$ Hz, 1H), 7.99 (t, $J = 7.5$ Hz, 1H), 7.95 (m, 1H).

$^{13}\text{C}\{^1\text{H}\}$ NMR (151 MHz, CD_2Cl_2) δ (ppm): 162.4 (HMBC)*, 140.3, 135.6, 135.2, 128.4, 126.0, 122.2.

IR (ATR) $\tilde{\nu}$ (cm^{-1}): 3878, 3456, 3095, 2232, 2106, 2008, 1964, 1849, 1720, 1624, 1588, 1457, 1302, 1223, 1183, 1159, 1119, 1053, 962, 787, 750, 665.

CI-MS (100 eV, methane) m/z : 310 (56) $[M+H]^+$, 184 (65) $[\text{Saccharin}+H]^+$.

EI-MS (70 eV) m/z : 309 (100) $[M]^+$, 254 (11), 229 (16), 127 (11), 118 (10), 90 (18), 76 (19), 50 (14).

CHN: Anal. Calcd for $\text{C}_7\text{H}_6\text{INO}_4\text{S}$ (NISac· H_2O): C, 25.70; H, 1.85; N, 4.28. Found C, 25.73; H, 1.76; N, 4.25.

The NMR spectroscopic data are in accordance with the literature.⁸

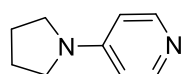
* Detected by ^1H - ^{13}C HMBC NMR spectroscopy

Elemental analysis of commercially available NISac that confirms the presence of a hydrate:

CHN: Anal. Calcd for $\text{C}_7\text{H}_4\text{INO}_3\text{S}$ (NISac): C, 27.20; H, 1.30; N, 4.53. Found C, 25.76; H, 1.71; N, 4.29.

CHN: Anal. Calcd for $\text{C}_7\text{H}_6\text{INO}_4\text{S}$ (NISac· H_2O): C, 25.70; H, 1.85; N, 4.28. Found C, 25.76; H, 1.71; N, 4.29.

4-Pyrrolidinopyridine (2b)



The title compound was prepared following GP1 using 4-chloropyridine hydrochloride (225.0 mg, 1.50 mmol, 1.00 equiv.) and pyrrolidine (0.75 mL, 8.98 mmol, 5.99 equiv.). The product was obtained as slightly yellow solid (196.0 mg, 1.32 mmol, 88%) after column chromatography ($\text{DCM}:\text{MeOH}$ 3:1→2:1→1:1).

mp: 49.4–52.0 °C.

¹H NMR (600 MHz, CD₂Cl₂) δ (ppm): 8.12 (m, 2H), 6.37 (m, 2H), 3.29 (m, 4H), 2.01 (m, 4H).

¹³C{¹H} NMR (151 MHz, CD₂Cl₂) δ (ppm): 152.3, 149.7, 107.4, 47.5, 25.8.

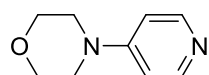
IR (ATR) $\tilde{\nu}$ (cm⁻¹): 3192, 3077, 3025, 2960, 2909, 2848, 2671, 2504, 2322, 2182, 2084, 1988, 1915, 1864, 1754, 1702, 1594, 1540, 1512, 1455, 1397, 1347, 1216, 1179, 1161, 1096, 987, 915, 863, 796.

CI-MS (100 eV, methane) m/z : 149 (100) [$M+H$]⁺, 148 (7) [M]⁺.

EI-MS (70 eV) m/z : 149 (100) [$M+H$]⁺, 148 (94) [M]⁺, 147 (100), 120 (11), 119 (20), 105 (12), 92 (12), 78 (14), 51 (14).

CHN: Anal. Calcd for C₉H₁₂N: C, 72.94; H, 8.16; N, 18.90. Found C, 71.02; H, 7.96; N, 18.45.

4-Morpholinopyridine (2c)



The title compound was prepared following GP1 using 4-chloropyridine hydrochloride (225.0 mg, 1.50 mmol, 1.00 equiv.) and morpholine (0.79 mL, 9.03 mmol, 6.02 equiv.). The product was obtained as slightly yellow solid (215.2 mg, 1.31 mmol, 87%) after column chromatography (EtOAc).

mp: 106.1–107.5 °C.

¹H NMR (400 MHz, CD₂Cl₂) δ (ppm): 8.27 (br s, 2H), 6.68 (d, J = 5.4 Hz, 2H), 3.80 (m, 4H), 3.25 (m, 4H).

¹³C{¹H} NMR (101 MHz, CD₂Cl₂) δ (ppm): 155.8, 150.8, 108.7, 66.9, 46.7.

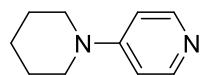
IR (ATR) $\tilde{\nu}$ (cm⁻¹): 3855, 3367, 3086, 2989, 2957, 2881, 2834, 2703, 2490, 2325, 2223, 2104, 2022, 1984, 1920, 1791, 1594, 1542, 1503, 1447, 1373, 1312, 1277, 1241, 1113, 1074, 1049, 987, 929, 859, 802, 737.

CI-MS (100 eV, methane) m/z : 165 (100) [$M+H$]⁺, 164 (9) [M]⁺.

EI-MS (70 eV) m/z : 165 (20) [$M+H$]⁺, 164 (100) [M]⁺, 106 (81), 105 (26), 78 (12), 51 (11).

CHN: Anal. Calcd for C₉H₁₂N₂O: C, 65.83; H, 7.37; N, 17.06. Found C, 65.52; H, 7.23; N, 17.17.

4-Piperidinopyridine (2d)



The title compound was prepared following GP1 using 4-chloropyridine hydrochloride (225.0 mg, 1.50 mmol, 1.00 equiv.) and piperidine (0.90 mL, 9.11 mmol, 6.07 equiv.). The product was obtained as yellow oil (205.1 mg, 1.26 mmol, 84%) after column chromatography (EtOAc).

¹H NMR (400 MHz, CD₂Cl₂) δ (ppm): 8.18 (br s, 2H), 6.65 (d, J = 5.6 Hz, 2H), 3.31 (m, 4H), 1.64 (m, 6H).

¹³C{¹H} NMR (101 MHz, CD₂Cl₂) δ (ppm): 155.5, 150.6, 108.8, 47.7, 25.7, 24.9.

IR (ATR) $\tilde{\nu}$ (cm⁻¹): 3858, 3391, 3086, 3027, 2989, 2931, 2853, 2507, 2325, 2088, 1994, 1916, 1592, 1538, 1508, 1446, 1392, 1361, 1244, 1126, 1023, 985, 924, 853, 803, 729.

CI-MS (100 eV, methane) m/z : 163 (100) $[M+H]^+$, 162 (11) $[M]^+$.

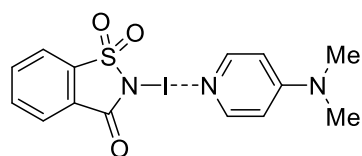
EI-MS (70 eV) m/z : 163 (100) $[M+H]^+$, 162 (95) $[M]^+$, 161 (100), 133 (11), 121 (16), 106 (19), 105 (13), 78 (11)

CHN: Anal. Calcd for $C_{10}H_{14}IN_2$: C, 74.03; H, 8.70; N, 17.27. Found C, 72.94; H, 8.50; N, 17.47.

7.2 Products

7.2.1 XB Complexes

NISac-DMAP (3a)



The title compound was prepared according to GP2 starting from NISac (100.0 mg, 0.324 mmol, 1.01 equiv.) and DMAP (39.4 mg, 0.322 mmol, 1.00 equiv.). The desired XB complex was obtained as a colorless solid (124.3 mg, 0.288 mmol, 89%).

mp: 160.9–163.4°C change from white to orange, 165.7–167.6 (decomp.).

1H NMR (600 MHz, CD_2Cl_2) δ (ppm): 8.18 (d, $J = 6.5$ Hz, 2H), 7.87 (m, 1H), 7.79 (m, 1H), 7.68 (m, 2H), 6.47 (m, 2H), 3.08 (s, 6H).

$^{13}C\{^1H\}$ NMR (151 MHz, CD_2Cl_2) δ (ppm): 155.9*, 152.2, 148.2, 133.6, 124.8, 120.9, 108.6, 39.9.

IR (ATR) $\tilde{\nu}$ (cm^{-1}): 3379, 3082, 2931, 2600, 2320, 2170, 2127, 2070, 2030, 1983, 19369, 1694, 1618, 1538, 1450, 1390, 1333, 1291, 1214, 1156, 1130, 1059, 1010, 958, 805, 778, 748, 707, 671.

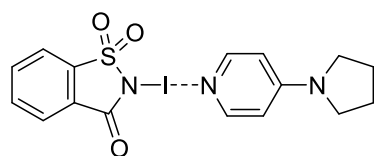
CI-MS (100 eV, methane) m/z : 310 (11) $[NISac+H]^+$, 184 (63) $[Saccharin+H]^+$, 183 (100) $[Saccharin]^+$, 123 (47) $[DMAP+H]^+$.

EI-MS (70 eV) m/z : 309 (88) $[NISac]$, 254 (27), 229 (15), 183 (20), 127 (16), 123 (14), 122 (100) $[DMAP]$, 121 (93), 94 (11), 92 (10), 90 (16), 78 (10), 76 (26), 51 (15), 50 (23).

CHN: Anal. Calcd for $C_{14}H_{14}IN_3O_3S$: C, 38.99; H, 3.27; N, 9.74. Found C, 39.01; H, 3.24; N, 9.67.

*Due to the low concentration caused by the low solubility, it was only detectable by 1H - ^{13}C HMBC NMR spectroscopy and more signals (the quaternary carbon atoms of the saccharin scaffold) are expected but could not be detected. The identity of the structure is confirmed by the other analytical data as well as the X-ray crystal structure.

NISac-PPY (3b)



The title compound was prepared according to GP2 starting from NISac (61.8 mg, 0.20 mmol, 1.00 equiv.) and PPY (29.6 mg, 0.20 mmol, 1.00 equiv.). The desired XB complex was obtained as a slightly yellowish solid (73.9 mg, 0.162 mmol, 81%).

mp: 139.2–144.1 °C (decomp.).

¹H NMR (600 MHz, CD₂Cl₂) δ (ppm): 8.16 (d, J = 6.5 Hz, 2H), 7.87 (m, 1H), 7.79 (m, 1H), 7.68 (m, 2H), 6.36 (d, J = 6.5 Hz, 2H), 3.37 (m, 4H), 2.06 (m, 4H).

¹³C{¹H} NMR (151 MHz, CD₂Cl₂) δ (ppm): 148.0, 133.5, 124.8, 120.8, 109.1, 48.26, 25.8.*

IR (ATR) $\tilde{\nu}$ (cm⁻¹): 3855, 3355, 3074, 2961, 2919, 2863, 2569, 2322, 2108, 1993, 1899, 1737, 1682, 1611, 1530, 1457, 1410, 1297, 1234, 1210, 1156, 1123, 1056, 1008, 946, 814, 772, 752, 706, 671.

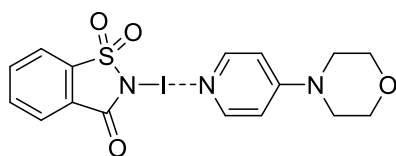
CI-MS (100 eV, methane) m/z : 310 (1) [NISac+H]⁺, 184 (100) [Saccharin+H]⁺, 149 (36) [PPY+H]⁺.

EI-MS (70 eV) m/z : 309 (32) [NISac], 254 (57), 183 (66), 164 (12), 149 (13), 148 (100) [PPY], 147 (99), 127 (21), 120 (36), 119 (52), 107 (11), 106 (19), 105 (22), 104 (14), 93 (10), 92 (38), 78 (23), 76 (46), 74 (12), 51 (24), 50 (34).

CHN: Anal. Calcd for C₁₆H₁₆IN₃O₃S: C, 42.03; H, 3.53; N, 9.19. Found C, 41.33; H, 3.32; N, 9.11.

* More signals (the quaternary carbon atoms of the saccharin scaffold) are expected but could not be detected, due to the low concentration caused by the low solubility. The identity of the structure is confirmed by the other analytical data as well as the X-ray crystal structure.

NISac-MPY (3c)



The title compound was prepared according to GP2 starting from NISac (100.1 mg, 0.324 mmol, 1.00 equiv.) and MPY (53.0 mg, 0.323 mmol, 1.00 equiv.). The desired XB complex was obtained as a colorless solid (138.6 mg, 0.293 mmol, 91%).

mp: 151.9–154.0 °C (decomp.).

¹H NMR (600 MHz, CD₂Cl₂) δ (ppm): 8.25 (d, J = 6.9 Hz, 2H), 7.88 (m, 1H), 7.79 (m, 1H), 7.69 (m, 2H), 6.64 (d, J = 6.5 Hz, 2H), 3.80 (m, 4H), 3.42 (t, J = 5.1 Hz, 4H).

¹³C{¹H} NMR (151 MHz, CD₂Cl₂) δ (ppm): 156.3, 148.8, 133.6, 124.9, 120.9, 109.4, 66.5, 46.2.*

IR (ATR) $\tilde{\nu}$ (cm⁻¹): 3086, 2981, 2865, 2583, 2324, 2149, 2111, 1907, 1740, 1680, 1616, 1514, 1454, 1384, 1335, 1300, 1278, 1258, 1228, 1162, 1126, 1071, 1007, 954, 872, 809, 779, 756, 711, 674.

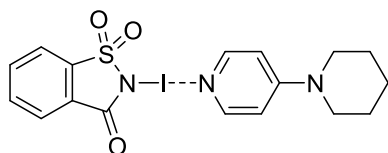
CI-MS (100 eV, methane) m/z : 310 (4) [NISac+H]⁺, 184 (100) [Saccharin+H]⁺, 165 (67) [MPY+H]⁺.

EI-MS (70 eV) m/z : 309 (59) [NISac], 254 (21), 229 (10), 183 (12), 165 (25), 164 (100) [MPY], 127 (12), 106 (62), 105 (20), 90 (10), 78 (10), 76 (14), 51 (10), 50 (12).

CHN: Anal. Calcd for C₁₆H₁₆IN₃O₄S: C, 40.60; H, 3.41; N, 8.88. Found C, 40.45; H, 3.20; N, 8.71.

* More signals (the quaternary carbon atoms of the saccharin scaffold) are expected but could not be detected, due to the low concentration caused by the low solubility. The identity of the structure is confirmed by the other analytical data as well as the X-ray crystal structure.

NISac-PiPY (3d)



The title compound was prepared according to GP2 starting from NISac (100.0, 0.324 mg, 1.00 equiv.) and PiPY (52.6 mg, 0.324 mmol, 1.00 equiv.). The desired XB complex was obtained as a colorless solid (130.1 mg, 0.276 mmol, 85%).

mp: 133.3–134.3 °C (decomp.).

¹H NMR (600 MHz, CD₂Cl₂) δ (ppm): 8.15 (d, J = 6.5 Hz, 2H), 7.87 (dd, J = 6.1, 2.4 Hz, 1H), 7.78 (m, 1H), 7.68 (m, 2H), 6.58 (m, 2H), 3.46 (m, 4H), 1.71 (m, 2H), 1.66 (m, 4H).

¹³C{¹H} NMR (151 MHz, CD₂Cl₂) δ (ppm): 165.0, 155.5, 148.6, 141.5, 133.6, 130.8, 124.8, 120.8, 109.3, 47.7, 25.7, 24.5.

IR (ATR) $\tilde{\nu}$ (cm⁻¹): 3358, 3220, 3061, 2935, 2860, 2578, 2322, 2065, 1998, 1903, 1735, 1683, 1611, 1526, 1456, 1413, 1332, 1306, 1276, 1218, 1158, 1124, 1063, 1024, 996, 948, 855, 808, 774, 751, 707, 672.

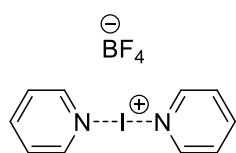
CI-MS (100 eV, methane) m/z : 310 (2) [NISac+H]⁺, 184 (100) [Saccharin+H]⁺, 163 (100) [PiPY+H]⁺.

EI-MS (70 eV) m/z : 309 (22) [NISac], 254 (42), 183 (32), 163 (15), 162 (87) [PiPY], 161 (100), 133 (10), 127 (11), 121 (15), 120 (12), 119 (14), 106 (21), 105 (15), 78 (12), 76 (17), 51 (10), 50 (12).

CHN: Anal. Calcd for C₁₇H₁₈IN₃O₃S: C, 43.32; H, 3.85; N, 8.92. Found C, 43.24; H, 3.71; N, 8.86.

7.2.2 Iodine(I) Complexes

[Bis(pyridine)iodine(I)]tetrafluoroborate – Barluenga's reagent



The title compound was prepared following a modified literature procedure.⁹ A 500 mL round bottom flask equipped with a magnetic stirring bar was charged with deionized water (50 mL). Then, HBF₄ (50% in water, 6.27 mL, 50.0 mmol, 1.00 equiv.) was added using a syringe and the solution was stirred for 2 min at rt. Next, Ag₂CO₃ (6894 mg, 25.0 mmol, 0.50 equiv.) was added in portions over 2 min at rt. The flask was wrapped in aluminum foil, and the reaction mixture was stirred at ambient temperature until all solids were dissolved. Afterwards, 10 g of silica gel were added, and the mixture was further stirred for 5 min. Then, the water was evaporated using a rotary evaporator until a slightly grey, free-floating

powder (AgBF₄@SiO₂) was observed. After cooling down to rt, the powder was suspended in 300 mL DCM and pyridine (8.09 mL, 100.0 mmol, 2.00 equiv.) was added. The suspension was stirred for 2 min at rt. Then, iodine (12691 mg, 50.0 mmol, 1.00 equiv.) was added in one portion, and the mixture was stirred for 1 h at ambient temperature protected from light. Afterwards, the reaction mixture was filtered over a Büchner filter funnel (porosity 3 glass frit, 125 mL capacity). The flask was washed with additional DCM and the filter cake was rinsed with DCM (100 mL). The solvent was removed under reduced pressure to yield a deep red solid. The solid was dissolved in DCM (100 mL) and placed in an ice bath. After 5 min, Et₂O (200 mL) were added, and a white precipitate started to form. After 10 min in the ice bath, the white precipitate was filtered off using a Büchner filter funnel (porosity 3 glass frit, 125 mL capacity) and was washed with ice cold Et₂O (100 mL) to remove remaining iodine. The mother lye was concentrated, and the precipitation procedure was repeated once. The precipitates were combined, dried in a stream of air for 10 min and further dried overnight in a vacuum desiccator to yield the product as fluffy, yellow powder (11774 mg, 31.7 mmol, 63%).

mp: 151.6 °C (turned into a wax like state), 168.9 °C (decomp.).

¹H NMR (400 MHz, CD₃CN) δ (ppm): 8.81 (d, J = 5.5 Hz, 4H), 8.28 (m, 2H), 7.66 (t, J = 6.8 Hz, 4H).

¹³C{¹H} NMR (101 MHz, CD₃CN) δ (ppm): 150.7, 143.3, 128.9.

¹¹B NMR (128 MHz, CD₃CN) δ (ppm): -1.16 (s).

¹⁹F NMR (376 MHz, CD₃CN) δ (ppm): -151.77 (s, ¹⁰BF₄⁻), -151.83 (s, ¹¹BF₄⁻).

IR (ATR) $\tilde{\nu}$ (cm⁻¹): 3079, 2326, 2080, 1930, 1654, 1600, 1452, 1352, 1287, 1249, 1205, 1161, 1094, 1042, 1004, 757, 685.

CI-MS (100 eV, methane) m/z : 207 (17) [Pyridine+HI]⁺, 80 (100) [Pyridine+H]⁺.

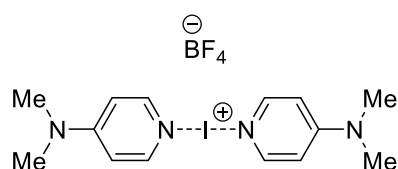
EI-MS (70 eV) m/z : 254 (63), 203 (10), 127 (21), 79 (100) [Pyridine], 78 (12), 52 (60), 51 (30), 50 (22), 49 (18).

ESI-MS (ESI) m/z : [M]⁺ calcd for C₁₀H₁₀IN₂ [Py-I-Py]⁺, 284.9883 found, 284.9884.

CHN: Anal. Calcd for C₁₀H₁₀BF₄IN₂: C, 32.30; H, 2.71; N, 7.53. Found C, 32.02; H, 2.74; N, 7.38.

The NMR spectroscopic data are in accordance with the literature.⁹

{Bis-[4-(dimethylamino)pyridine]iodine(I)} tetrafluoroborate



The title compound was prepared following a modified literature procedure.⁹ A 250 mL round bottom flask equipped with a magnetic stirring bar was charged with deionized water (15 mL). Then, HBF₄

(8 mol/L in water, 1.88 mL, 15.0 mmol, 1.00 equiv.) was added using a syringe and the solution was stirred for 2 min at rt. Next, Ag_2CO_3 (2068 mg, 7.50 mmol, 0.50 equiv.) was added in portions over 2 min at rt. The flask was wrapped in aluminum foil, and the reaction mixture was stirred at ambient temperature until all solids were dissolved. Afterwards, 3 g of silica gel were added, and the mixture was further stirred for 5 min. Then, the water was evaporated using a rotary evaporator until a slightly grey, free-floating powder ($\text{AgBF}_4@\text{SiO}_2$) was observed. After cooling down to rt, the powder was suspended in DCM (90 mL) and DMAP (3702 mg, 30.0 mmol, 2.00 equiv.) was added. The suspension was stirred for 2 min at rt. Then, iodine (3807 mg, 15.0 mmol, 1.00 equiv.) was added in one portion, and the mixture was stirred for 1 h at ambient temperature protected from light. Afterwards, the reaction mixture was filtered over a Büchner filter funnel (porosity 3 glass frit, 125 mL capacity). The flask was washed with additional DCM and the filter cake was rinsed with DCM (100 mL). The solvent was removed under reduced pressure to yield a deep red solid. The solid was dissolved in DCM (100 mL) and placed in an ice bath. After 5 min, Et_2O (100 mL) were added, and a white precipitate started to form. After 10 min in the ice bath, the white precipitate was filtered off using a Büchner filter funnel (porosity 3 glass frit, 125 mL capacity) and was washed with ice cold Et_2O (50 mL) to remove remaining iodine. The mother lye was concentrated, and the precipitation procedure was repeated once. The precipitates were combined, dried in a stream of air for 10 min and further dried overnight in a vacuum desiccator. NMR analysis revealed a mixture of the corresponding Ag(I) and iodine(I) complexes. To fully convert the silver complex, all precipitate was transferred to a 500 mL round bottom flask equipped with a magnetic stirring bar and dissolved in DCM (200 mL). Then iodine (850 mg, 3.35 mmol, 0.22 equiv.) was added in one portion and the reaction mixture was stirred at rt protected from light for 90 min. The precipitated AgI was filtered off using a Büchner filter funnel (porosity 3 glass frit, 125 mL capacity) and washed with additional DCM (50 mL) to complete the transfer. The filtrate was concentrated using a rotary evaporator. Then, it was dissolved in DCM (150 mL) under slight heating using a water bath (40 °C). When everything was dissolved, it was placed in an ice bath and Et_2O (100 mL) were added. After 15 min stirring in the ice bath, the precipitate was filtered off using a Büchner filter funnel (porosity 3 glass frit, 125 mL capacity) and was washed with additional Et_2O (50 mL). The precipitate was dried in a stream of air, then further in vacuo. The precipitation procedure using Et_2O was repeated for the mother lye. The precipitates were combined to yield the product as beige solid (4019 mg, 8.77 mmol, 59%).

mp: turned yellow during heating, 136.1–139.3 °C (decomp.).

^1H NMR (600 MHz, CD_2Cl_2) δ (ppm): 8.06 (m, 4H), 6.51 (m, 4H), 3.10 (s, 12H).

$^{13}\text{C}\{^1\text{H}\}$ NMR (151 MHz, CD_2Cl_2) δ (ppm): 156.1, 147.1, 109.0, 40.0.

^{11}B NMR (192 MHz, CD_2Cl_2) δ (ppm): -1.15 (s).

^{19}F NMR (564 MHz, CD_2Cl_2) δ (ppm): -153.30 (s, $^{10}\text{BF}_4^-$), -151.35 (s, $^{11}\text{BF}_4^-$).

IR (ATR) $\tilde{\nu}$ (cm⁻¹): 3628, 3552, 3115, 3061, 2928, 2601, 2298, 2159, 2035, 1766, 1619, 1542, 1447, 1392, 1344, 1303, 1221, 1052, 1007, 811, 756, 657.

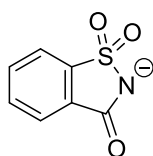
CI-MS (100 eV, methane) m/z : 371 (1) [I(DMAP)₂]⁺, 245 (16) [2DMAP+H]⁺, 123 (57) [DMAP+H]⁺.

EI-MS (70 eV) m/z : 254 (32), 248 (8) [DMAP+I]⁺, 127 (17), 123 (30), 122 (100) [DMAP]⁺, 121 (82), 83 (13), 51 (11).

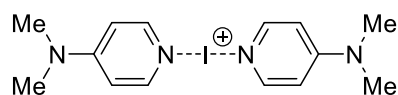
ESI-MS m/z : [*M*]⁺ calcd for C₁₀H₂₀IN₄ [I(DMAP)₂]⁺, 371.0727; found, 371.0717.

CHN: Anal. Calcd for C₁₄H₂₀BF₄IN₄: C, 36.71; H, 4.40; N, 12.23. Found C, 36.73; H, 4.44; N, 12.84.

[Bis(DMAP)iodine(I)] saccharinate (**4a**)



The title compound was prepared quantitatively following GP7 using NISac (309.1 mg, 1.00 mmol, 1.00 equiv.) and DMAP (244.3 mg, 2.00 mmol, 2.00 equiv.)



mp: turned yellow, then orange during heating, 143.6–146.3 (decomp.).

NMR: NMR data are not given as the title compound was too labile in solution.

IR (ATR) $\tilde{\nu}$ (cm⁻¹): 3753, 3541, 3260, 3108, 3068, 2924, 2822, 2603, 2288, 2215, 2160, 2095, 2010, 1987, 1943, 1896, 1768, 1722, 1615, 1540, 1447, 1390, 1336, 1250, 1220, 1143, 1054, 1008, 945, 810, 760, 703, 677.

CI-MS (100 eV, methane) m/z : 371 (1) [I(DMAP)₂]⁺, 123 (100) [DMAP+H]⁺, 122 [DMAP]⁺ (11).

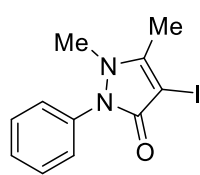
EI-MS (70 eV) m/z : 309 (43) [NISac], 254 (14), 123 (32) [DMAP+H]⁺, 122 (100) [DMAP], 121 (82), 50 (10).

ESI-MS m/z : [*M*]⁺ calcd for C₁₀H₂₀IN₄ [I(DMAP)₂]⁺, 371.0727; found, 371.0739.

CHN: Anal. Calcd for C₂₁H₂₄IN₅O₃S: C, 45.58; H, 4.37; N, 12.65. Found C, 45.52; H, 4.64; N, 12.80.

7.2.3 Iodinated Products

4-Iodoantipyridine (6)



The title compound was prepared following GP9 using antipyridine (37.6 mg, 0.20 mmol, 1.00 equiv.) and Barluenga's reagent (74.4 mg, 0.20 mmol, 1.00 equiv). After purification by column chromatography (SiO₂, EtOAc) it was obtained a colorless solid (57.1 mg, 0.182 mmol, 91%). The yield could be increased to 96%, when 3 agate balls (10 mm in Ø) were used.

R_f = 0.53 (EtOAc), UV-active.

mp: 159.1–160.2 °C.

¹H NMR (600 MHz, CDCl₃) δ (ppm): 7.44 (m, 2H), 7.36 (m, 2H), 7.29 (m, 1H), 3.13 (s, 3H), 2.33 (s, 3H).

¹³C{¹H} NMR (151 MHz, CDCl₃) δ (ppm): 164.1, 157.7, 135.2, 129.3, 127.1, 124.3, 61.4, 36.7, 14.8.

IR (ATR) $\tilde{\nu}$ (cm⁻¹): 3288, 3058, 2922, 2854, 2659, 2326, 2181, 2083, 1993, 1952, 1872, 1741, 1649, 1590, 1555, 1486, 1454, 1397, 1365, 1329, 1309, 1240, 1137, 1095, 1063, 1029, 960, 908, 880, 832, 781, 746, 691.

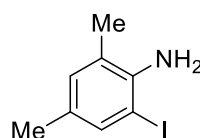
CI-MS (100 eV, methane) m/z : 629 (38) [2M+H]⁺, 315 (100) [M+H]⁺.

EI-MS (70 eV) m/z : 315 (17) [M+H]⁺, 314 (100) [M]⁺, 222 (12), 169 (18), 67 (12), 56 (13).

CHN: Anal. Calcd for C₁₁H₁₁IN₂O: C, 42.06; H, 3.53; N, 8.92. Found C, 41.90; H, 3.41; N, 8.76.

The NMR spectroscopic data are in accordance with the literature.¹⁰

2-Iodo-4,6-dimethylaniline (8)



A 10 mL screw cap vial equipped with a magnetic stirring bar was charged with 2,4-xylidine (24.2 mg, 0.2 mmol, 1.00 equiv.), which was dissolved in DCM (0.5 mL). Then, Barluenga's reagent (74.4 mg, 0.20 mmol, 1.00 equiv.), and the reaction mixture was stirred for 15 min at rt. It was separated between DCM and water (each 20 mL) and aq. sat. Na₂S₂O₃ solution (10 mL) were added. After phase separation, the organic phase was dried over Na₂SO₄, and the product was purified by column chromatography. After purification by column chromatography (SiO₂, pentane:EtOAc 4:1) it was obtained as colorless solid (41.4 mg, 0.168 mmol, 84%).

R_f = 0.86 (pentane:EtOAc 4:1), UV-active, stains with I₂@SiO₂.

mp: 63.1–64.3 °C.

¹H NMR (600 MHz, CDCl₃) δ (ppm): 7.36 (m, 1H), 6.84 (m, 1H), 3.92 (br s, 2H), 2.20 (s, 3H), 2.18 (s, 3H).

¹³C{¹H} NMR (151 MHz, CDCl₃) δ (ppm): 142.5, 137.0, 131.6, 129.4, 122.6, 84.9, 20.0, 19.0.

IR (ATR) $\tilde{\nu}$ (cm⁻¹): 3818, 3396, 3312, 3209, 3016, 2919, 2854, 2731, 2323, 2171, 2104, 1887, 1778, 1741, 1621, 1552, 1474, 1377, 1280, 1238, 1149, 1057, 1012, 986, 890, 852, 809, 760, 717.

CI-MS (100 eV, methane) m/z : 495 (65) [2M+H]⁺, 248 (98) [M+H]⁺, 247 (100) [M]⁺.

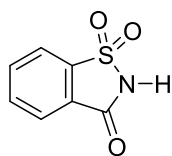
EI-MS (70 eV) m/z : 248 (11) [M+H]⁺, 247 [M]⁺, 120 (18).

CHN: Anal. Calcd for C₈H₁₀IN: C, 38.89; H, 4.08; N, 5.67. Found C, 39.28; H, 4.14; N, 5.59.

The NMR spectroscopic data are in accordance with the literature.¹¹

7.2.4 Recovery of Starting Materials

Saccharin



Following a 1 mmol approach of **GP9**. After product **6** was purified, the remaining substances were recovered from the column using MeOH as eluent. After evaporation of the solvent a mixture containing DMAP, and saccharin was recovered. The mixture was dissolved in DCM (25 mL) and extracted with 1 M HCl (25 mL). The aqueous phase was extracted twice using DCM (25 mL) and then kept for the recovery of DMAP. The organic phases were combined and washed with aqueous saturated Na₂S₂O₃ (10 mL) to remove the pink colour. This aqueous phase was extracted with EtOAc (3 × 20 mL), the organic phases combined, dried over Na₂SO₄. Then, saccharin was purified by running two consecutive column chromatographies (1st column: SiO₂, EtOAc; 2nd column: SiO₂, pentane:EtOAc 1:0 → 19:1 → 9:1 → 4:1 → 2:1 → 1:1 → 0:1) and was obtained as white solid (20.2 mg, 0.11 mmol, 11%).

mp: 224.1–225.9 °C.

¹H NMR (600 MHz, (CD₃)₂SO) δ (ppm): 8.14 (d, J = 7.6 Hz, 1H), 7.98 (m, 2H), 7.93 (td, J = 7.5 Hz, 1.1 Hz, 1H), 4.66 (br s, 4H). The broad signal should only be 1H, but due to the presence of water in the solvent it does not add up to one. The other data support the presence of saccharin.

¹³C{¹H} NMR (151 MHz, (CD₃)₂SO) δ (ppm): 161.1, 139.6, 135.4, 134.6, 127.8, 124.7, 121.1.

IR (ATR) $\tilde{\nu}$ (cm⁻¹): 3446, 3092, 2966, 2695, 2296, 2230, 2160, 2109, 2052, 1986, 1865, 1718, 1592, 1460, 1332, 1296, 1255, 1176, 1139, 1119, 1054, 1012, 969, 898, 756, 702.

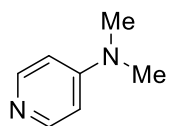
CI-MS (100 eV, methane) m/z : 184 [M+H]⁺ (100).

EI-MS (70 eV) m/z : 184 $[M+H]^+$ (14), 183 $[M]^+$ (100), 120 (47), 119 (58), 104 (21), 103 (17), 92 (44), 76 (83), 75 (15), 74 (20), 64 (15), 63 (15), 50 (64).

CHN: Anal. Calcd for $C_7H_5NO_3S$: C, 45.90; H, 2.75; N, 7.65. Found C, 44.71; H, 2.82; N, 7.03.

The NMR spectroscopic data of the $^{13}C\{^1H\}$ spectrum are in accordance with the literature.¹²

4-*N,N*-Dimethylaminopyridine (DMAP)



The acidic aqueous phase was made basic using 1 M NaOH and it was extracted twice with DCM (25 mL), then EtOAc (3×25 mL). The organic phases were combined, dried over Na_2SO_4 , and the solvent evaporated to yield the title compound as colourless solid (143.1 mg, 1.17 mmol, 59%).

mp: 109.8–111.9 °C.

1H NMR (600 MHz, $CDCl_3$) δ (ppm): 8.17 (dd, $J = 4.9, 1.6$ Hz, 2H), 6.43 (dd, $J = 4.9, 1.6$ Hz, 2H), 2.94 (s, 6H).

$^{13}C\{^1H\}$ NMR (151 MHz, $CDCl_3$) δ (ppm): 154.2, 149.8, 106.6, 39.0.

IR (ATR) $\tilde{\nu}$ (cm^{-1}): 3397, 3031, 2996, 2906, 2825, 2546, 2487, 2340, 2202, 2122, 1928, 1811, 1735, 1594, 1515, 1440, 1371, 1218, 1103, 1067, 981, 941, 803, 744, 660.

CI-MS (100 eV, methane) m/z : 123 $[M+H]^+$ (100), 122 $[M]^+$ (7).

EI-MS (70 eV) m/z : 123 $[M+H]^+$ (58), 122 $[M]^+$ (100), 121 (96), 83 (11), 51 (11).

CHN: Anal. Calcd for $C_7H_{10}N_2$: C, 68.82; H, 8.25; N, 22.93. Found C, 68.50; H, 8.24; N, 22.82.

The analytical data are in accordance with the literature.¹³

8 References

- (1) Hoof, R. W. W.; Nonius. Collect. Nonius BV: Delft, The Netherlands 1998.
- (2) Otwinowski, Z.; Minor, W. B. T.-M. in E. [20] Processing of X-Ray Diffraction Data Collected in Oscillation Mode. In *Macromolecular Crystallography Part A*; Academic Press, 1997; Vol. 276, pp 307–326. [https://doi.org/10.1016/S0076-6879\(97\)76066-X](https://doi.org/10.1016/S0076-6879(97)76066-X).
- (3) Fulmer, G. R.; Miller, A. J. M.; Sherden, N. H.; Gottlieb, H. E.; Nudelman, A.; Stoltz, B. M.; Bercaw, J. E.; Goldberg, K. I. NMR Chemical Shifts of Trace Impurities: Common Laboratory Solvents, Organics, and Gases in Deuterated Solvents Relevant to the Organometallic Chemist. *Organometallics* **2010**, *29* (9), 2176–2179. <https://doi.org/10.1021/om100106e>.
- (4) Lu, N.; Chang, W.-H.; Tu, W.-H.; Li, C.-K. A Salt Made of 4-N,N-Dimethylaminopyridine (DMAP) and Saccharin as an Efficient Recyclable Acylation Catalyst: A New Bridge between Heterogeneous and Homogeneous Catalysis. *Chem. Commun.* **2011**, *47* (25), 7227–7229. <https://doi.org/10.1039/C1CC11556A>.
- (5) Groom, C. R.; Bruno, I. J.; Lightfoot, M. P.; Ward, S. C. The Cambridge Structural Database. *Acta Crystallogr. Sect. B* **2016**, *72* (2), 171–179. <https://doi.org/10.1107/S2052520616003954>.
- (6) Makhotkina, O.; Lieffrig, J.; Jeannin, O.; Fourmigué, M.; Aubert, E.; Espinosa, E. Cocrystal or Salt: Solid State-Controlled Iodine Shift in Crystalline Halogen-Bonded Systems. *Cryst. Growth Des.* **2015**, *15* (7), 3464–3473. <https://doi.org/10.1021/acs.cgd.5b00535>.
- (7) Narayan, S.; Seelhammer, T.; Gawley, R. E. Microwave assisted solvent free amination of halo-(pyridine or pyrimidine) without transition metal catalyst. *Tetrahedron Letters* **2004**, *45*, 757–759. <https://doi.org/10.1016/j.tetlet.2003.11.030>
- (8) Dolenc, D. *N*-Iodosaccharin - a New Reagent for Iodination of Alkenes and Activated Aromatics. *Synlett* **2000**, *2000* (04), 544–546. <https://doi.org/10.1055/s-2000-6561>.
- (9) Chalker, J. M.; Thompson, A. L.; Davis, B. G.; Zaware, N.; Wipf, P. Safe and Scalable Preparation of Barluenga's Reagent: (Bis(Pyridine) Iodonium(I) Tetrafluoroborate). *Organic Syntheses*. 2010, pp 288–298. <https://doi.org/10.15227/orgsyn.087.0288>.
- (10) Narobe, R.; Düsel, S. J. S.; Iskra, J., König, B. Photocatalytic Oxidative Iodination of Electron-Rich Arenes. *Adv. Synth. Catal.* **2019**, *361*, 3998–4004. <https://doi.org/10.1002/adsc.201900298>
- (11) Alharbi, H.; Elsherbini, M.; Qurban, J.; Wirth, T. C–N Axial Chiral Hypervalent Iodine Reagents: Catalytic Stereoselective α -Oxytosylation of Ketones. *Chem. – A Eur. J.* **2021**, *27* (13), 4317–4321. <https://doi.org/10.1002/chem.202005253>.
- (12) Kleinpeter, E.; Ströhl, D.; Jovanovski, G.; Šoptrajanov, B. Metal-to-Ligand Bonding in Some

Metal Saccharinates: A ^{13}C NMR Study. *J. Mol. Struct.* **1991**, 246 (1), 185–188.
[https://doi.org/https://doi.org/10.1016/0022-2860\(91\)80025-Y](https://doi.org/https://doi.org/10.1016/0022-2860(91)80025-Y).

- (13) Bläsing, K.; Labbow, R.; Schulz, A.; Villinger, A. Silylated Sulfuric Acid: Preparation of a Tris(Trimethylsilyl)Oxosulfonium $[(\text{Me}_3\text{Si}-\text{O})_3\text{SO}]^+$ Salt. *Angew. Chem. Int. Ed.* **2021**, 60 (25), 13798–13802. <https://doi.org/https://doi.org/10.1002/anie.202104733>.

9 Spectra

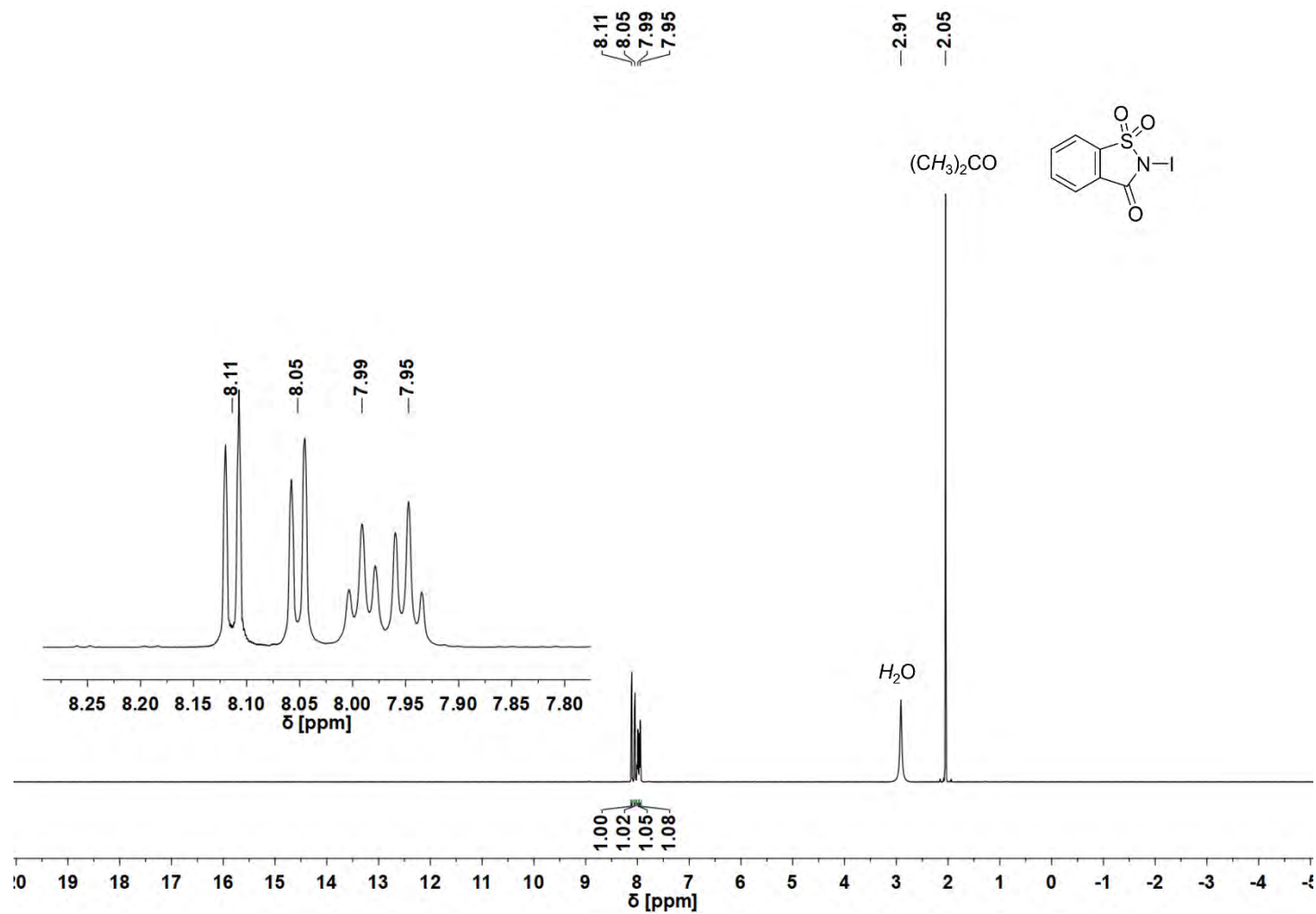


Figure S89. ^1H NMR spectrum (600 MHz, $(\text{CD}_3)_2\text{CO}$) of NISac (1).

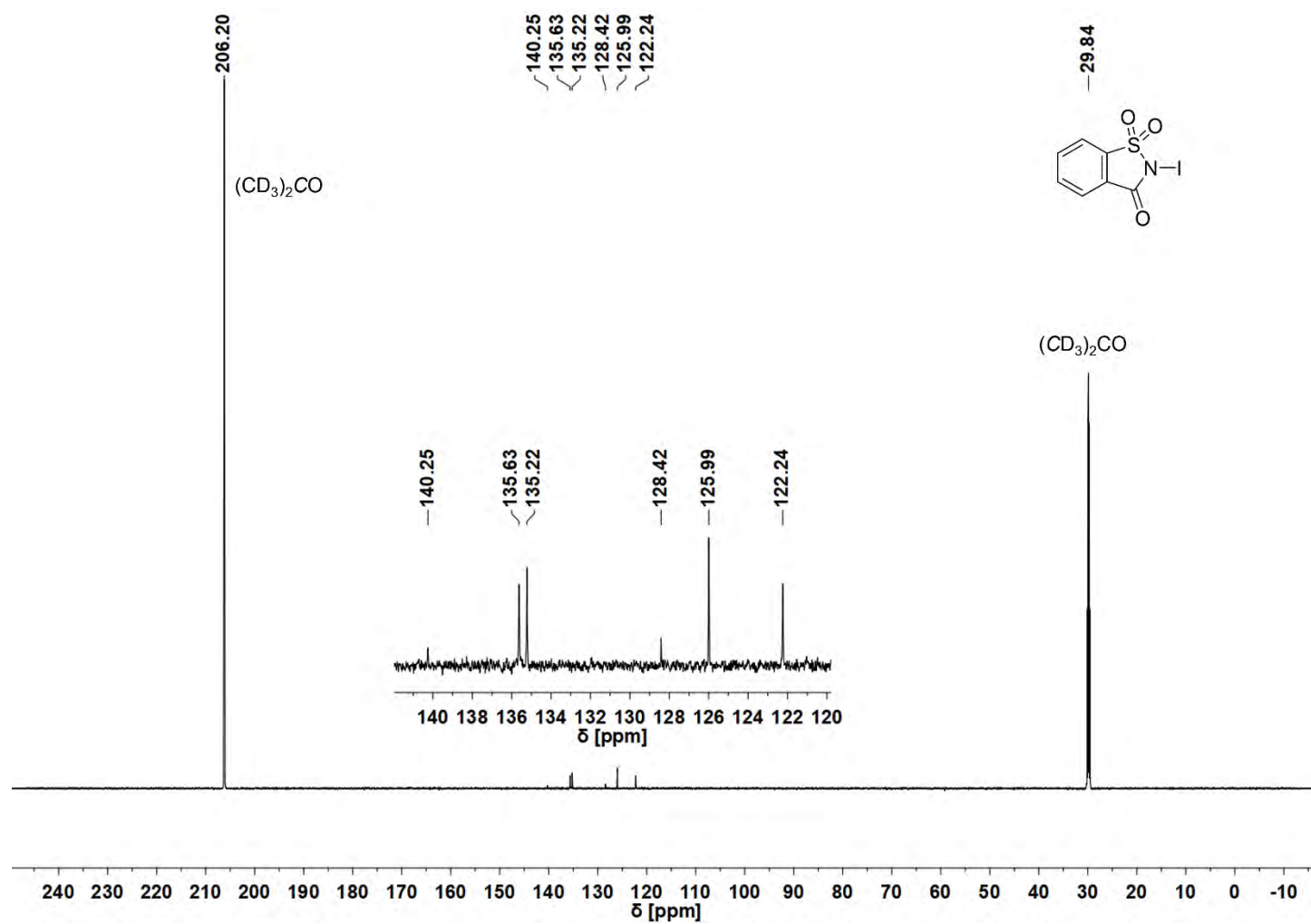


Figure S90. $^{13}\text{C}\{^1\text{H}\}$ NMR spectrum (151 MHz, $(\text{CD}_3)_2\text{CO}$) of NISac (**1**).

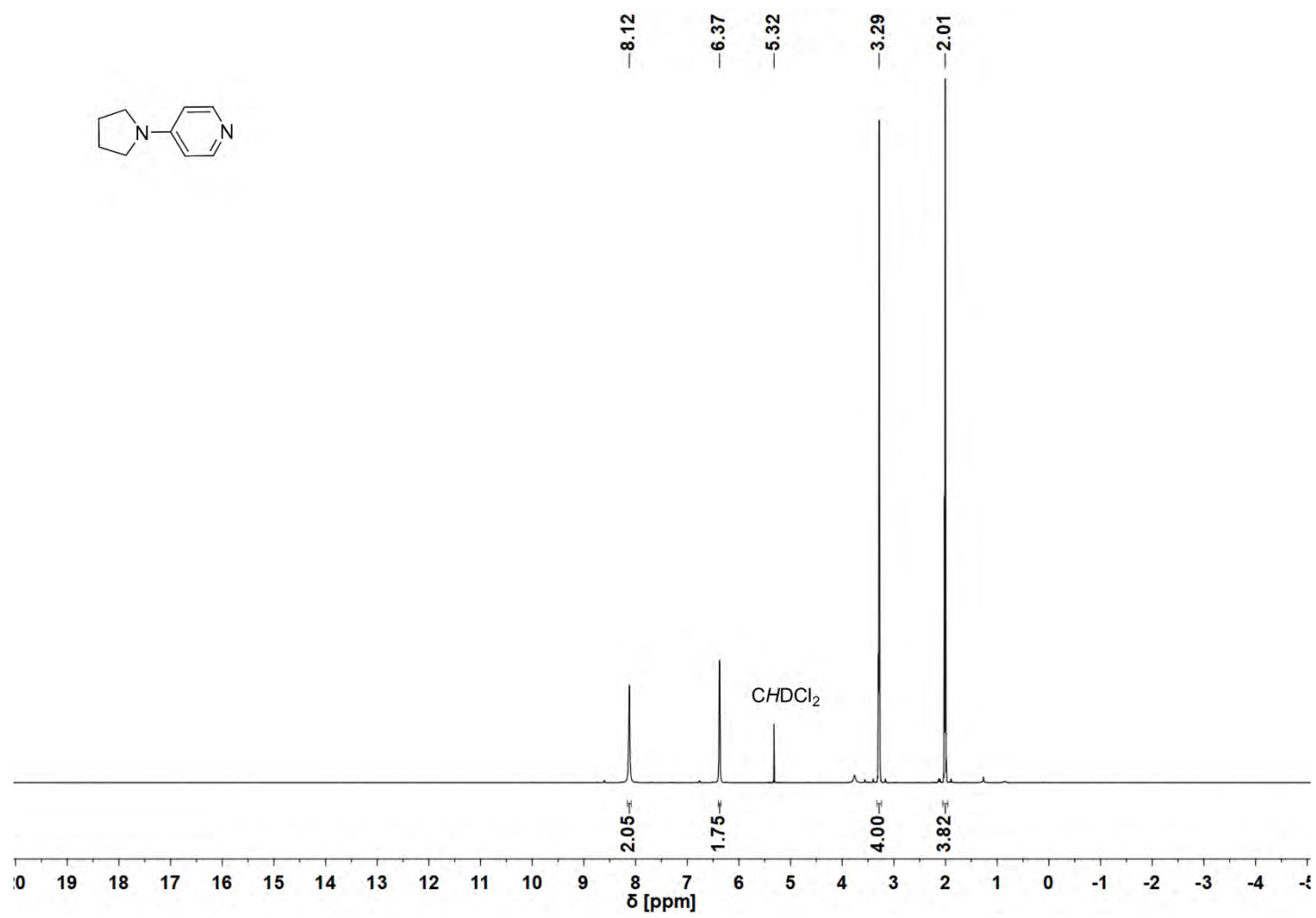


Figure S91. ¹H NMR spectrum (600 MHz, CD₂Cl₂) of PPY (**2b**).

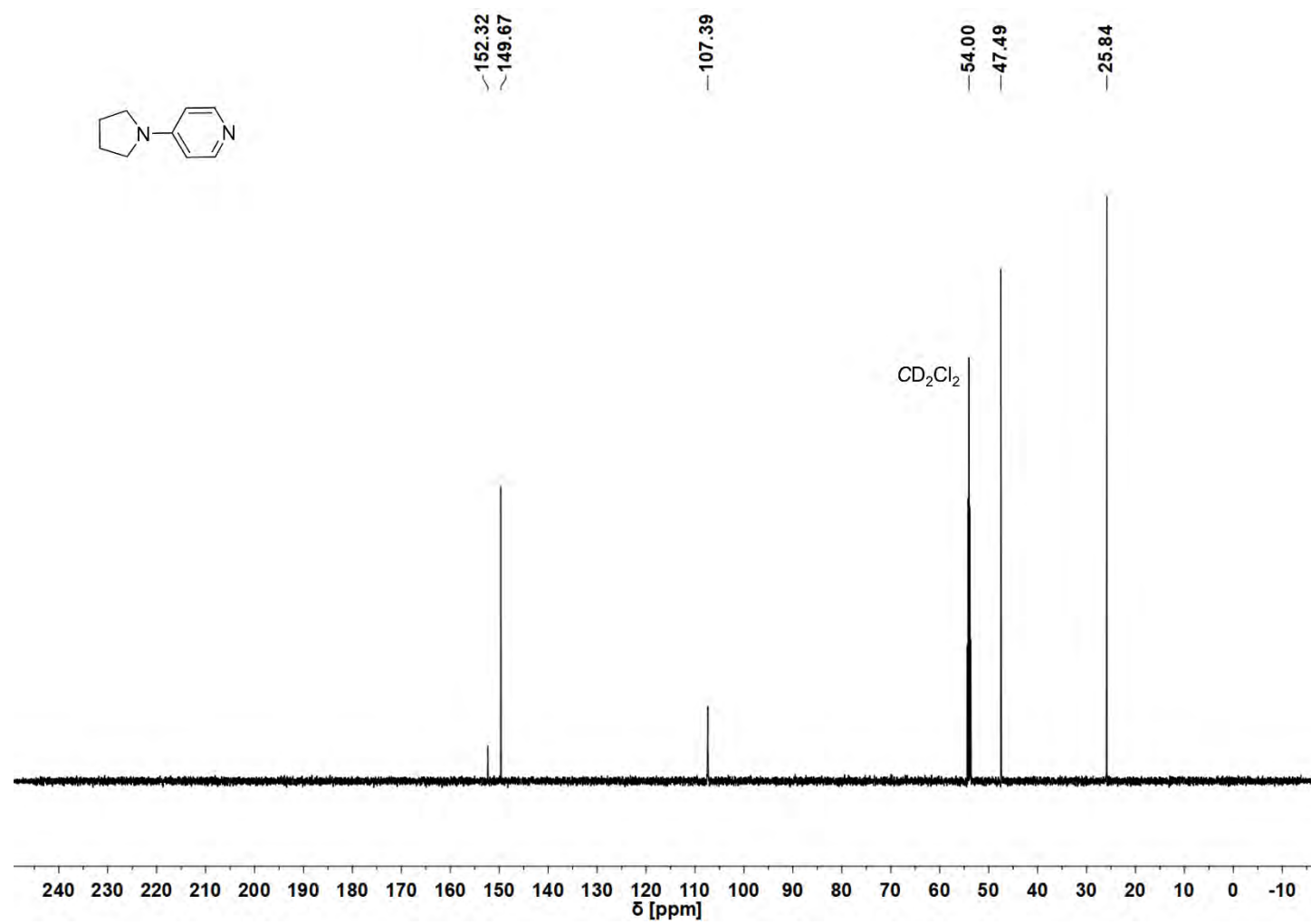


Figure S92. $^{13}\text{C}\{^1\text{H}\}$ NMR spectrum (151 MHz, CD_2Cl_2) of PPY (2b).

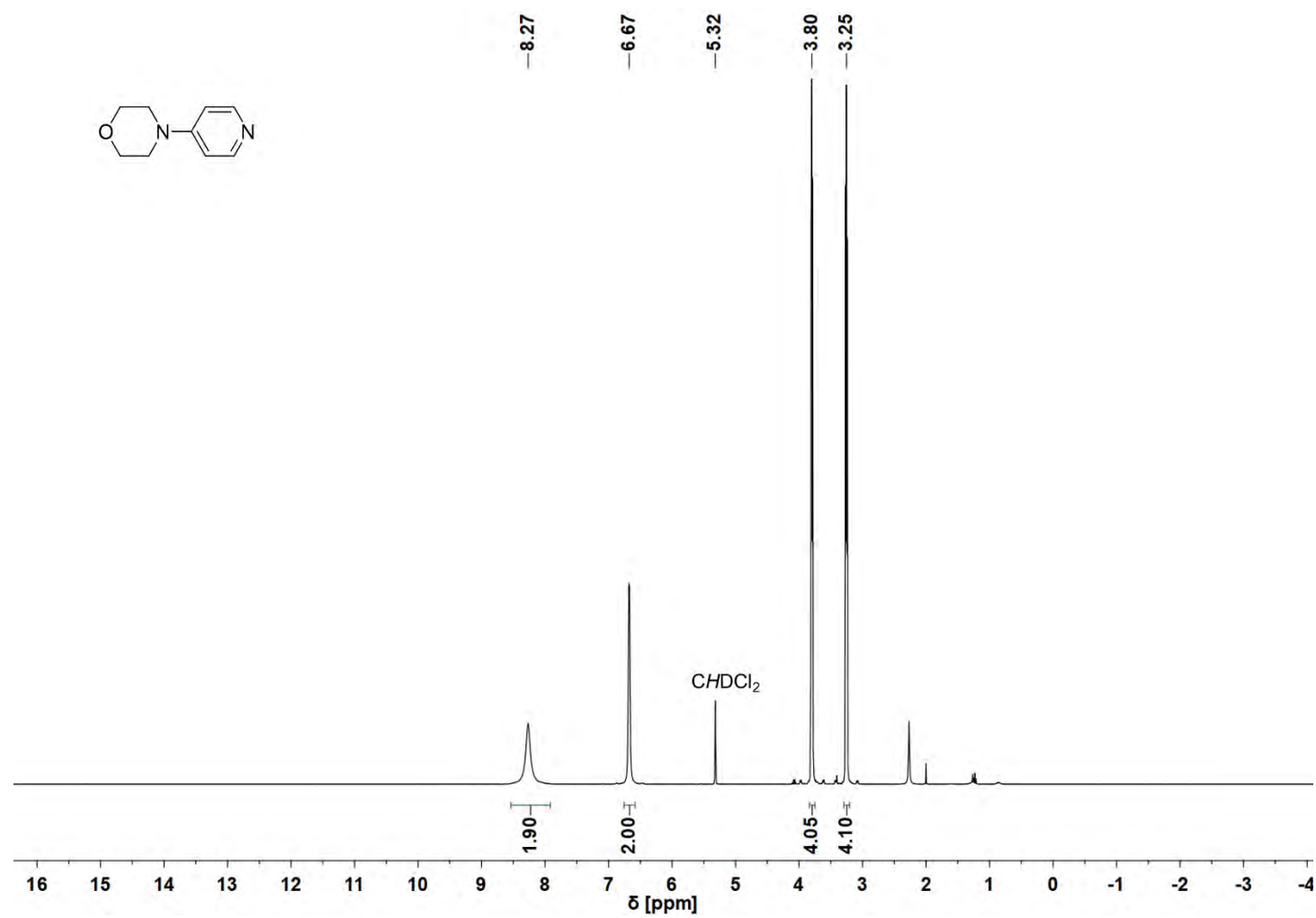


Figure S93. ¹H NMR spectrum (400 MHz, CD₂Cl₂) of MPY (2c).

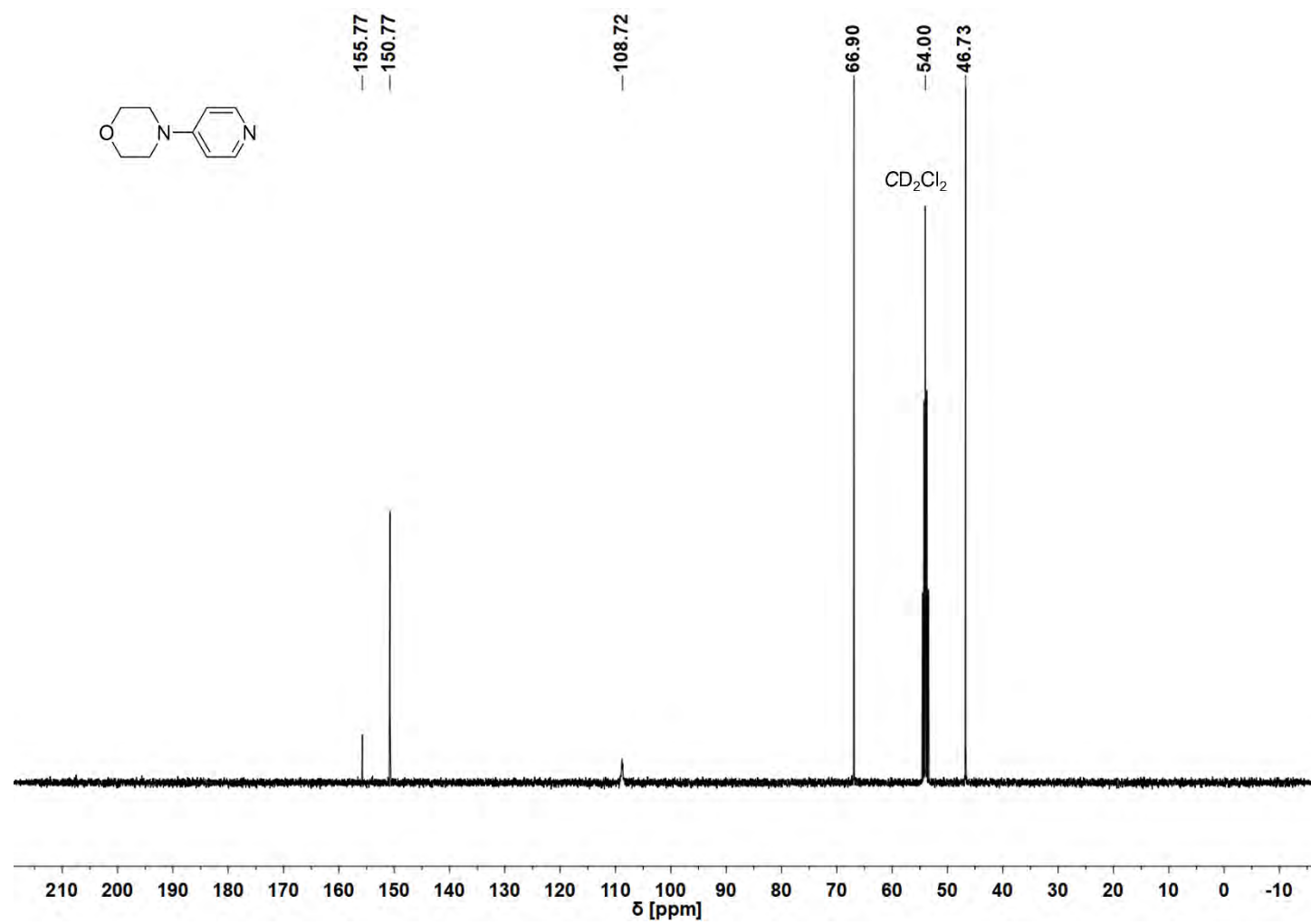


Figure S94. $^{13}\text{C}\{^1\text{H}\}$ NMR spectrum (101 MHz, CD_2Cl_2) of MPY (2c).

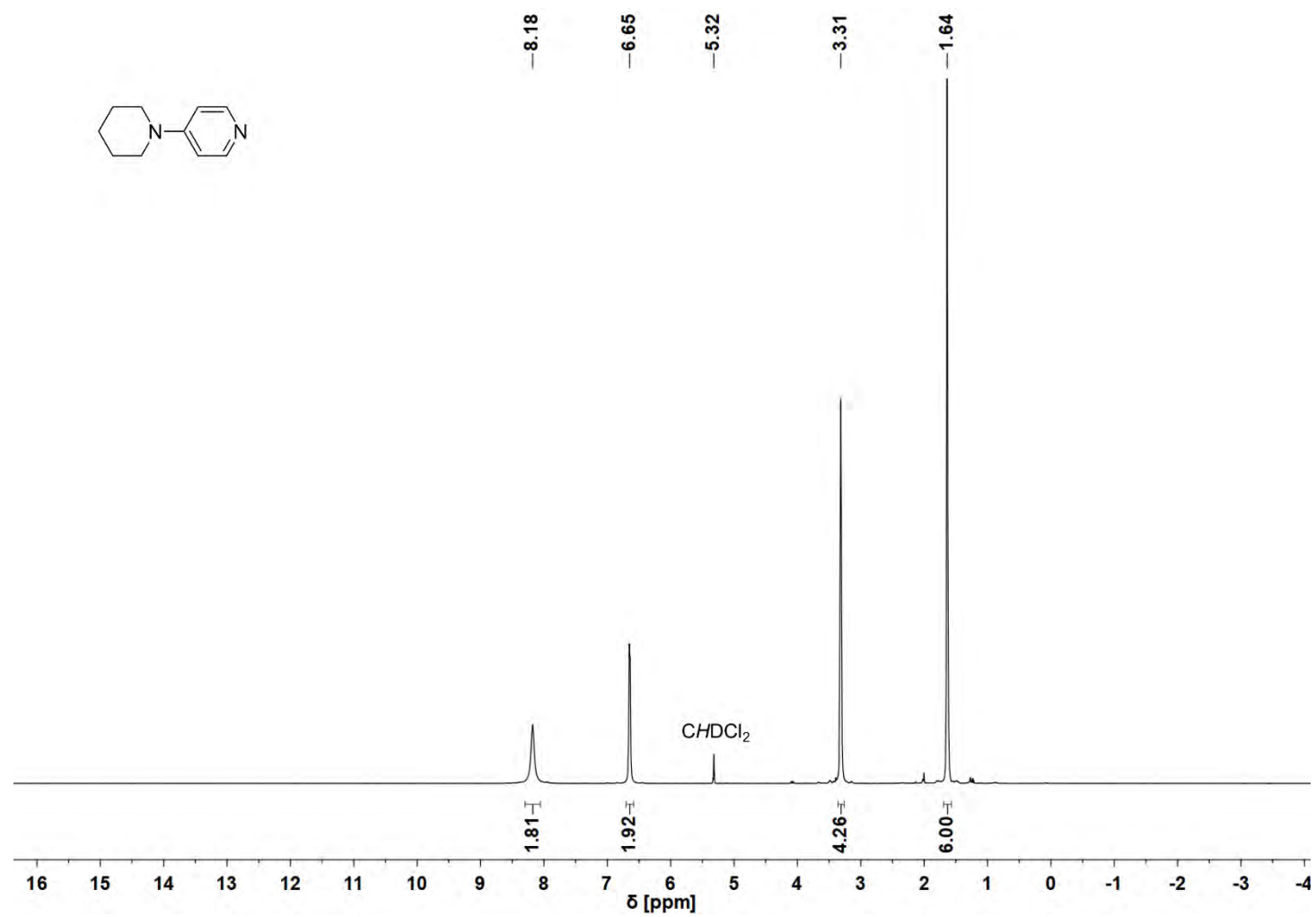


Figure S95. ¹H NMR spectrum (400 MHz, CD₂Cl₂) of PiPY (2d).

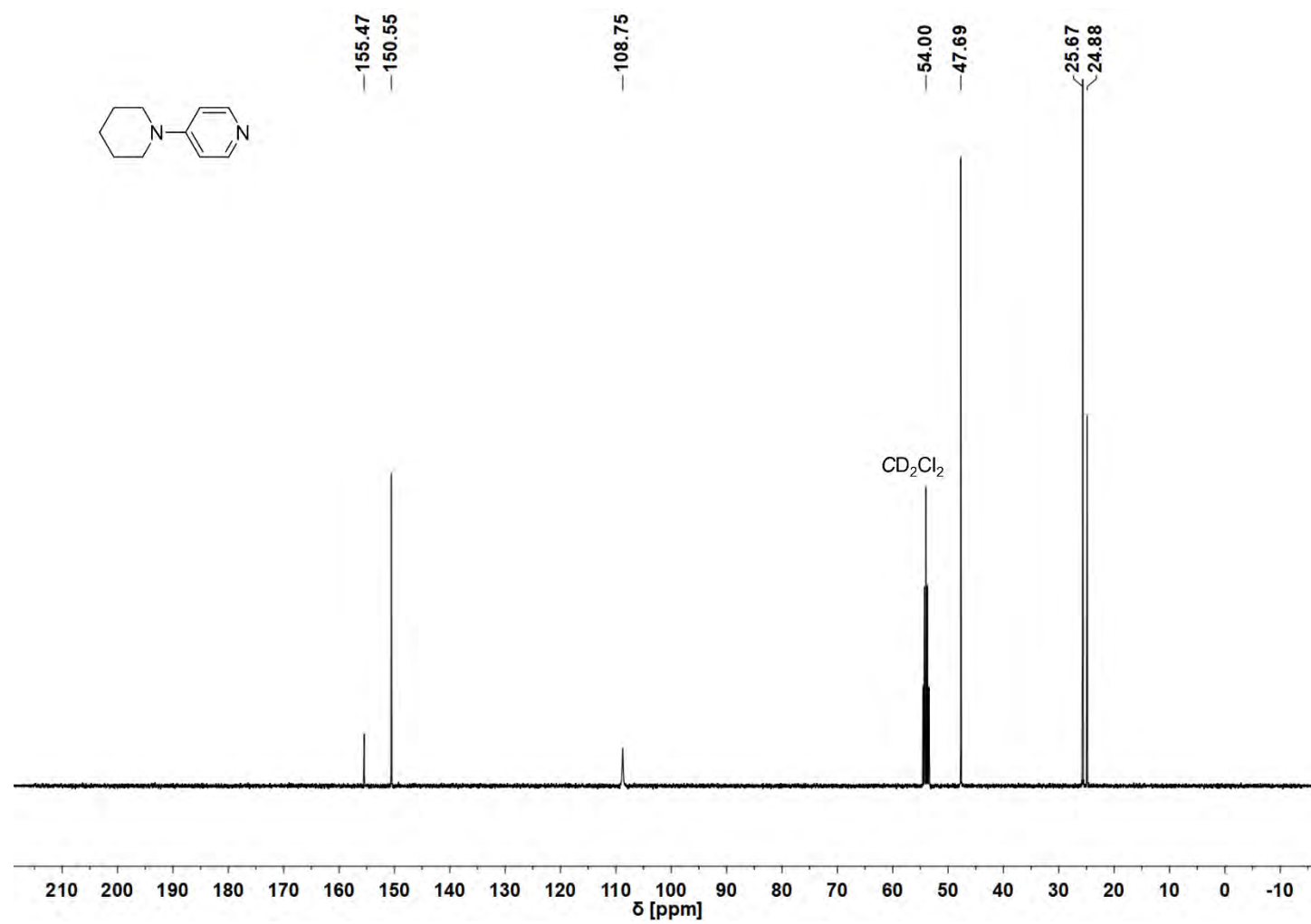


Figure S96. $^{13}\text{C}\{^1\text{H}\}$ NMR spectrum (101 MHz, CD_2Cl_2) of PiPY (2d).

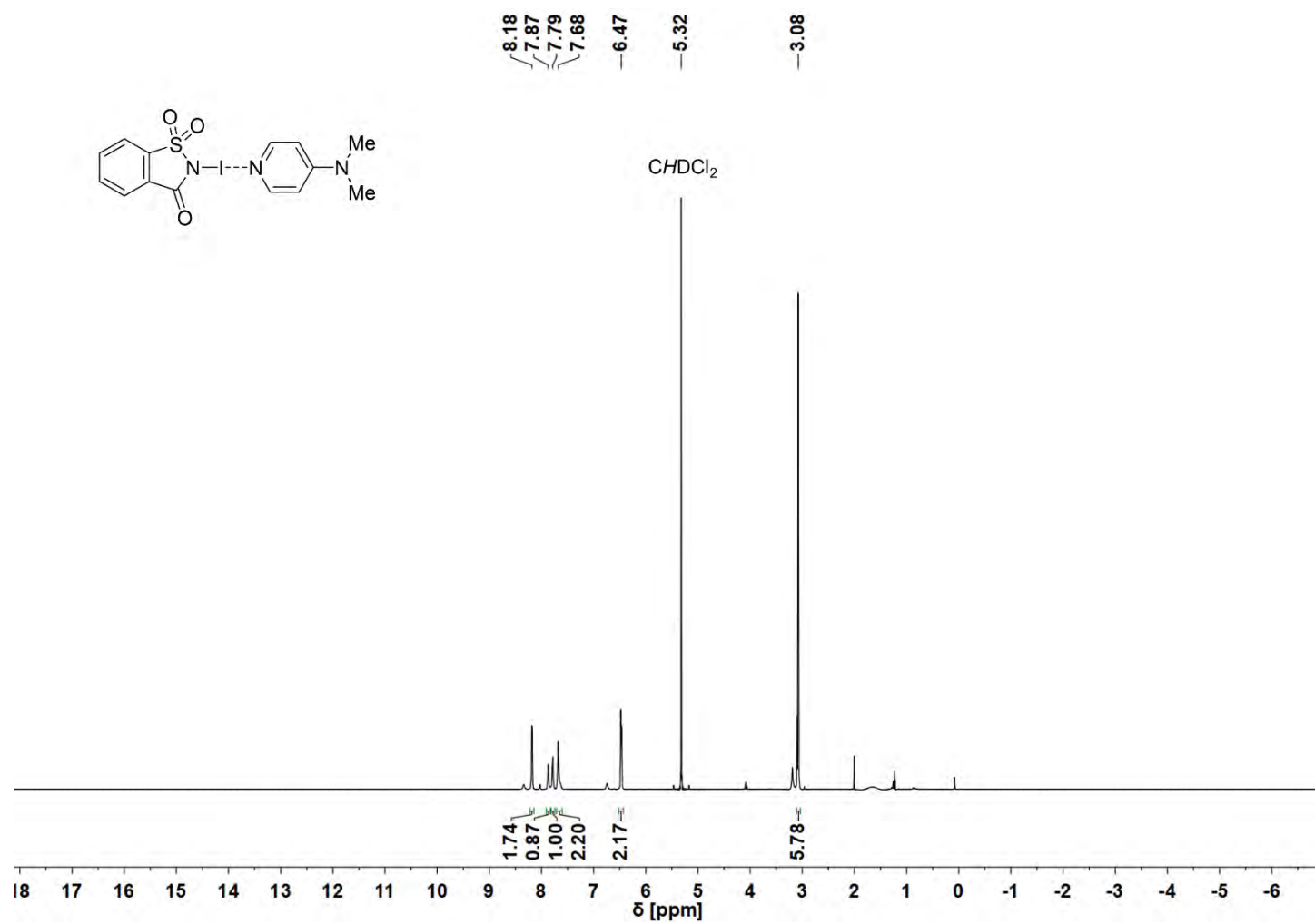


Figure S97. ¹H NMR spectrum (600 MHz, CD₂Cl₂) of [DMAP-NISac] (3a).

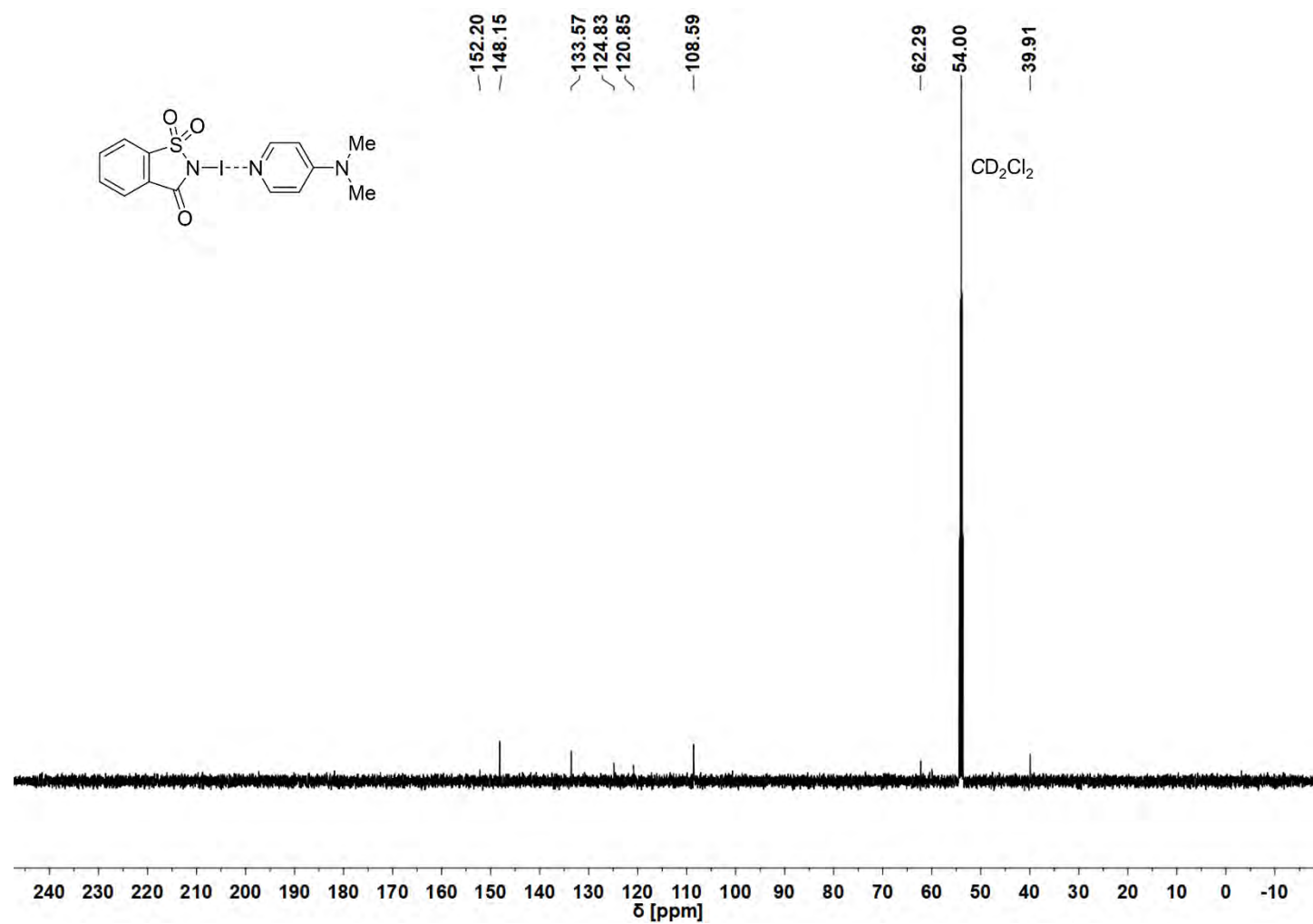


Figure S98. $^{13}\text{C}\{^1\text{H}\}$ NMR spectrum (151 MHz, CD_2Cl_2) of [DMAP-NISac] (**3a**).

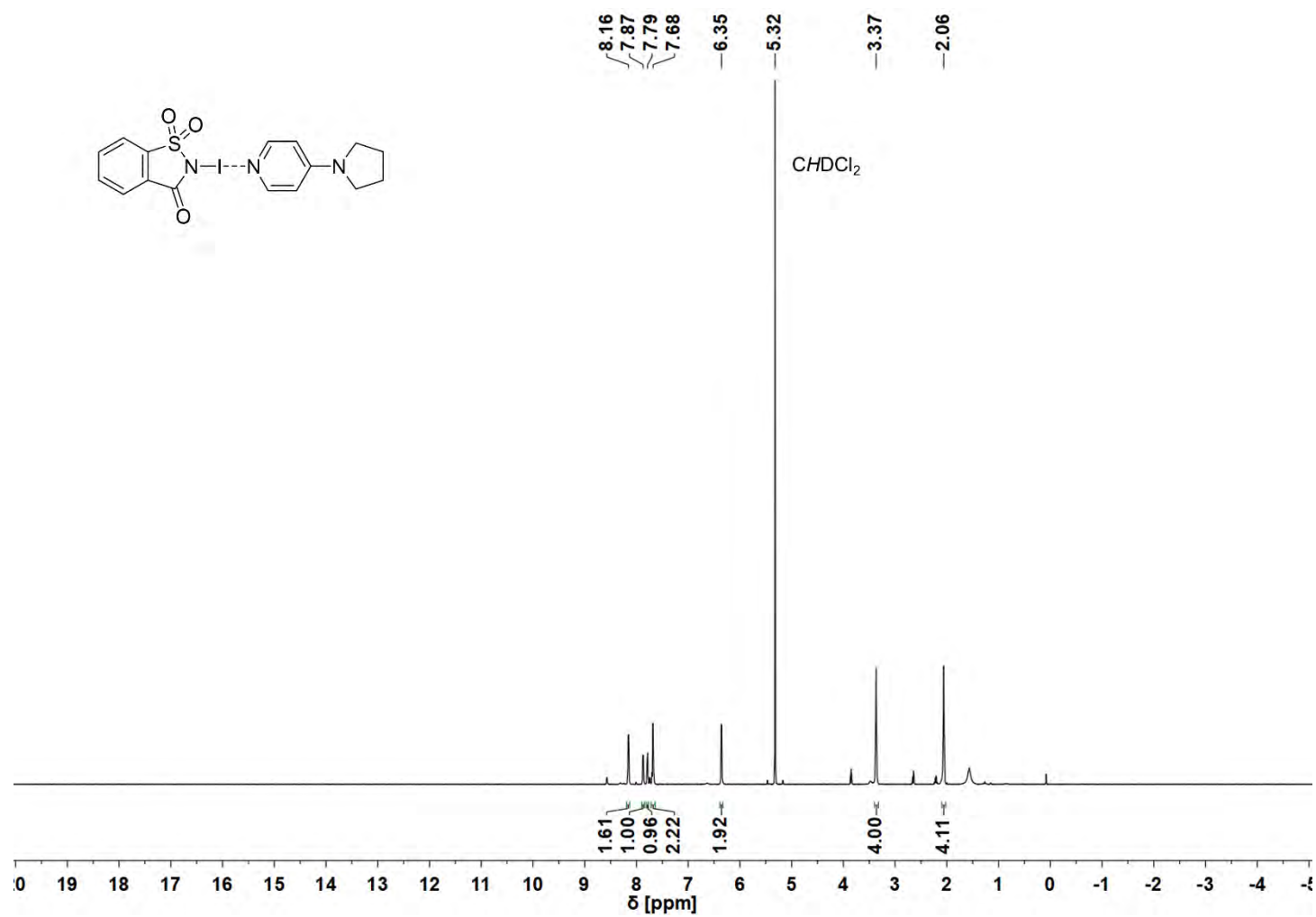


Figure S99. ¹H NMR spectrum (600 MHz, CD₂Cl₂) of [PPY-NISac] (**3b**).

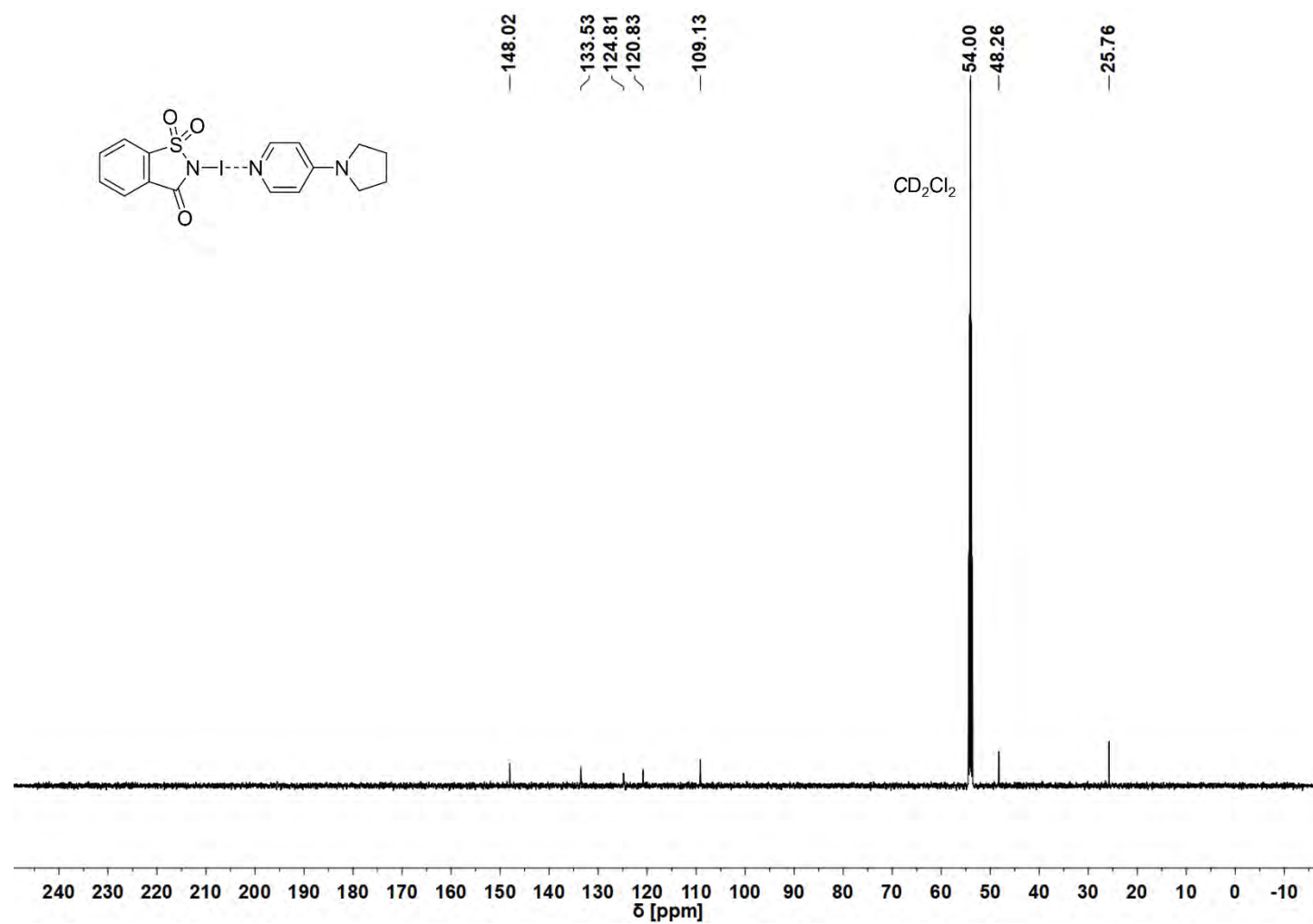


Figure S100. $^{13}\text{C}\{^1\text{H}\}$ NMR spectrum (151 MHz, CD_2Cl_2) of [PPY-NISac] (3b).

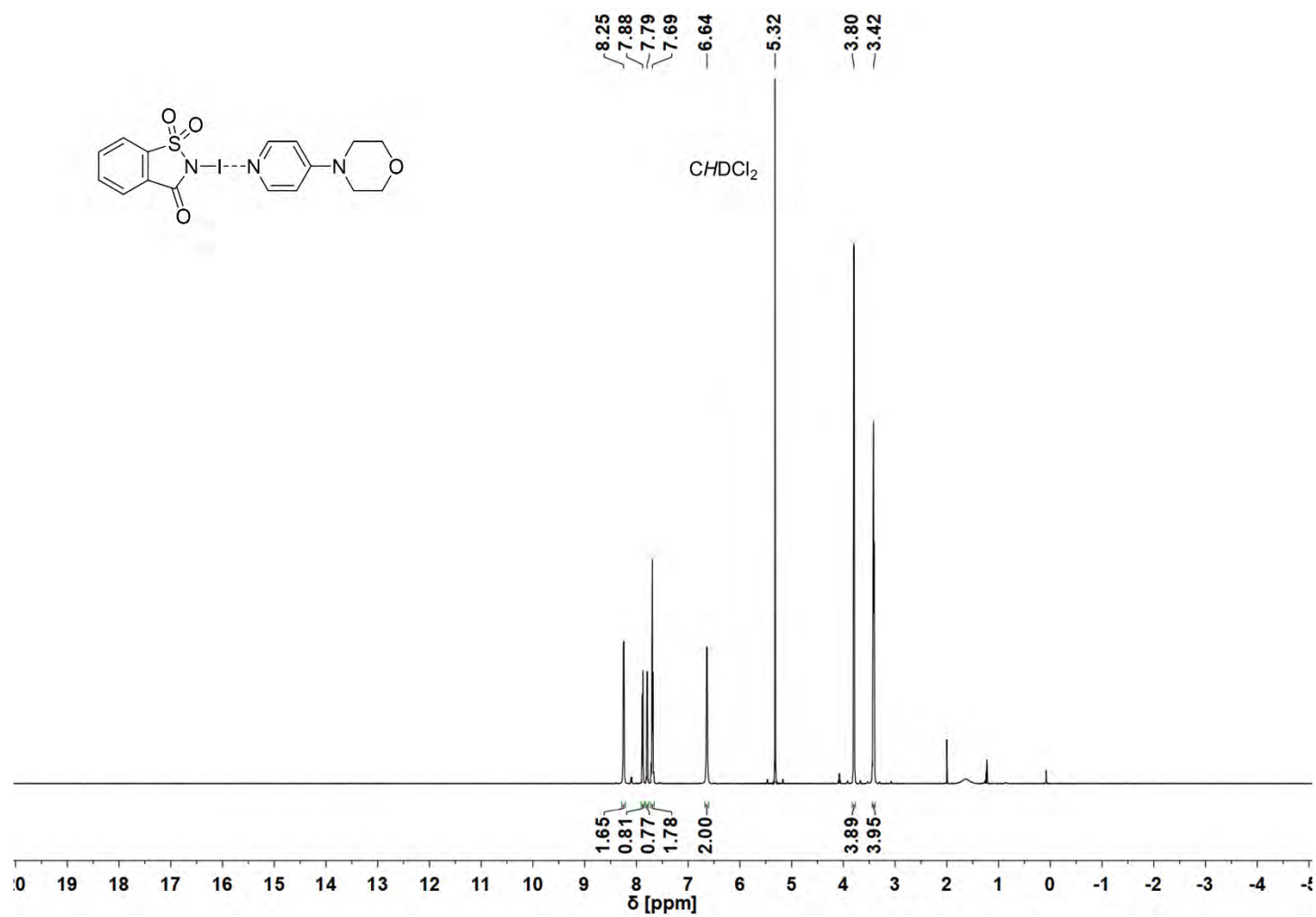


Figure S101. ^1H NMR spectrum (600 MHz, CD_2Cl_2) of [MPY-NISac] (3c).

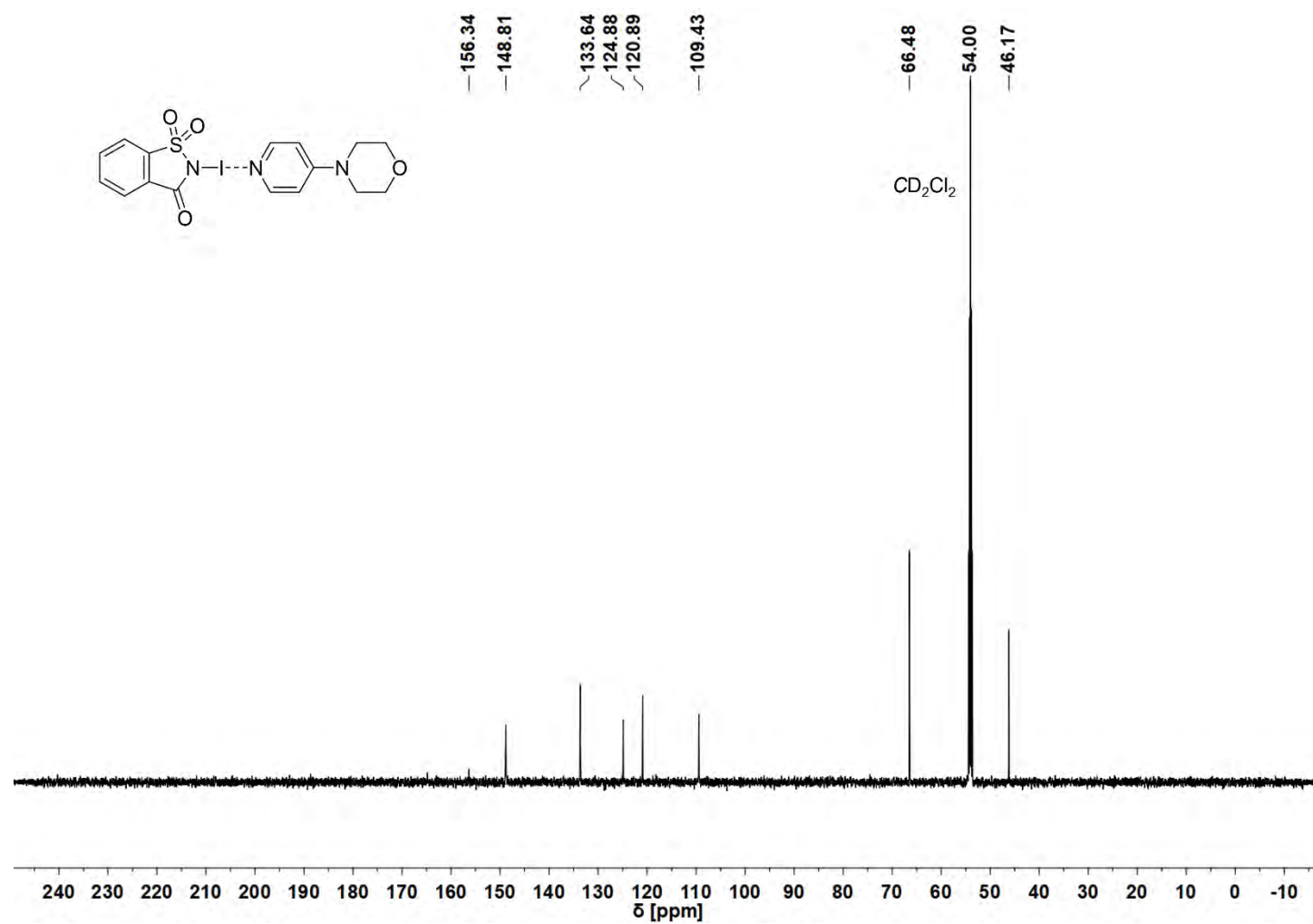


Figure S102. $^{13}\text{C}\{^1\text{H}\}$ NMR spectrum (151 MHz, CD_2Cl_2) of [MPY-NISac] (3c).

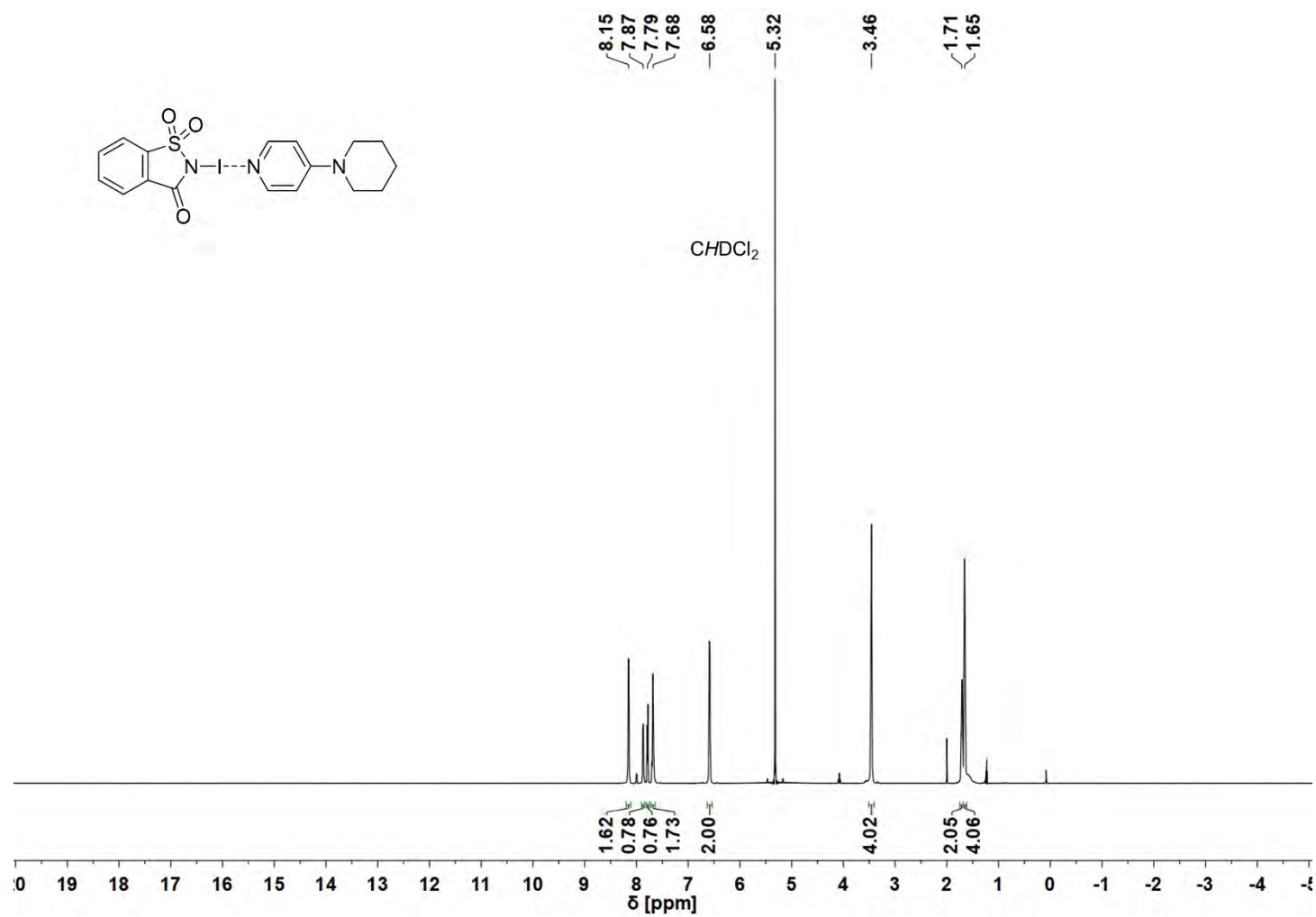


Figure S103. ¹H NMR spectrum (600 MHz, CD₂Cl₂) of [PiPY-NISac] (**3d**).

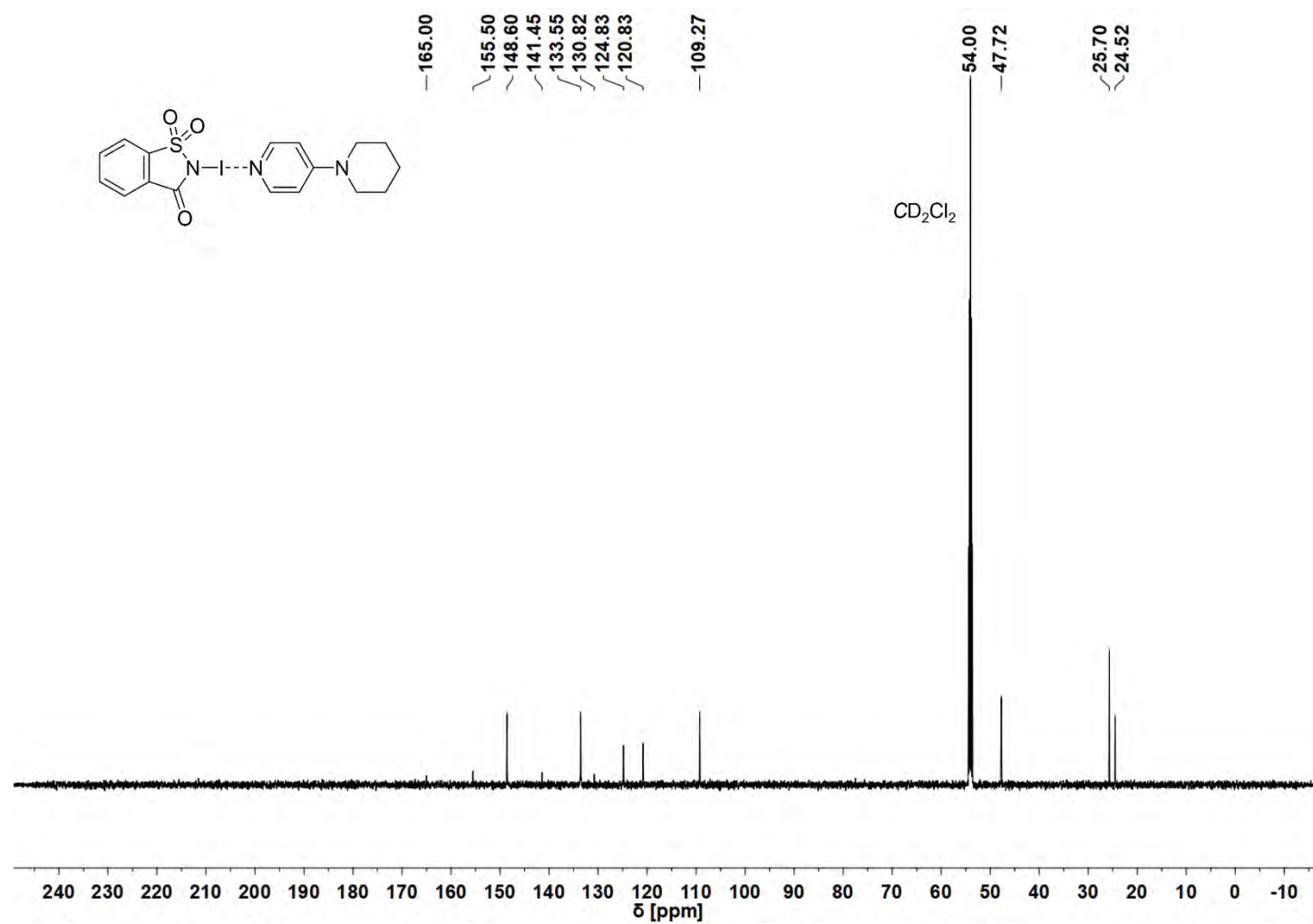


Figure S104. $^{13}\text{C}\{^1\text{H}\}$ NMR spectrum (151 MHz, CD_2Cl_2) of [PiPY-NISac] (3d).

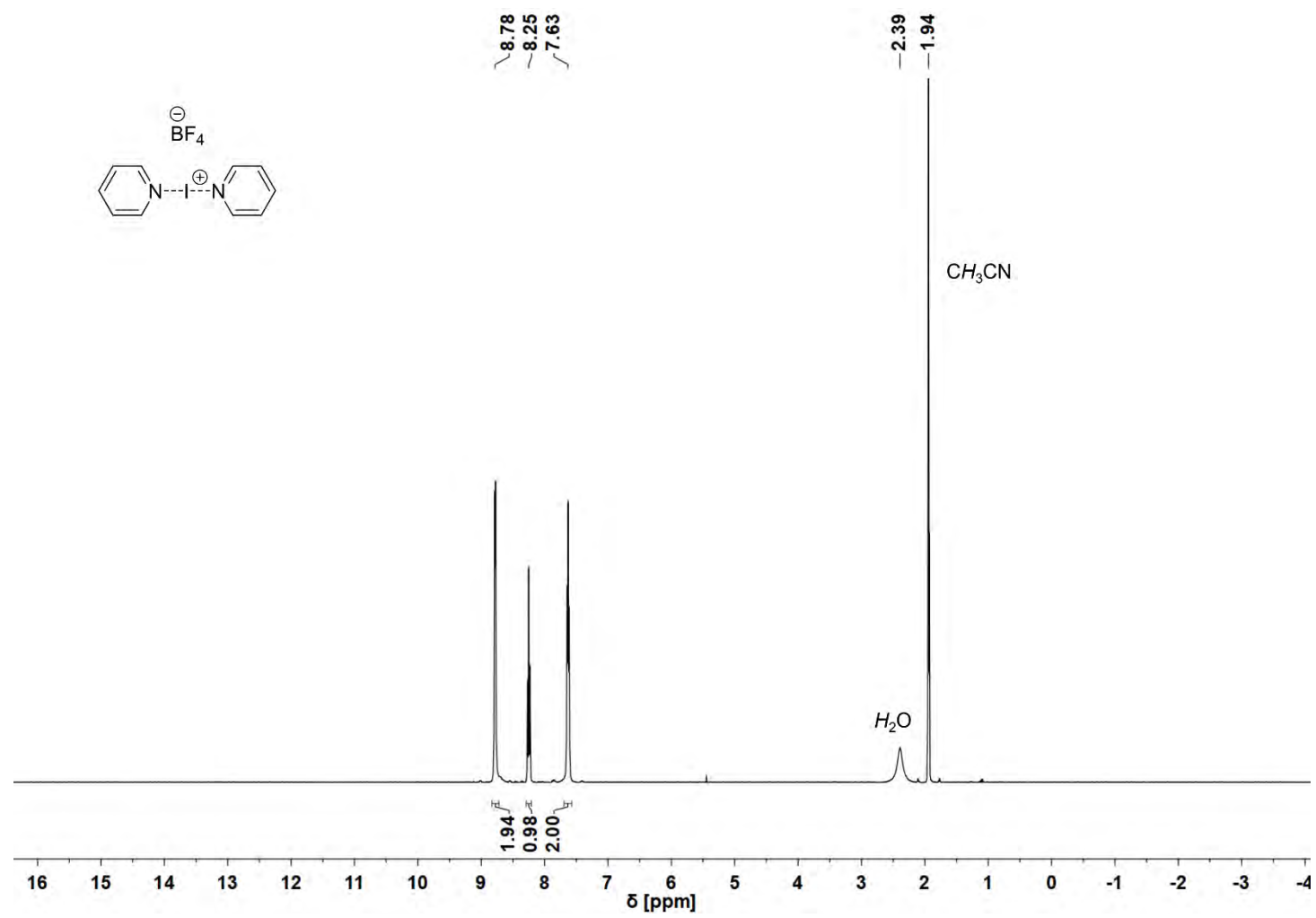


Figure S105. ^1H NMR spectrum (400 MHz, CD_3CN) of Barluenga's reagent.

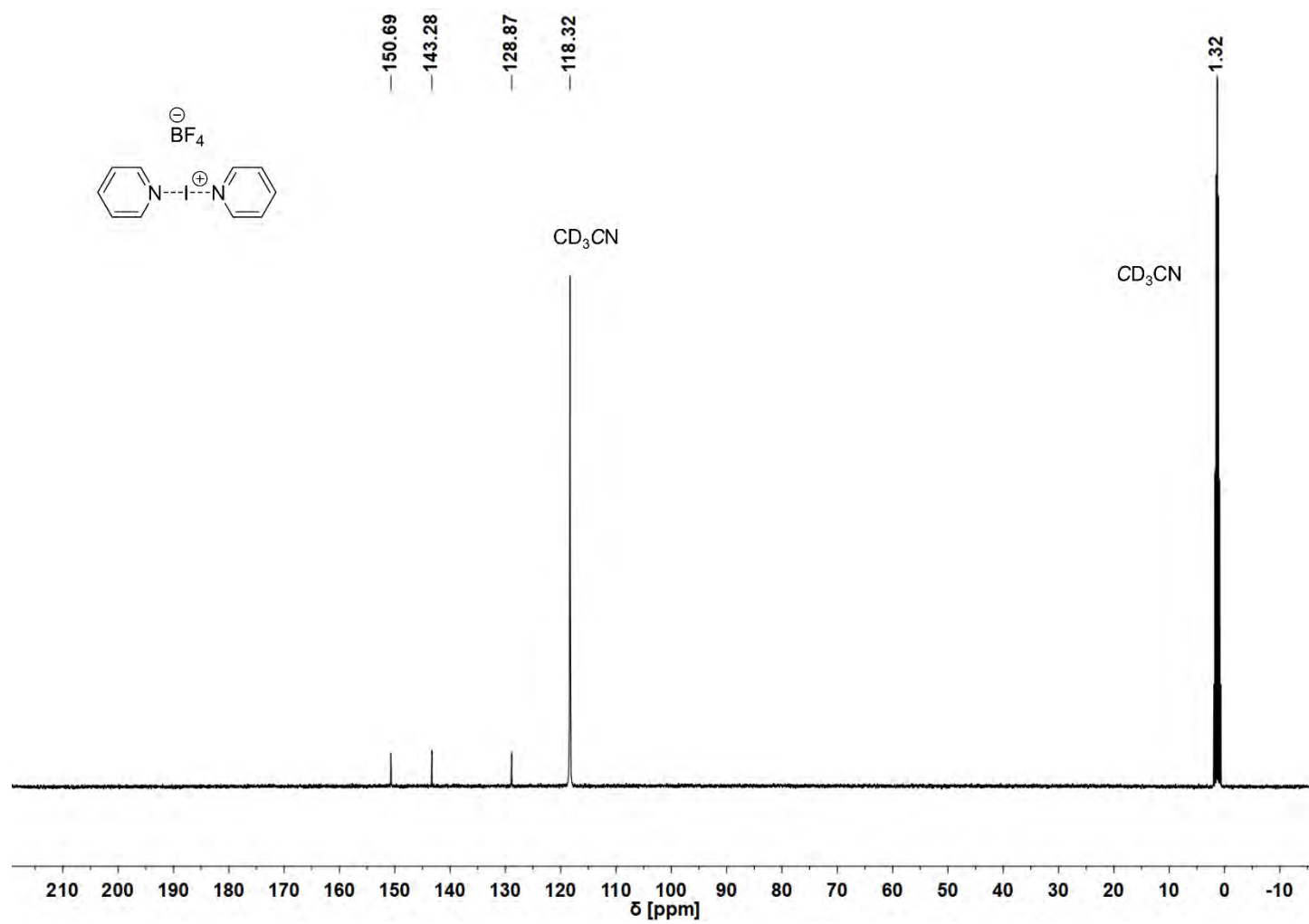


Figure S106. $^{13}\text{C}\{^1\text{H}\}$ NMR spectrum (101 MHz, CD_3CN) of Barluenga's reagent.

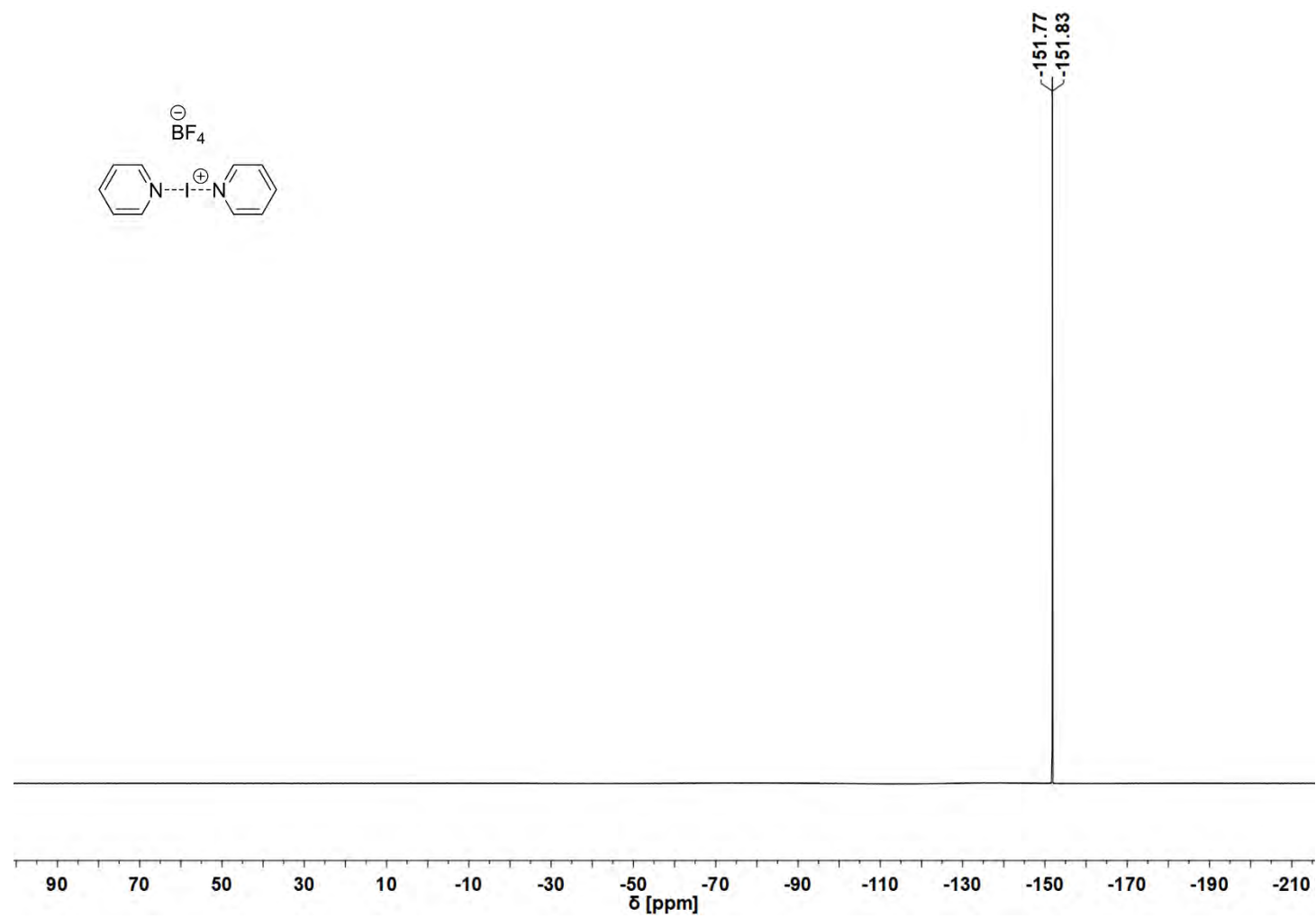


Figure S107. ^{19}F NMR spectrum (376 MHz, CD_3CN) of Barluenga's reagent.

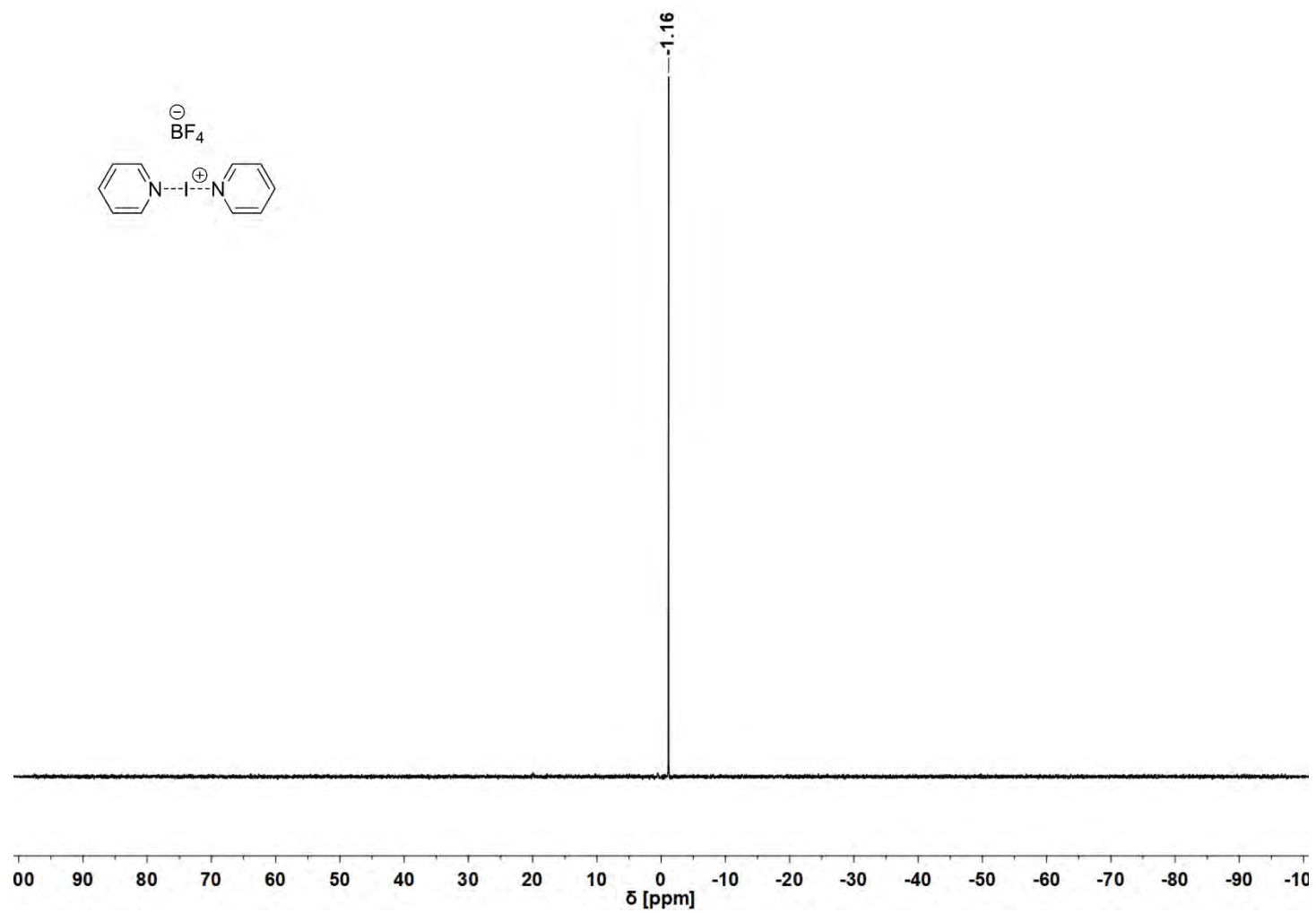


Figure S108. ¹¹B NMR spectrum (128 MHz, CD₃CN) of Barluenga's reagent.

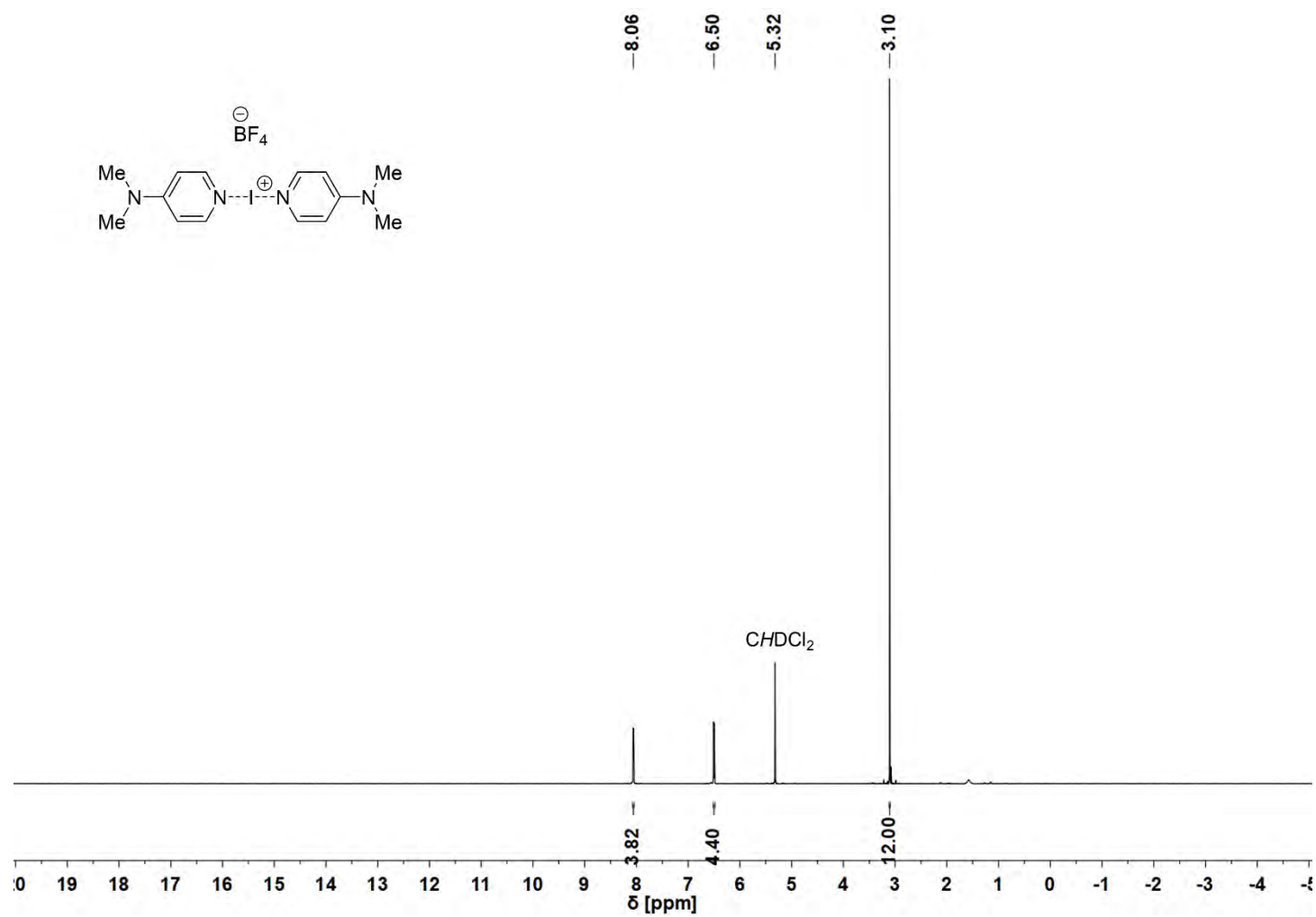


Figure S109. ¹H NMR spectrum (600 MHz, CD₂Cl₂) of [I(DMAP)₂]⁺BF₄⁻.

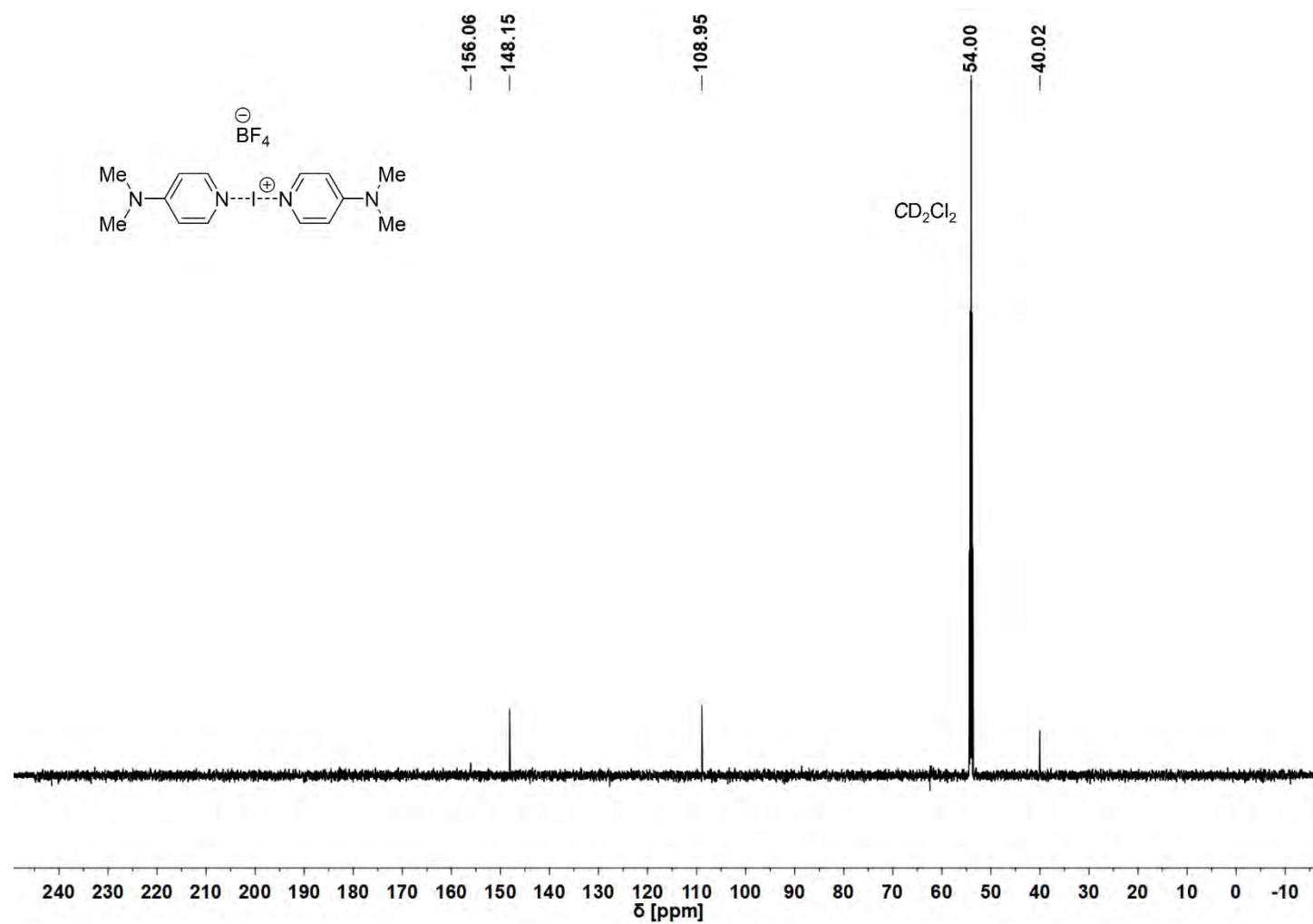


Figure S110. $^{13}\text{C}\{^1\text{H}\}$ NMR spectrum (151 MHz, CD_2Cl_2) of $[\text{I}(\text{DMAP})_2]\text{BF}_4$.

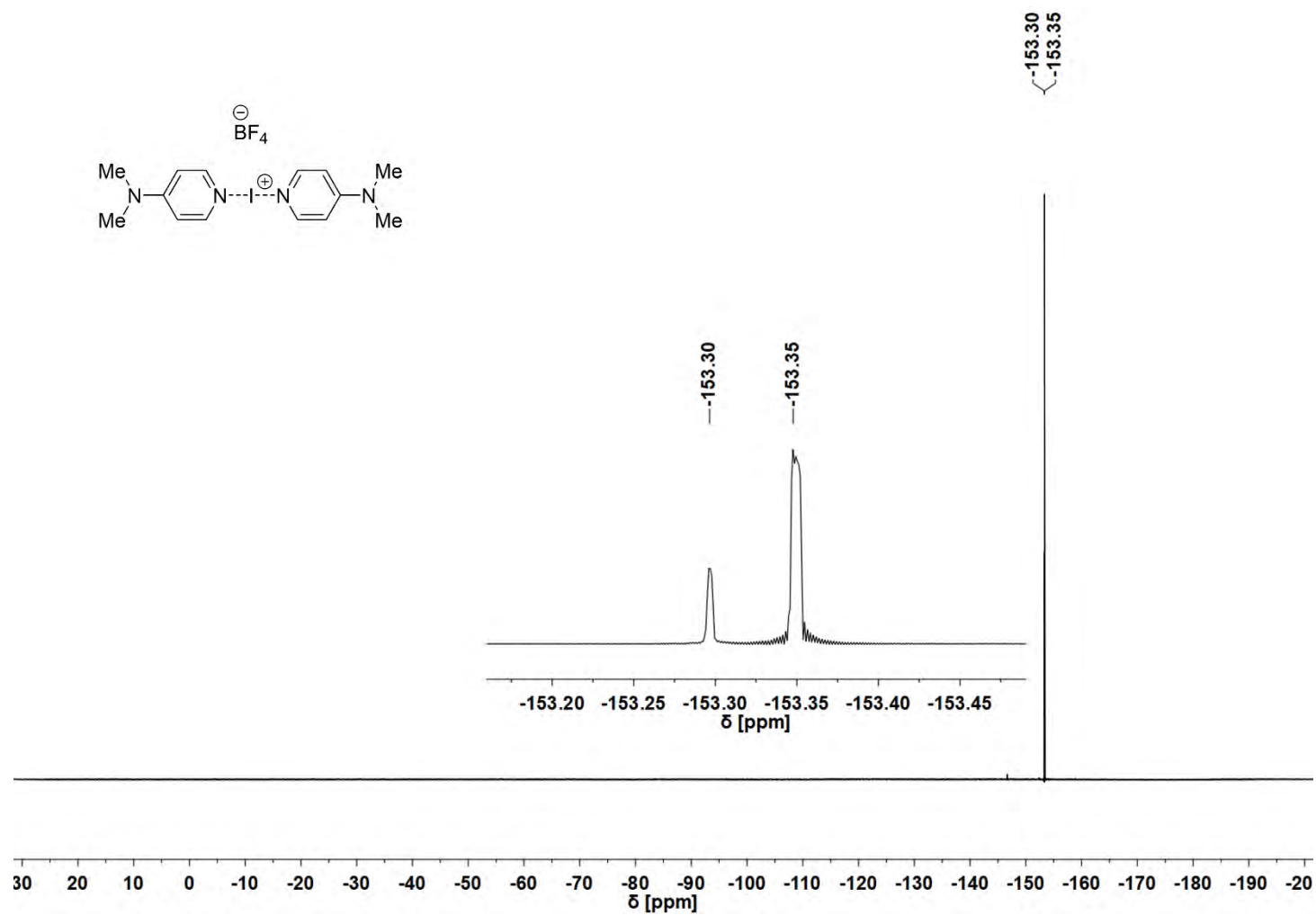


Figure S111. ¹⁹F NMR spectrum (564 MHz, CD₂Cl₂) of [I(DMAP)₂]⁺BF₄⁻.

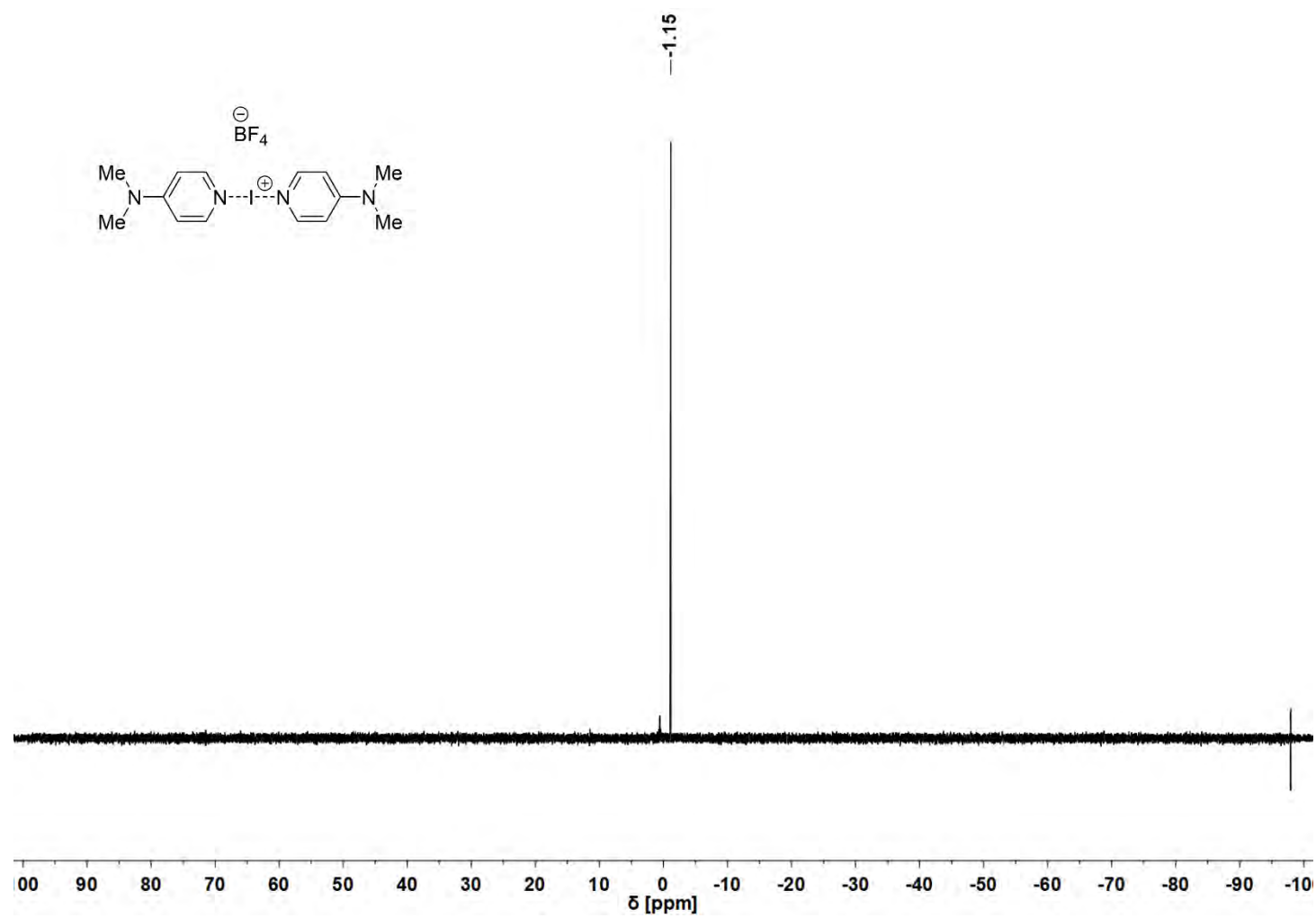


Figure S112. ^{11}B NMR spectrum (192 MHz, CD_2Cl_2) of $[I(DMAP)_2]BF_4$.

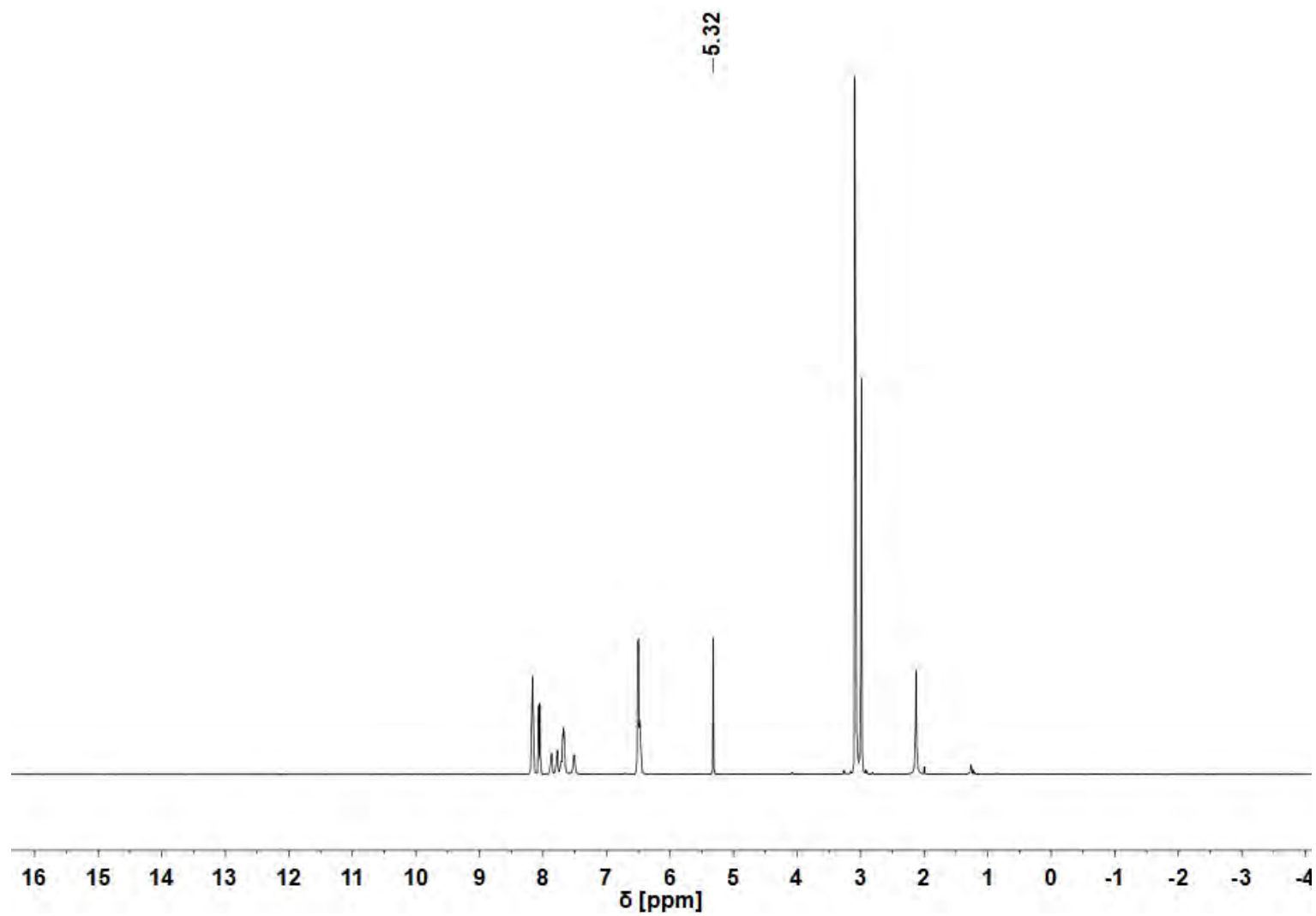


Figure S113. ^1H NMR spectrum (600 MHz, CD_2Cl_2) of $[\text{I}(\text{DMAP})_2]\text{NSac}$ (**4a**) showing decomposition of the product.

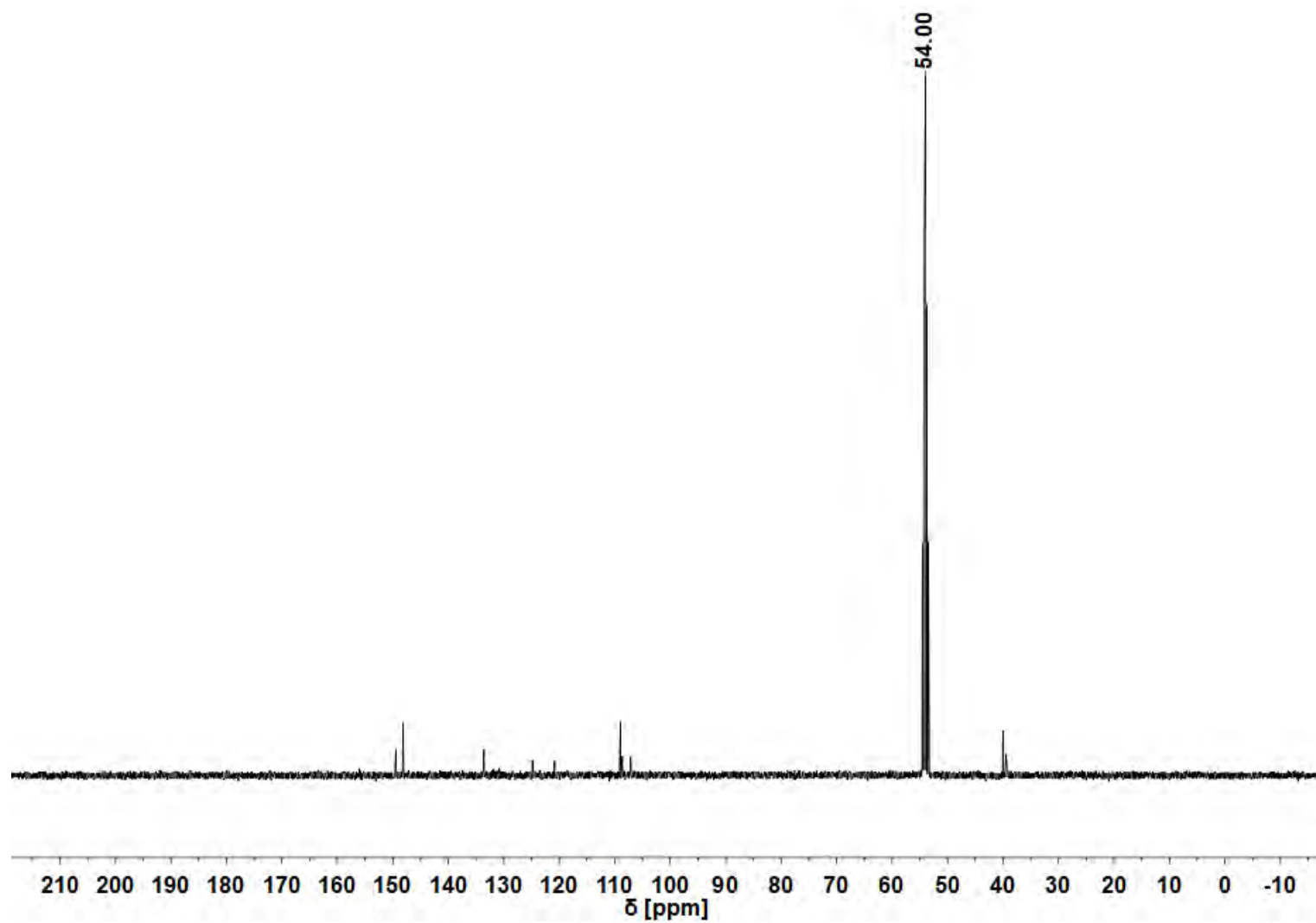


Figure S114. $^{13}\text{C}\{^1\text{H}\}$ NMR spectrum (151 MHz, CD_2Cl_2) of $[\text{I}(\text{DMAP})_2]\text{NSac}$ (**4a**) showing decomposition of the product.

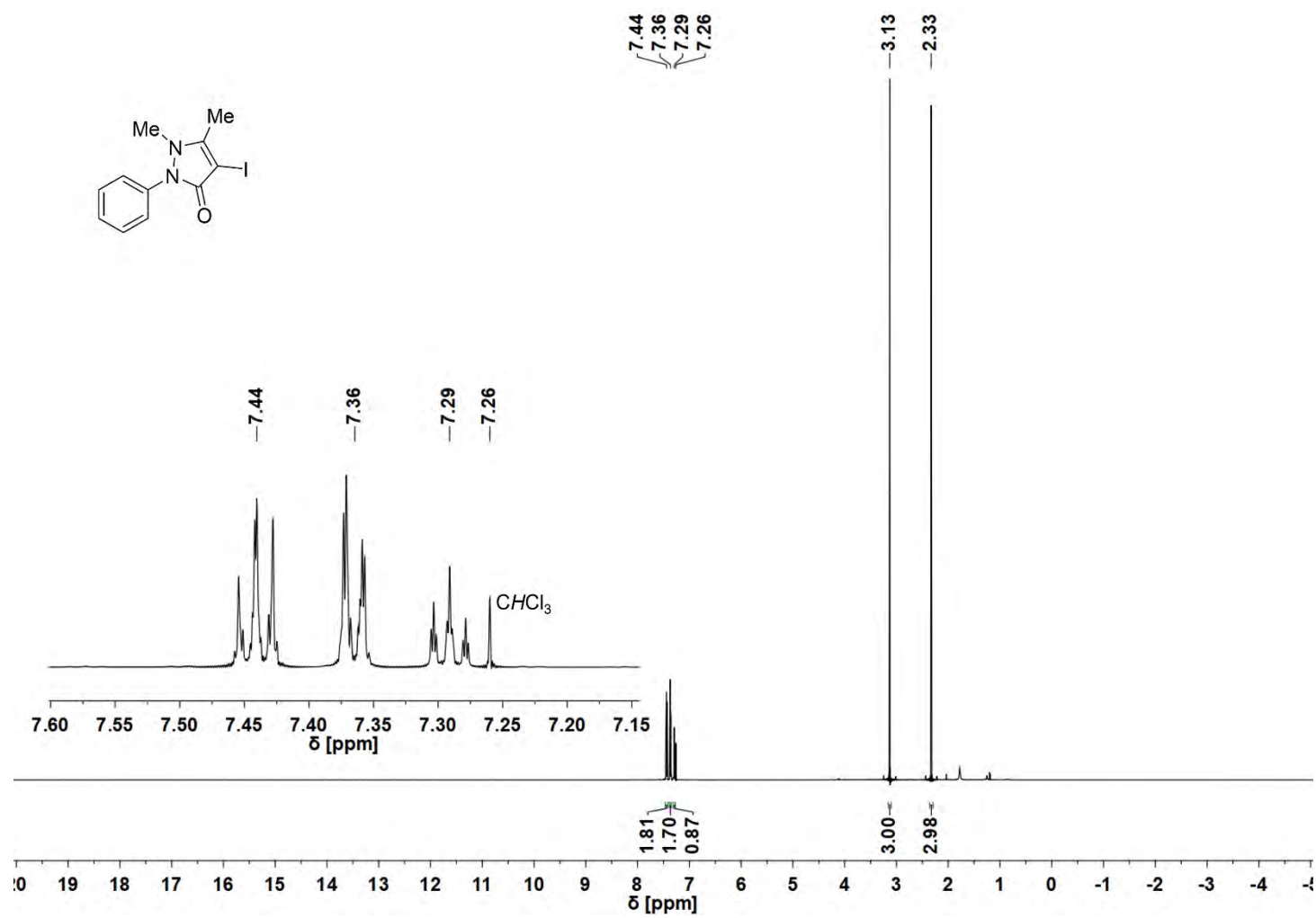


Figure S115. ¹H NMR spectrum (600 MHz, CDCl₃) of 4-iodoantipyrene (6).

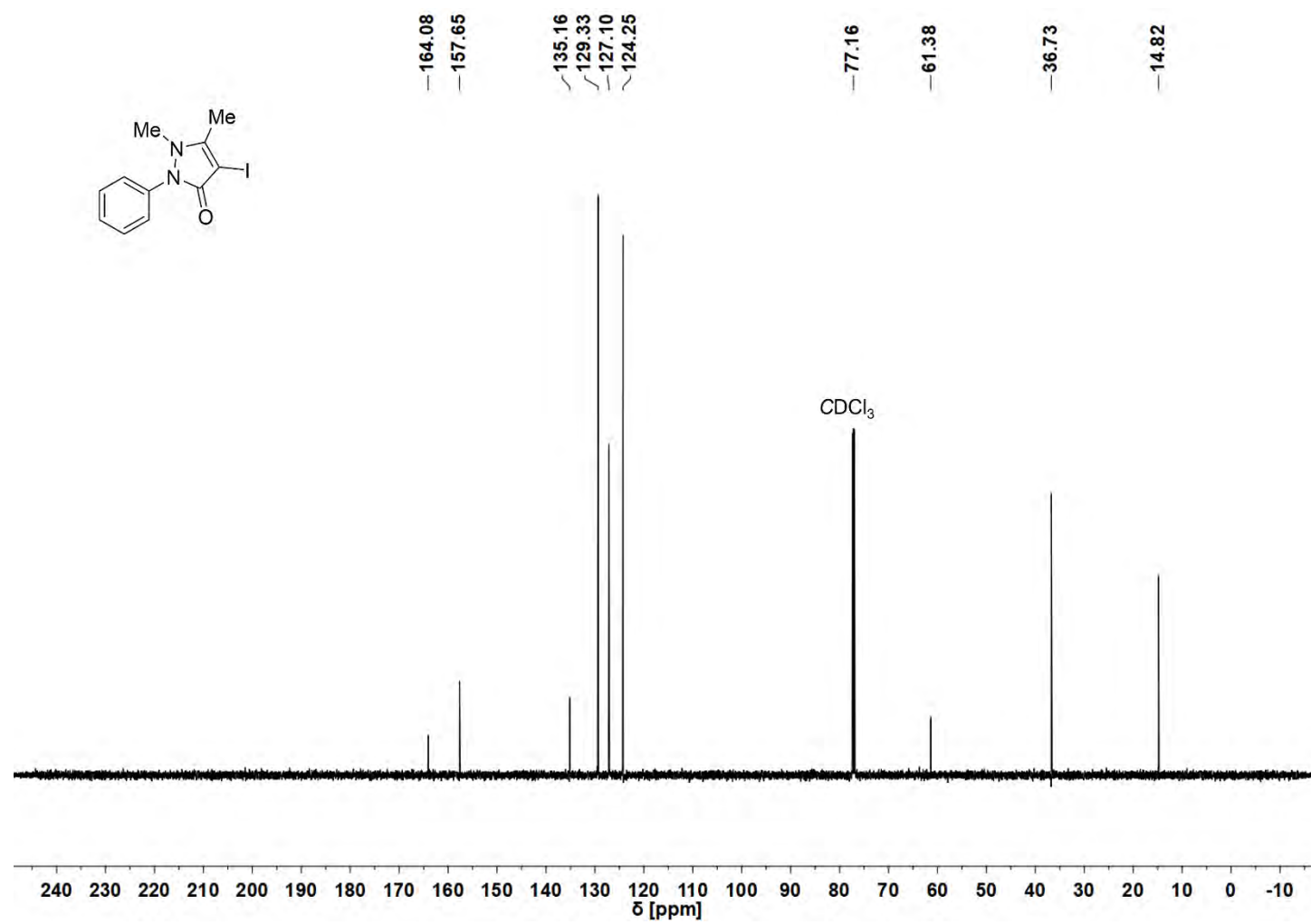


Figure S116. $^{13}\text{C}\{^1\text{H}\}$ NMR spectrum (151 MHz, CDCl_3) of 4-iodoantipyrine (**6**).

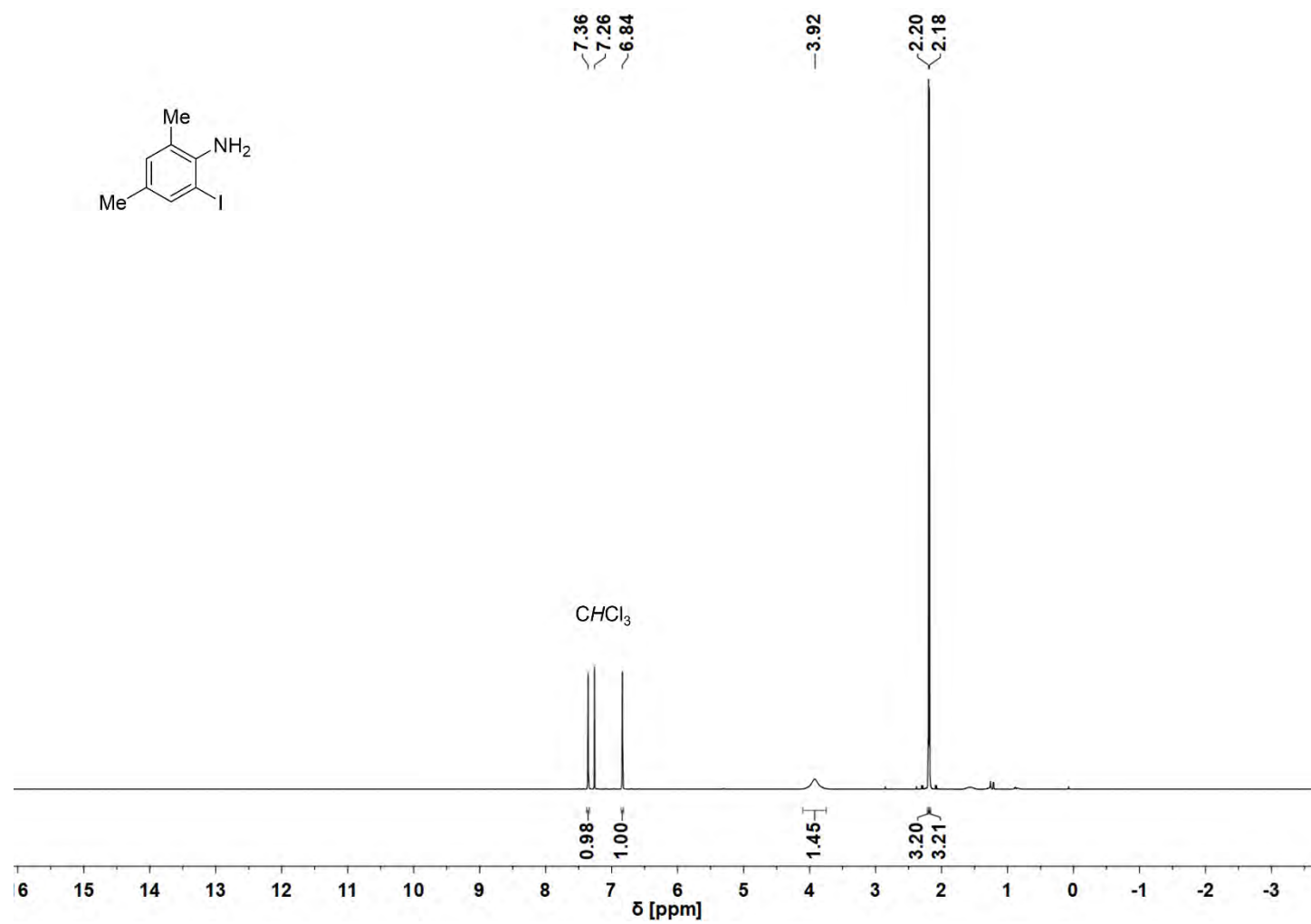


Figure S117. ^1H NMR spectrum (600 MHz, CDCl_3) of 2-iodo-4,6-dimethylaniline (**8**).

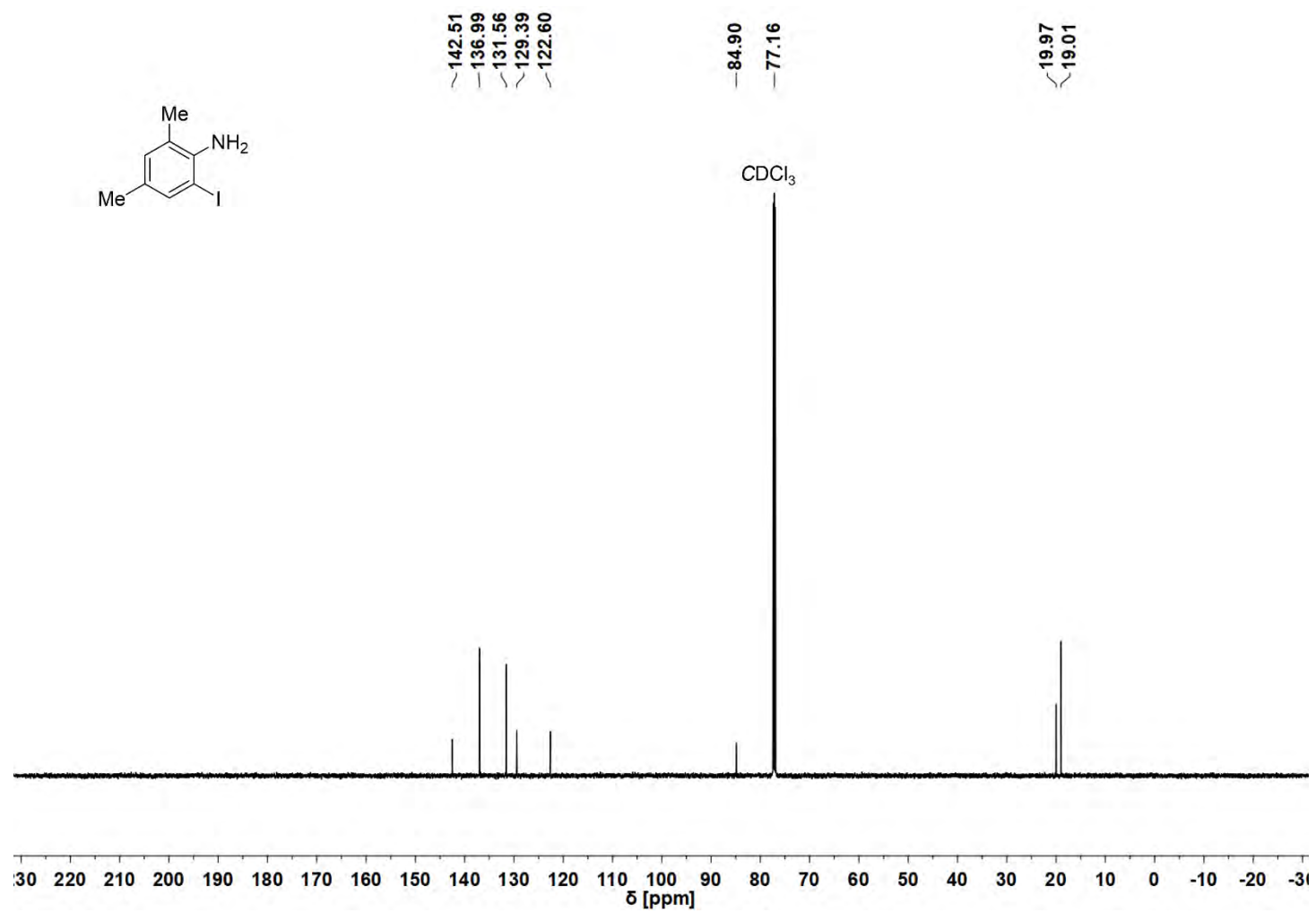


Figure S118. $^{13}\text{C}\{^1\text{H}\}$ NMR spectrum (151 MHz, CDCl_3) of 2-iodo-4,6-dimethylaniline (**8**).

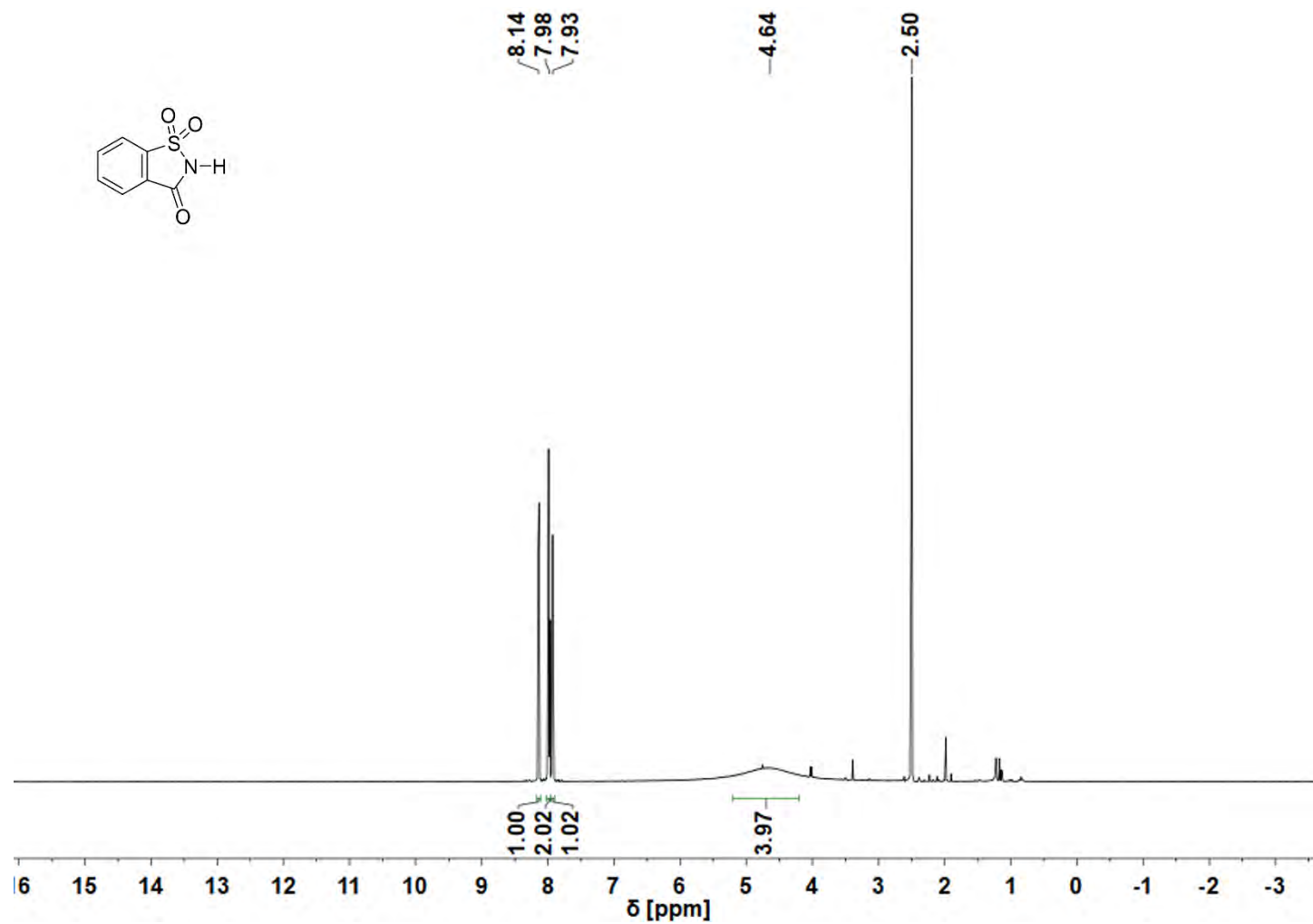


Figure S119. ^1H NMR spectrum (600 MHz, $(\text{CD}_3)_2\text{SO}$) of recovered saccharin.

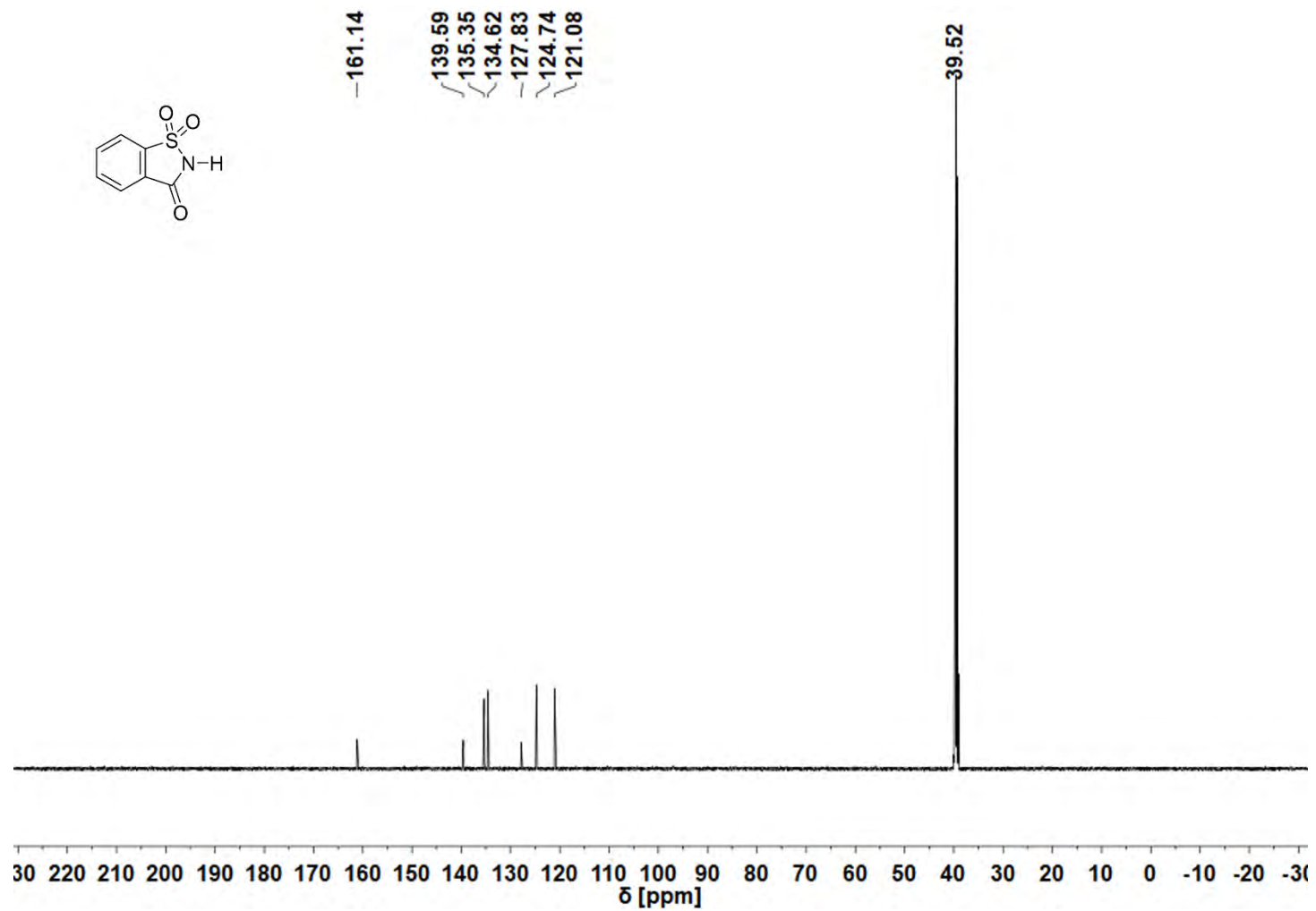


Figure S120. $^{13}\text{C}\{^1\text{H}\}$ NMR spectrum (151 MHz, $(\text{CD}_3)_2\text{SO}$) of recovered saccharin.

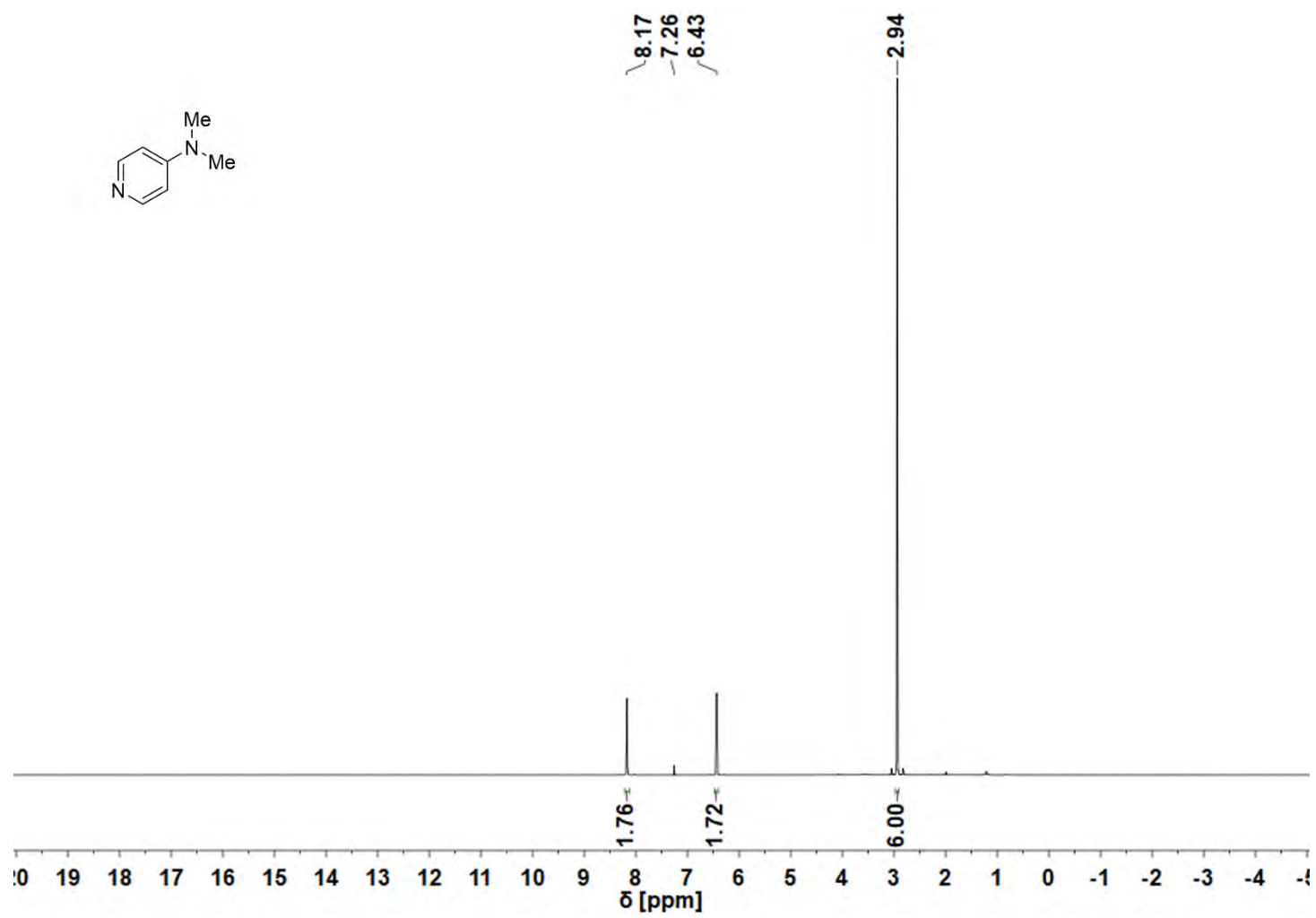


Figure S121. ^1H NMR spectrum (600 MHz, CDCl_3) of recovered DMAP (**2a**).

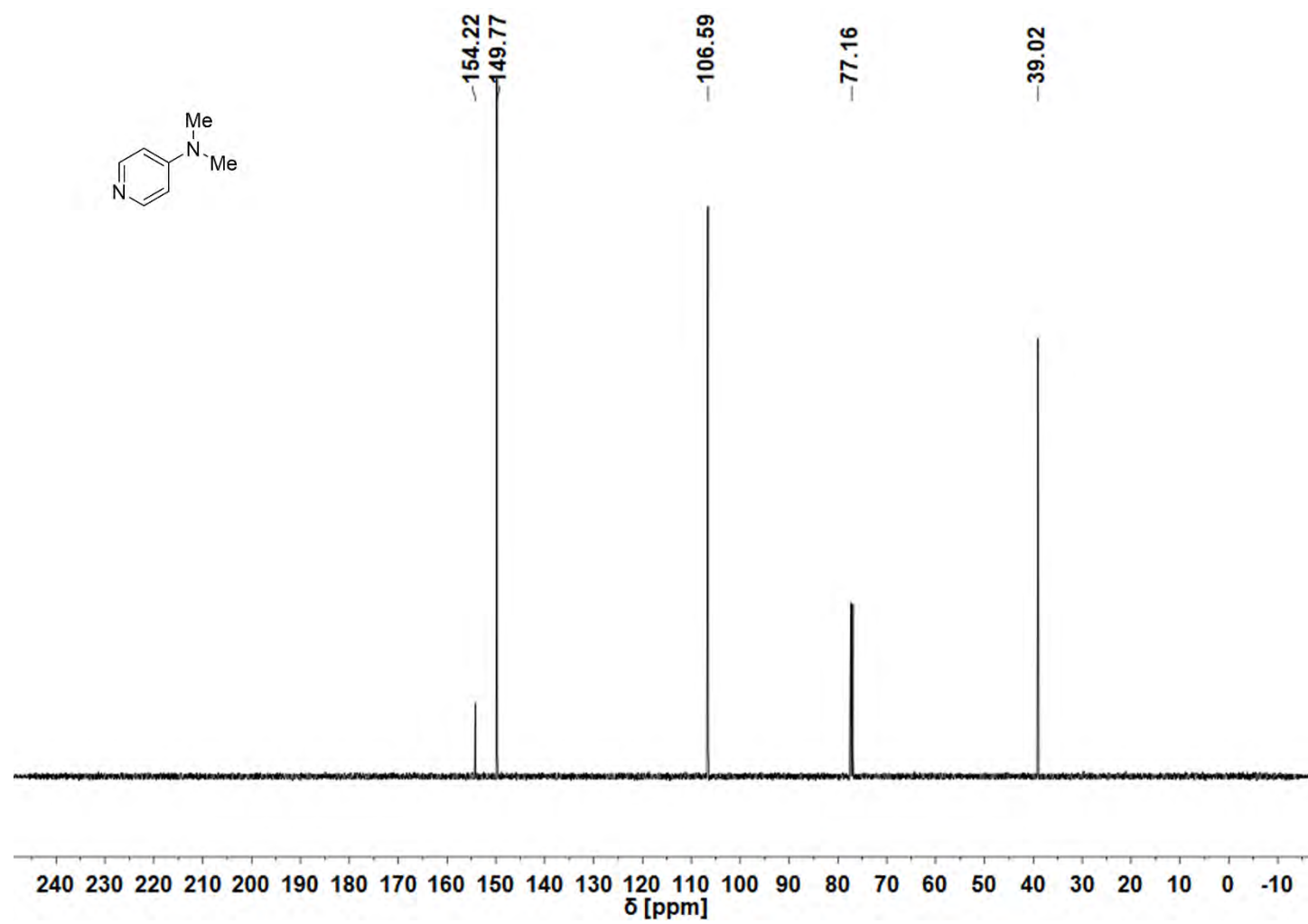


Figure S122. $^{13}\text{C}\{^1\text{H}\}$ NMR spectrum (151 MHz, CDCl_3) of recovered DMAP (**2a**).